The Genetic Architecture of Biological Age in Nine Human Organ Systems

Junhao Wen[1*], Ye Ella Tian[2], Ioanna Skampardoni[3], Zhijian Yang[3], Yuhan Cui[3], Filippos Anagnostakis[4], Elizabeth Mamourian[3], Bingxin Zhao[5], Arthur W. Toga[6], Andrew Zaleskey[2], Christos Davatzikos[3]

[1]Laboratory of AI and Biomedical Science (LABS), Stevens Neuroimaging and Informatics Institute, Keck School of Medicine of USC, University of Southern California, Los Angeles, California, USA
[2]Melbourne Neuropsychiatry Centre, Department of Psychiatry, Melbourne Medical School, The University of Melbourne, Melbourne, Victoria, Australia
[3]Artificial Intelligence in Biomedical Imaging Laboratory (AIBIL), Center for AI and Data Science for Integrated Diagnostics (AI^{2}D), Perelman School of Medicine, University of Pennsylvania, Philadelphia, USA
[4]Department of Medical and Surgical Sciences, University of Bologna, 40126 Bologna, Italy
[5]Department of Statistics and Data Science, University of Pennsylvania, Philadelphia, PA, USA
[6]Laboratory of Neuro Imaging (LONI), Stevens Neuroimaging and Informatics Institute, Keck School of Medicine of USC, University of Southern California, Los Angeles, California, USA

[*]Corresponding author:
Junhao Wen, junhaowe@usc.edu
2025 Zonal Ave, Los Angeles, CA 90033, United States

eMethod 1: The definition of genomic loci, independent significant SNP, lead SNP, candidate SNP

FUMA defined the significant independent SNPs, lead SNPs, candidate SNPs, and genomic risk loci as follows (https://fuma.ctglab.nl/tutorial#snp2gene):

Independent significant SNPs
They are defined as SNPs with $P \leq 5 \times 10^{-8}$ that are independent of each other at the user-defined r^2 (set to 0.6 in the current study). We further describe *candidate SNPs* as those in linkage disequilibrium (LD) with independent significant SNPs. FUMA then queries each candidate SNP in the GWAS Catalog to check whether any clinical traits have been reported to be associated with previous GWAS studies.

Lead SNPs
Lead SNPs are defined as independent significant SNPs that are also independent of each other at $r^2 < 0.1$. If multiple independent significant SNPs are correlated at $r^2 \geq 0.1$, then the one with the lowest individual *P*-value becomes the lead SNP. If r^2 threshold is set to 0.1 for the independent significant SNPs, then they would constitute the identical set as the lead SNPs by definition. FUMA thus advises setting r^2 to be 0.6 or higher.

Genomic risk loci
FUMA defines genomic risk loci to include all independent signals physically close or overlapping in a single locus. First, independent significant SNPs dependent on each other at $r^2 \geq 0.1$ are assigned to the same genomic risk locus. Then, independent significant SNPs with less than the user-defined distance (250 kb by default) away from one another are merged into the same genomic risk locus - the distance between two LD blocks of two independent significant SNPs is the distance between the closest points from each LD block. Each locus is represented by the SNP within the locus with the lowest *P*-value.

eText 1: Sensitivity check analyses for the main GWAS of the nine BAGs using European ancestry

We fully considered linkage disequilibrium and only included the independent significant SNPs in this sensitivity check analysis. We exemplified this analysis in the split-sample GWAS. We first used the Plink *clump* command *(--clump-p1 0.00000005 --clump-p2 0.05 --clump-r2 0.60 --clump-kb 250*) to define the independent significant SNPs for the split1 and split2 GWAS. We then included all the unique independent significant SNPs in either of the two split GWASs. We then calculated three statistics to scrutinize the concordance of the two split GWASs:

- *r-β*: Pearson's *r* between the two sets of *β* coefficients from the two splits;
- *C-β*: concordance rate of the sign of the *β* coefficients from the two splits – if the same SNP exerts the same protective/risk effect between the two splits;
- *P-β*: the difference between the two sets of *β* coefficients from the two splits – if the two sets of *β* coefficients (mean) statistically differ.

The two metrics were calculated for sex-stratified, fastGWA, and non-Euroepan GWAS sensitivity check analyses.

Split-sample GWAS

P-values:

In the split1 GWAS, we found 6, 28, 20, 117, 62, 160, 37, 40, and 127 independent significant SNPs for the brain, cardiovascular, eye, hepatic, immune, metabolic, musculoskeletal, pulmonary, and renal BAGs, and 5, 30, 21, 110, 55, 164, 45, 43, and139 independent significant SNPs in split2 GWAS.

For the brain BAG, we obtained an *r-β* of -0.06 (P-value=0.84; *N*=11), but the two sets of coefficients did not statistically differ (*P-β*=0.70). All the 11 independent significant SNPs showed the same direction of effect (*C-β*=1). The low *r-β* was likely due to small sample sizes in the brain BAG. For all the other 8 BAGs, we obtained significantly h70h *r-β* estimates ($0.90<r\text{-}\beta<0.99$; P-value$<1\times10^{-19}$). The two sets of coefficients did not statistically differ (*P-β*>0.48). All independent significant SNPs showed the same direction of effect (*C-β*=1). Detailed results of these SNPs are presented in **Supplementary eFile 2** for split-sample GWAS. The scatter plot of the independent SNPs' *β* coefficients is shown below.

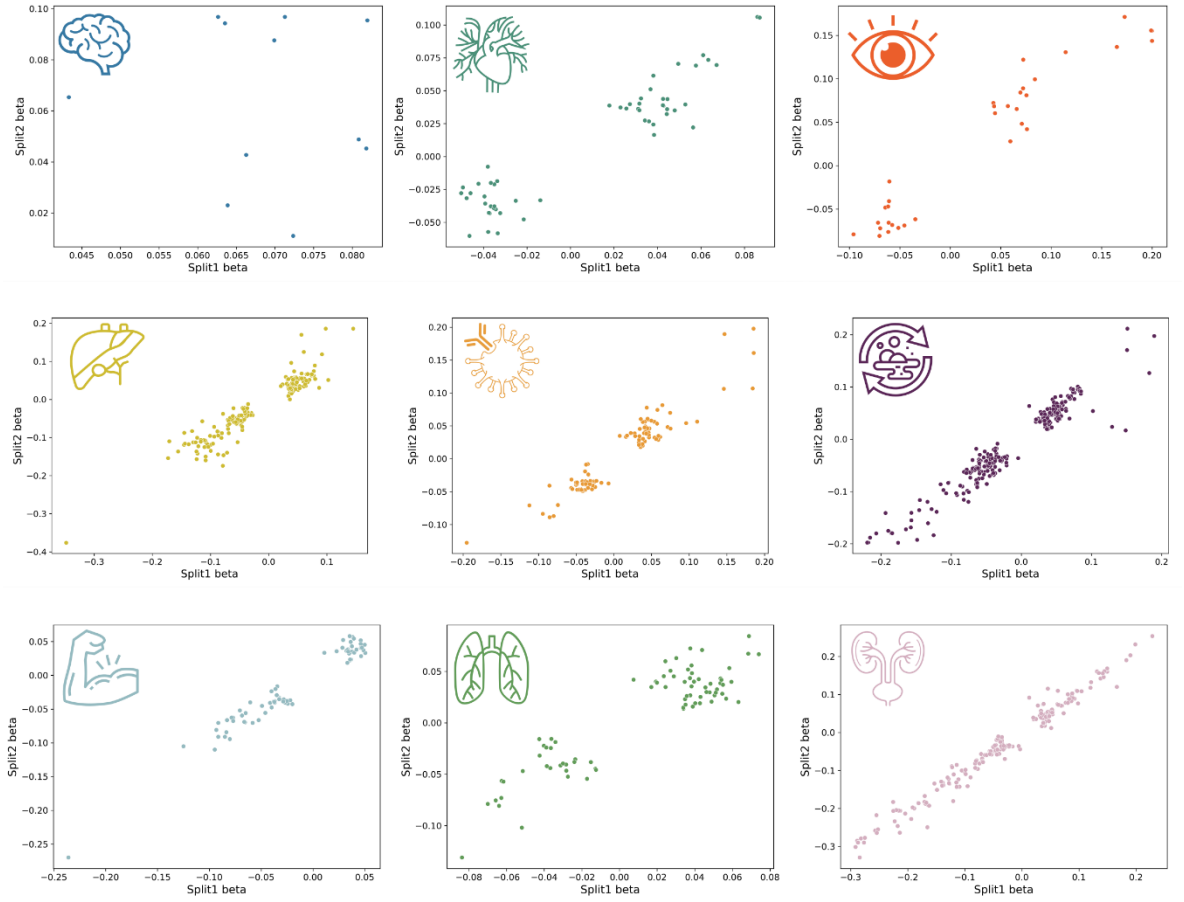

The figures present the scatter plots for the two sets of beta coefficients estimated from different splits.

Sex-stratified GWAS

In the female GWAS, we found 7, 24, 23, 286, 116, 142, 153, 30, and 131 independent significant SNPs for the brain, cardiovascular, eye, hepatic, immune, metabolic, musculoskeletal, pulmonary, and renal BAGs, and 7, 38, 22, 126, 275, 286, 42, 71, and 167 independent significant SNPs in the male GWAS.

For the brain BAG, we obtained an *r-β* of -0.869 (P-value=5.29x10^{-5}, *N*=14), but the two sets of coefficients did not statistically differ (*P-β*=0.66). 13 out of the 14 independent significant SNPs showed the same direction of effect (*C-β*=0.93). The one independent significant SNP (rs1634777) that had the opposite *β* sign in males compared to females was because the *β* coefficient was close to 0 (*β*=-0.000417162) and was not statistically significant (P-value=0.99). For all the other 8 BAGs, we obtained significantly high *r-β* estimates (0.30<*r-β*<0.96; P-value<2.57x10^{-7}). The two sets of coefficients did not statistically differ (*P-β*>0.40), except for the immune BAG (*P-β*=0.013). Most independent significant SNPs showed the same direction of effect (*C-β*>0.89), except for the immune (0.54) and musculoskeletal BAGs (0.70). Detailed results of these SNPs are presented in **Supplementary eFile 3** for sex-stratified GWAS. The scatter plot of the independent SNPs' *β* coefficients is shown below.

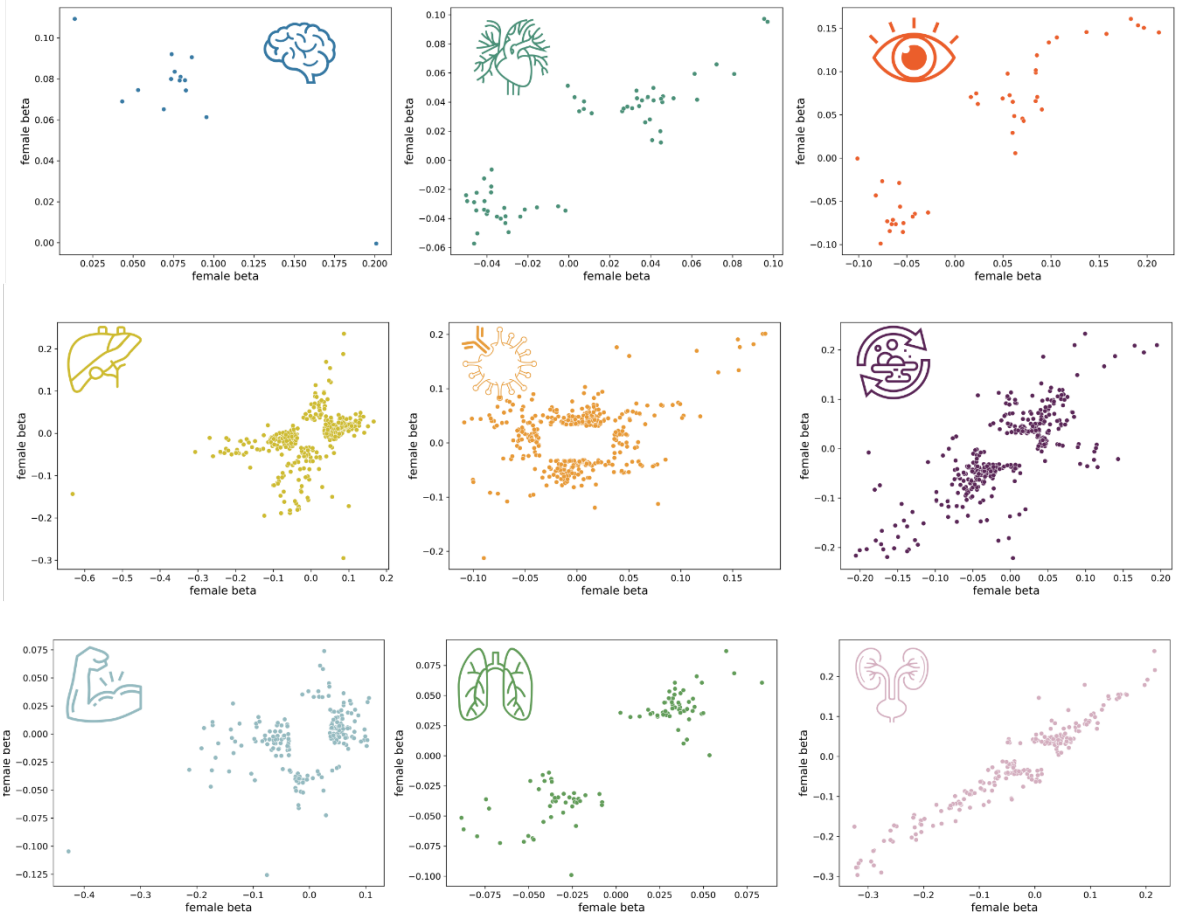

The figures present the scatter plots for the two sets of beta coefficients estimated from different genders.

fastGWA vs PLINK GWAS

In the PLINK GWAS, we found 27, 124, 69, 289, 217, 422, 147, 272, and 331 independent significant SNPs for the brain, cardiovascular, eye, hepatic, immune, metabolic, musculoskeletal, pulmonary, and renal BAGs, and 27, 124, 69, 292, 218, 422, 148, 269, and 333 independent significant SNPs in fastGWA GWAS.

For all the nine BAGs, we found almost perfect concordance between the PLINK and fastGWA GWASs using the three proposed metrics (r-β=1; C-β=1; P-β=1). Detailed results of these SNPs are presented in **Supplementary eFile 4** for method-specific GWAS. The scatter plot of the independent SNPs' β coefficients is shown below.

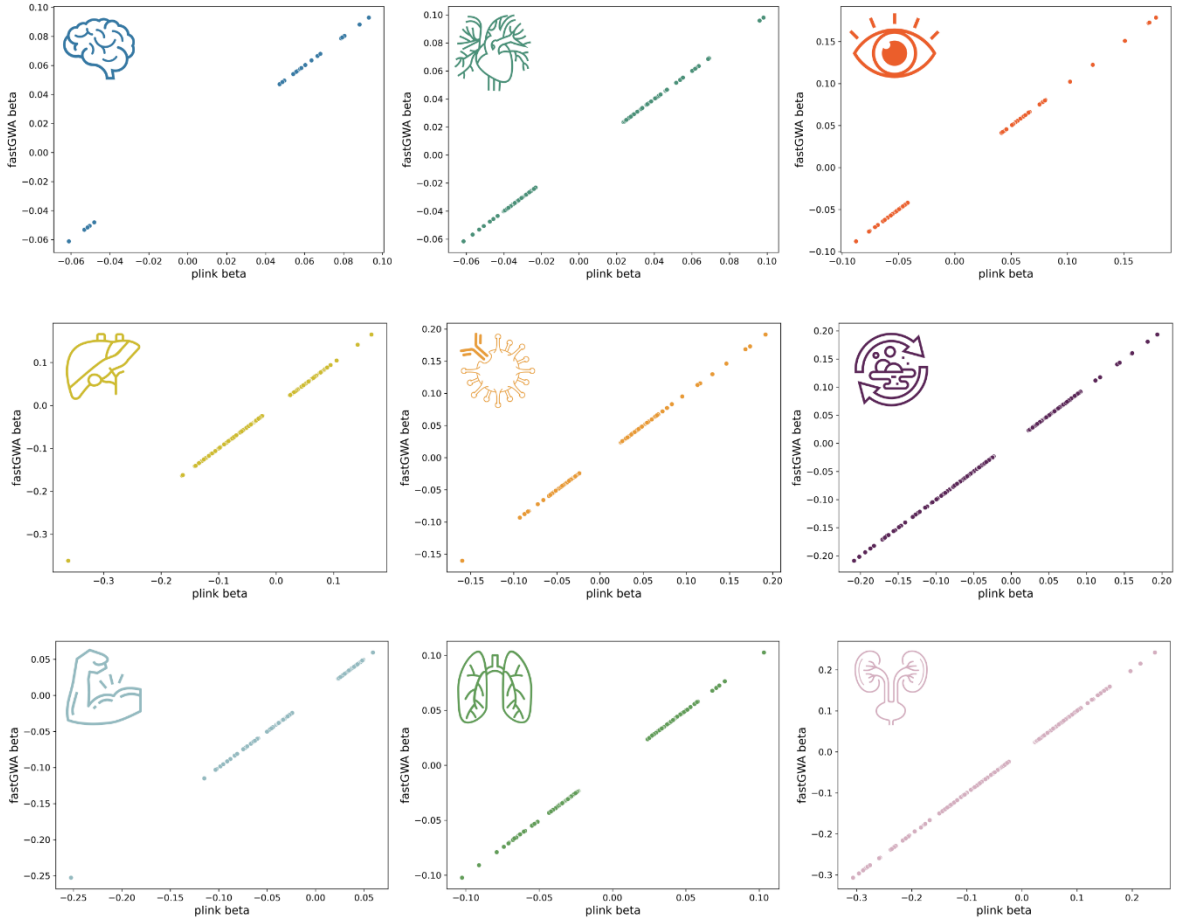

The figures present the scatter plots for the two sets of beta coefficients estimated from different GWAS methods.

European vs. non-European GWAS

In the European GWAS, we found 27, 124, 69, 289, 217, 422, 147, 272, and 331 independent significant SNPs for the brain, cardiovascular, eye, hepatic, immune, metabolic, musculoskeletal, pulmonary, and renal BAGs, and 0, 2, 1, 16, 2, 23, 1, 1, and 35 independent significant SNPs in non-European GWAS (with much smaller sample sizes).

For all the nine BAGs, we found a high concordance between the European and non-Euroropean GWASs using the three proposed metrics ($0.85<r\text{-}\beta<0.95$; $0.89<C\text{-}\beta<1$). The two sets of β coefficients did not significantly differ ($P\text{-}\beta>0.12$). Detailed results of these SNPs are presented in **Supplementary eFile 5** for ancestry-specific GWAS. The scatter plot of the independent SNPs' β coefficients is shown below.

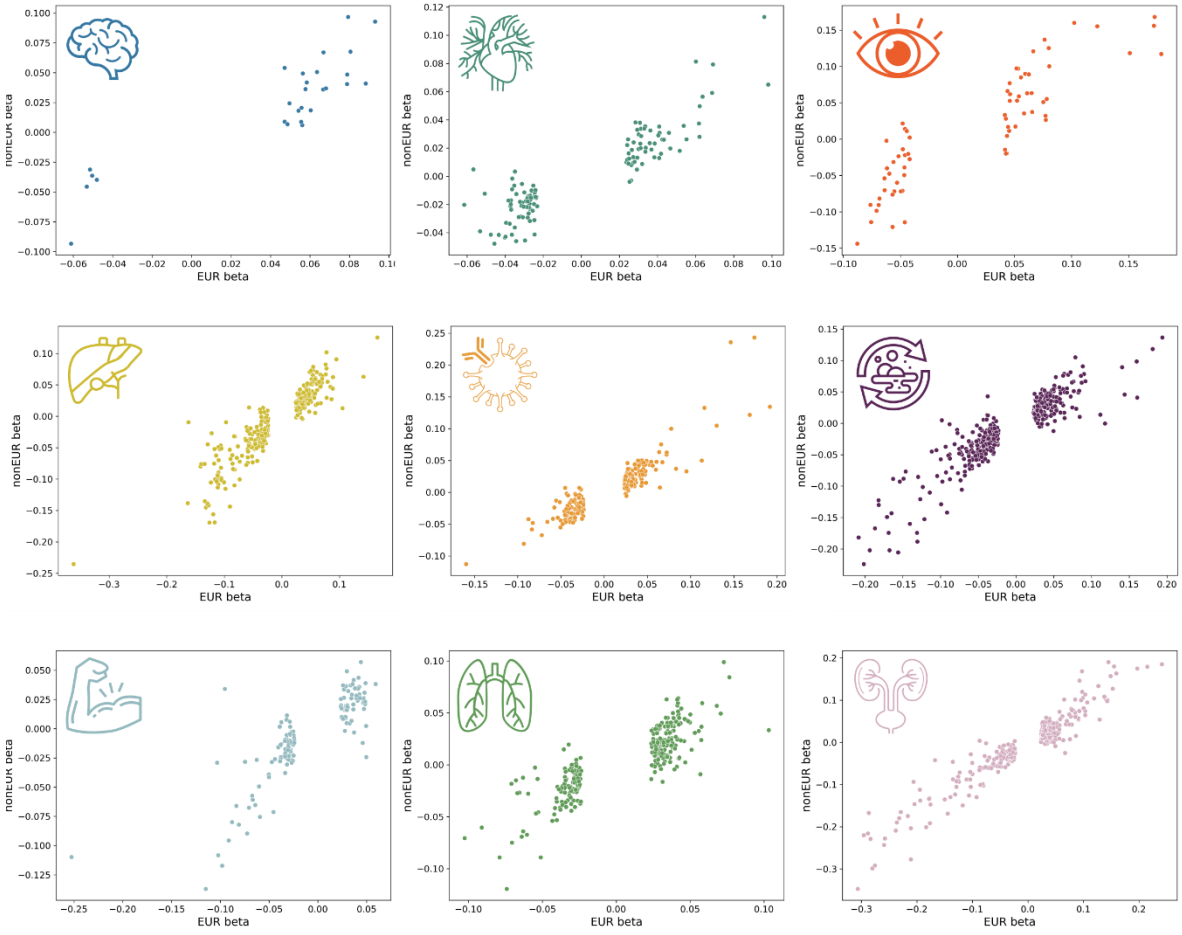

The figures present the scatter plots for the two sets of beta coefficients estimated from different GWAS ancestry groups.

eText 2: Phenome-wide association query using the GWAS Atlas platform

To comprehensively encompass the genetic landscape reported in previous literature, we comparatively conducted a phenome-wide association query using the GWAS Atlas platform (https://atlas.ctglab.nl/PheWAS). We applied the same P-value threshold search criteria as those used in the EMBL-EBI GWAS Catalog (P-value<$1x10^{-5}$). These findings are presented as a supplementary search to complement the results shown in **Fig. 2a**. The details of this comparative search are presented in **Supplementary eFile 7**.

It's important to note that the two platforms may exhibit variations in their curated GWAS datasets, the genome build versions utilized, and the specific P-value thresholds set for their search analyses by default. We tried our best to harmonize the query criteria. Hence, this comparative search was not exhaustive, and the results may differ. Rather, we intend to offer a broad overview of the two platforms commonly employed for phenome-wide association studies (PheWAS). Given the rapid updates in GWAS summary statistics in the field, it's worth mentioning that this comparative search was originally conducted on October 23, 2023, and revised on January 13, 2024, based on the reviewer's comments. The results from the GWAS Atlas are shown in the figure below.

In the GWAS Atlas platform, we identified 8,576 significant associations between the identified loci in our GWAS and clinical traits. The genomic loci associated with the brain BAG exhibited the highest proportion of associations (109 out of 308) with traits related to the brain. The brain BAG loci were also largely linked to many other traits related to other organ systems, evidencing inter-organ connections, including metabolic (*N*=78/308), lifestyle factor (*N*=13/308), neurodegenerative traits (*N*=5/308), and immune (*N*=35/308). For the eye BAG loci, most associations were found in the musculoskeletal (*N*=139/279), eye (*N*=14/279), and mental traits (*N*=19/279), among many others.

For the seven body organ systems, among the loci associated with the cardiovascular BAG, most associations were observed with musculoskeletal traits (*N*=249/611) and cardiovascular traits (166/611). 29 out of 1009 associations were related to hepatic traits (e.g., blood protein, cirrhosis, and bilirubin) for the hepatic BAG loci. Among the loci associated with the immune BAG, abundant associations were found enriched in immune (*N*=467/1062) traits. For the metabolic BAG loci, most associations were observed in metabolic traits (*N*=993/1990). We found a significant intertwining of musculoskeletal systems with other organ systems in the GWAS Atlas platform. Details of the phenome-wide associations are presented in **Supplementary eFile 7**.

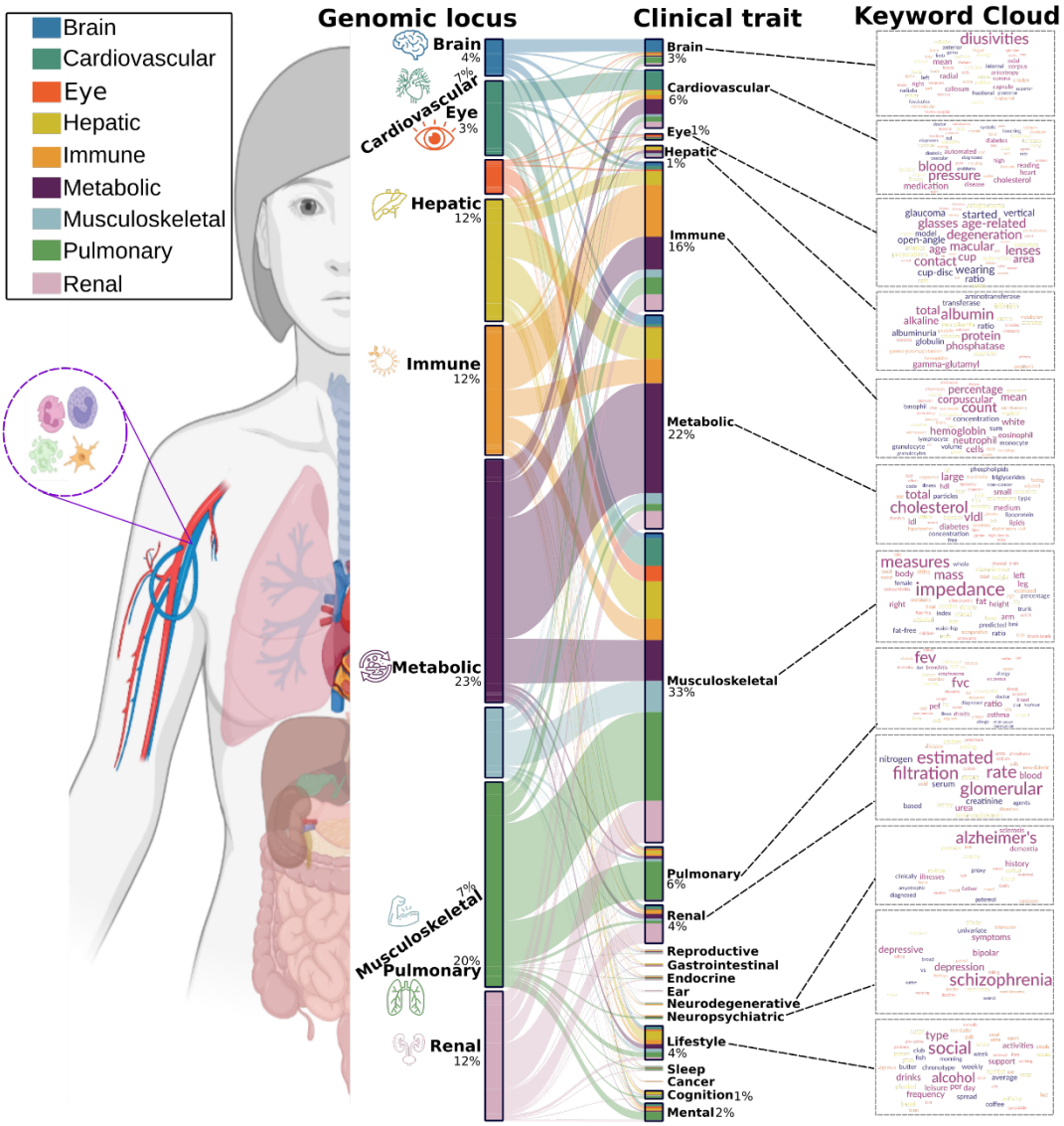

Figure. We queried the clumped independent significant SNPs using the PheWAS functionaly provided by the GWAS Atlas platforms.

eText 3: Sensitivity check analyses for the causality between the hepatic BAG and musculoskeletal BAG

A) Sensitivity analyses on body weight for the bi-directional causality between the hepatic and musculoskeletal BAGs

We conducted a revised Mendelian randomization analysis by introducing body weight as a covariate in the split-sample GWASs for hepatic and musculoskeletal BAGs. In this approach, we employed hepatic BAG as the exposure variable in split1 GWAS and musculoskeletal BAG as the outcome variable in split2 GWAS. Likewise, we reversed the roles, using musculoskeletal BAG as the exposure variable in split1 GWAS and hepatic BAG as the outcome variable in split2 GWAS, thus assessing the inverse causal relationship. This methodology ensured the absence of overlapping populations while effectively controlling for the influence of body weight.

Compared to the original results, this bi-directional causality persisted while adjusting the body weight as a covariate, shown in the tables below:

1) GWAS without and with body weight as a covariate for the causal relationship from the hepatic BAG to the musculoskeletal BAG.

Weight	Outcome (split2)	Exposure (split1)	Method	nSNP	BETA	SE	P	OR	CI_low	CI_high
N	Musculoskeletal	Hepatic	MR Egger	19	0.51783336	0.14070786	0.00185593	1.67838725	1.27385274	2.21138886
	Musculoskeletal	Hepatic	Weighted median	19	0.35295633	0.06606437	9.16E-08	1.42326899	1.25040832	1.62002649
	Musculoskeletal	Hepatic	Inverse variance weighted	19	0.38344296	0.07834137	9.85E-07	1.46732785	1.25846644	1.71085295
	Musculoskeletal	Hepatic	Simple mode	19	0.15733154	0.10700058	0.15872332	1.17038357	0.94895908	1.44347395
	Musculoskeletal	Hepatic	Weighted mode	19	0.46614953	0.08121762	1.93E-05	1.59384531	1.35929067	1.86887391
Y	Musculoskeletal	Hepatic	MR Egger	18	0.51517011	0.14245065	0.00231711	1.67392323	1.26613232	2.21305384
	Musculoskeletal	Hepatic	Weighted median	18	0.35613857	0.06002398	2.97E-09	1.42780539	1.26933301	1.60606258
	Musculoskeletal	Hepatic	Inverse variance weighted	18	0.38926537	0.0792834	9.12E-07	1.47589615	1.2634801	1.72402356
	Musculoskeletal	Hepatic	Simple mode	18	0.24697399	0.11293776	0.04302518	1.28014581	1.02594689	1.59732761
	Musculoskeletal	Hepatic	Weighted mode	18	0.47542746	0.06925444	2.74E-06	1.60870171	1.40451037	1.84257891

2) GWAS without and with body weight as a covariate for the causal relationship from the musculoskeletal BAG to the hepatic BAG.

Weight	Outcome (split2)	Exposure (split1)	Method	nSNP	BETA	SE	P	OR	CI_low	CI_high
N	Hepatic	Musculoskeletal	MR Egger	9	1.8282501	0.24293965	0.00013439	6.22298749	3.8654897	10.018283
	Hepatic	Musculoskeletal	Weighted median	9	0.92114305	0.13768954	2.23E-11	2.51216028	1.9179781	3.2904178
	Hepatic	Musculoskeletal	Inverse variance weighted	9	1.02402966	0.18103365	1.54E-08	2.78439235	1.9526818	3.97035541

	Hepatic	Musculoskeletal	Simple mode	9	1.20577311	0.18620161	0.000193	3.33933976	2.31826245	4.81014995
	Hepatic	Musculoskeletal	Weighted mode	9	1.25833413	0.13034769	1.10E-05	3.51955347	2.7260472	4.54403601
Y	Hepatic	Musculoskeletal	MR Egger	9	1.69092352	0.35916855	0.00218827	5.42448802	2.68304718	10.9670342
	Hepatic	Musculoskeletal	Weighted median	9	0.85408009	0.13197703	9.71E-11	2.34921232	1.81376558	3.04272978
	Hepatic	Musculoskeletal	Inverse variance weighted	9	0.99179962	0.19767923	5.24E-07	2.69608204	1.83005923	3.97192521
	Hepatic	Musculoskeletal	Simple mode	9	1.23665687	0.15851732	5.23E-05	3.44408019	2.52429777	4.6990052
	Hepatic	Musculoskeletal	Weighted mode	9	1.27628794	0.1538585	3.36E-05	3.58331353	2.65043899	4.84453174

B) Sensitivity analysis for the hepatic BAG on musculoskeletal BAG excluding the *APOE* gene

We conducted a revised Mendelian randomization analysis by excluding SNPs within the *APOE* gene for the causal relationship from the hepatic BAG to the musculoskeletal BAGs; all other significant causality did not involve the two common *APOE* gene SNPs (rs429358 and rs7412). In this approach, we employed hepatic BAG as the exposure variable in split1 GWAS and musculoskeletal BAG as the outcome variable in split2 GWAS.

Compared to the original results, this causality persisted while excluding the SNP (rs429358) as an IV, shown in the tables below:

GWAS without and with rs429358 as an IV for the causal relationship from the hepatic BAG to the musculoskeletal BAG.

rs429358	Outcome (split2)	Exposure (split1)	Method	nSNP	BETA	SE	P	OR	CI_low	CI_high
N	Musculoskeletal	Hepatic	MR Egger	18	0.51522659	0.12736616	0.00093844	1.67401778	1.30419881	2.14870271
	Musculoskeletal	Hepatic	Weighted median	18	0.36478773	0.06339608	8.71E-09	1.44020827	1.27192489	1.63075657
	Musculoskeletal	Hepatic	Inverse variance weighted	18	0.41660503	0.07146014	5.55E-09	1.5168033	1.31856385	1.74484706
	Musculoskeletal	Hepatic	Simple mode	18	0.15924454	0.09710274	0.11938508	1.17262466	0.96940109	1.41845167
	Musculoskeletal	Hepatic	Weighted mode	18	0.45942325	0.07899932	2.07E-05	1.58316063	1.35606155	1.84829191
Y	Musculoskeletal	Hepatic	MR Egger	19	0.51783336	0.14070786	0.00185593	1.67838725	1.27385274	2.21138886
	Musculoskeletal	Hepatic	Weighted median	19	0.35295633	0.06606437	9.16E-08	1.42326899	1.25040832	1.62002649
	Musculoskeletal	Hepatic	Inverse variance weighted	19	0.38344296	0.07834137	9.85E-07	1.46732785	1.25846644	1.71085295
	Musculoskeletal	Hepatic	Simple mode	19	0.15733154	0.10700058	0.15872332	1.17038357	0.94895908	1.44347395
	Musculoskeletal	Hepatic	Weighted mode	19	0.46614953	0.08121762	1.93E-05	1.59384531	1.35929067	1.86887391

C) Sensitivity analyses for metabolic BAG on body weight

We showcased sensitivity analyses to investigate potential violations of the three IV assumptions (**Method 3j**). To illustrate this, we showcased the sensitivity analysis results for the causal effect

of the metabolic BAG on body weight (**Supplementary eFigure 33**). In a leave-one-out analysis, no single SNP overwhelmingly drove the overall effect. There was evidence for minor heterogeneity[1] of the causal effect amongst SNPs (Cochran's Q value=57.33, P-value<$1x10^{-5}$). Some SNPs exerted opposite causal effects compared to the model using all SNPs. The scatter plot indicated two obvious SNP outliers (rs117233107 and rs33959228), and the funnel plot showed slight asymmetry. Finally, the MR Egger estimator allows for pleiotropic effects independent of the effect on the exposure of interest (i.e., the InSIDE assumption[2]). Our results from the Egger estimator showed a small but not significant positive intercept ($3.62x10^{-4}$±$1.67x10^{-3}$, P-value=0.83), which may indicate that the IVW estimate is not likely biased[2]. We re-analyzed the IVW MR analyses by excluding the two outliers identified in **Supplementary eFigure 33** (rs117233107 and rs33959228), which led to a similar OR [0.94 (0.91, 0.97) vs. 0.95 (0.92, 0.98)] and a less significant P-value [$6.9x10^{-4}$ vs. $1.2x10^{-3}$].

eFigure 1: GWAS Manhattan plots for the brain BAG

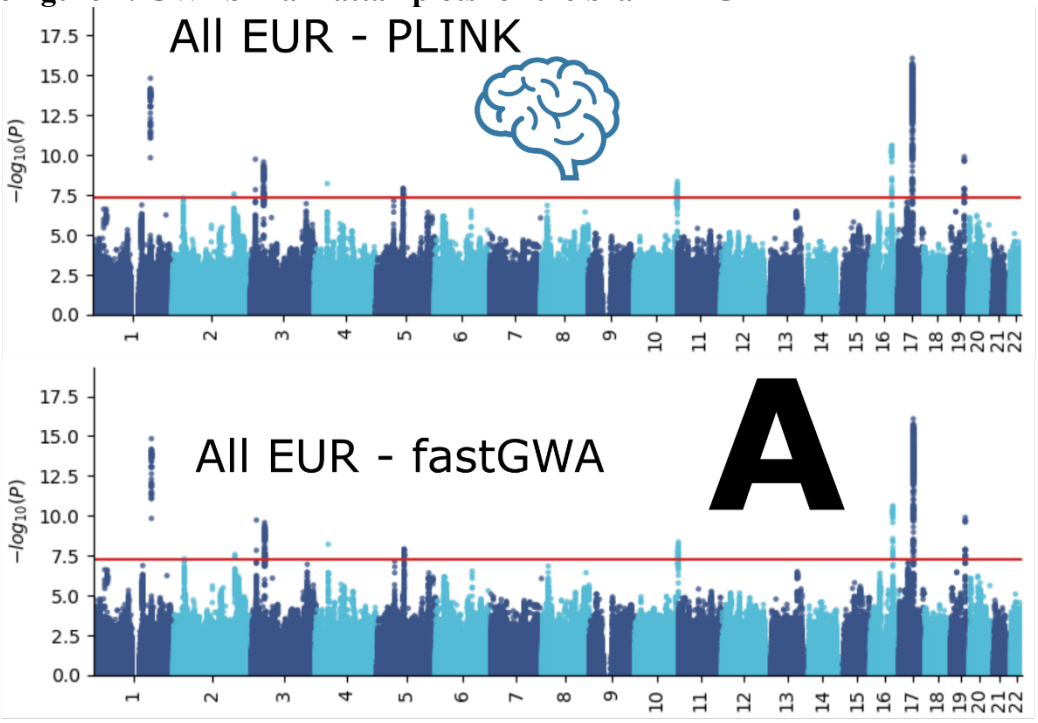

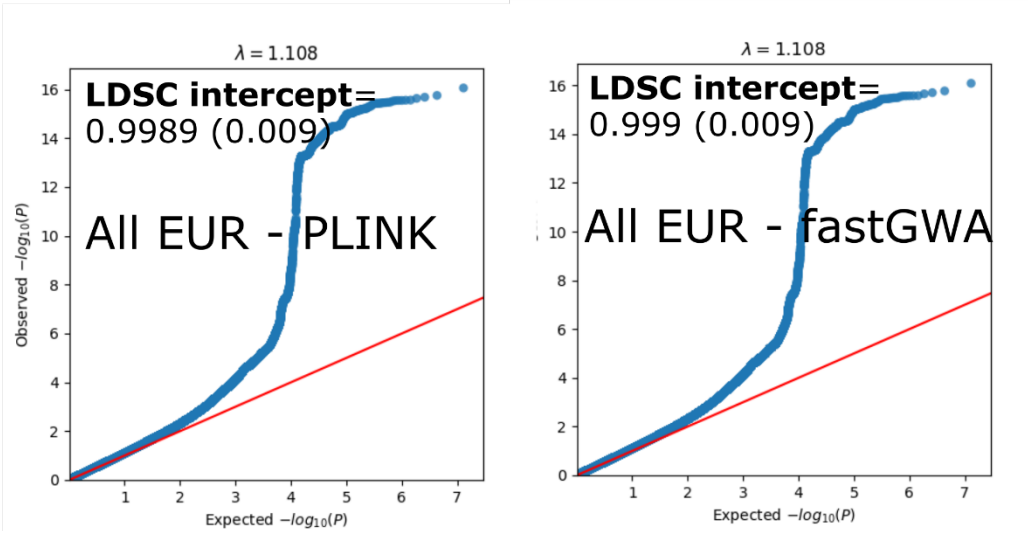

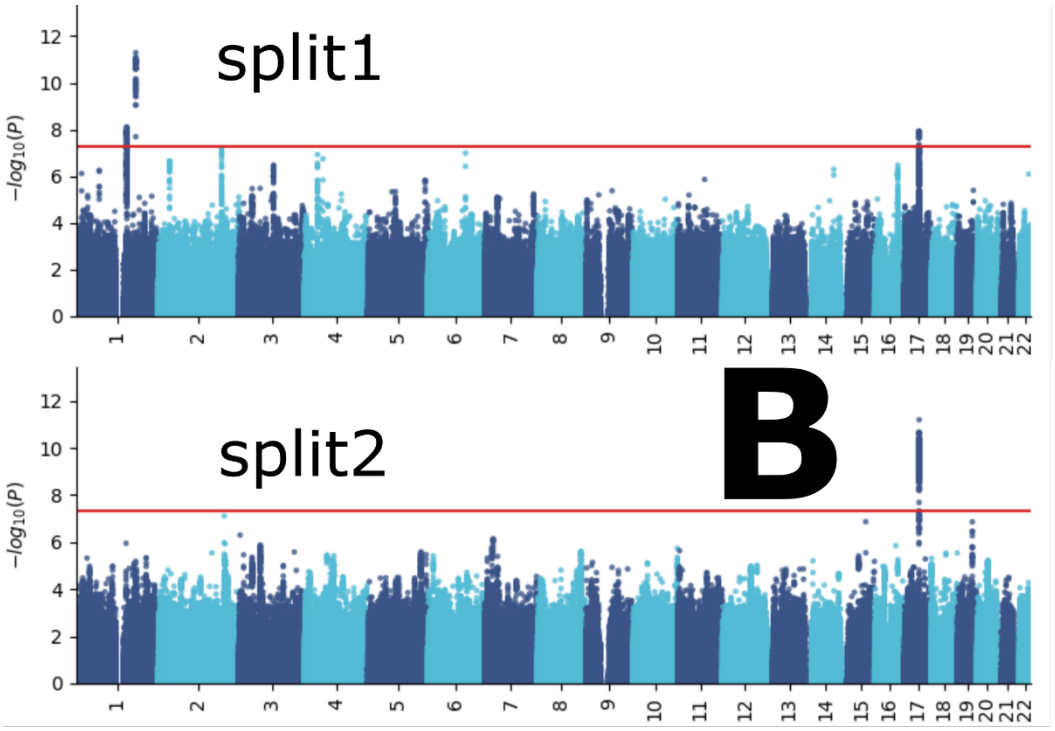
split1
split2
B
$-log_{10}(P)$

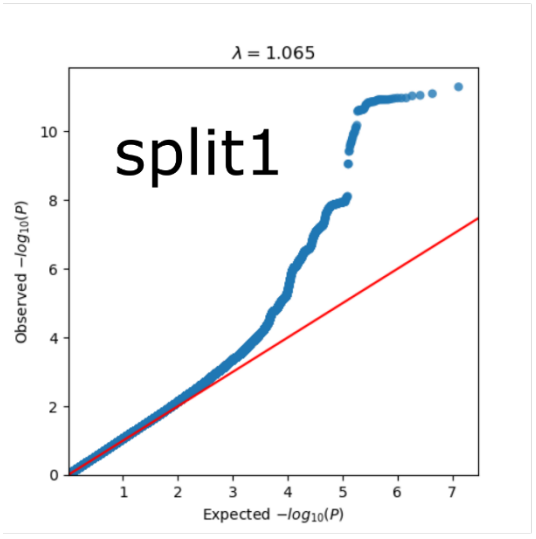
$\lambda = 1.065$
split1
Observed $-log_{10}(P)$
Expected $-log_{10}(P)$

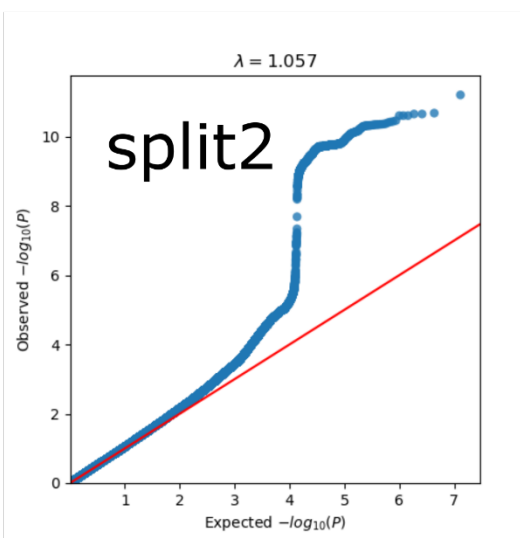
$\lambda = 1.057$
split2
Observed $-log_{10}(P)$
Expected $-log_{10}(P)$

286

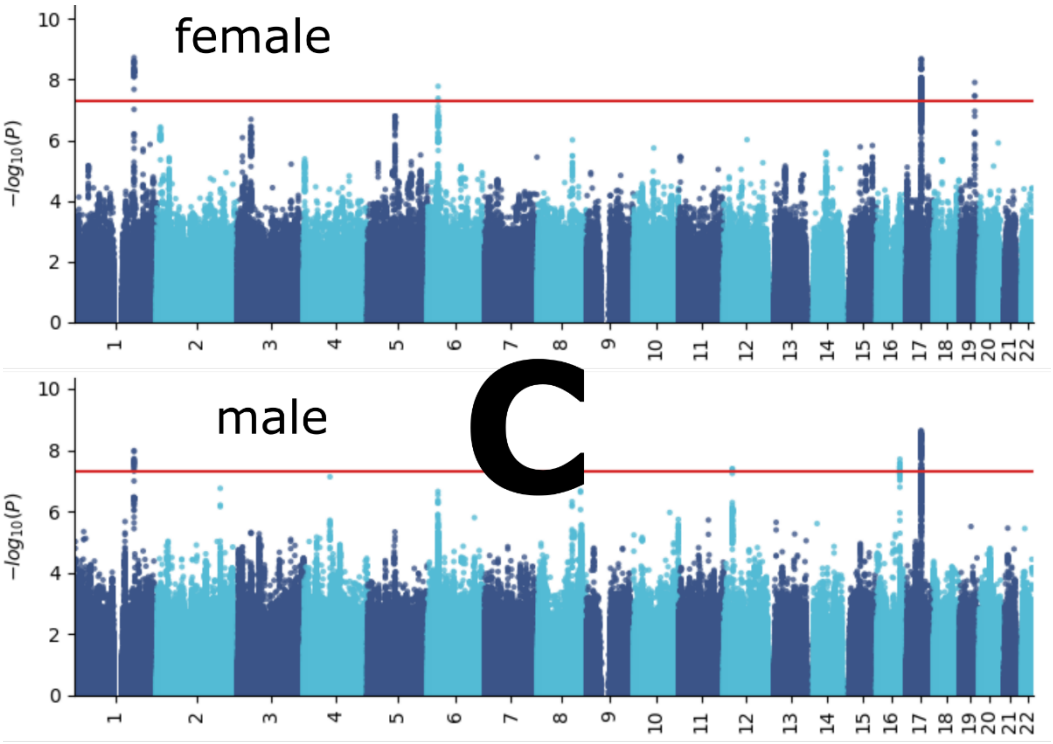
female
male
C
$-log_{10}(P)$
1
2
3
4
5
6
7
8
9
10
11
12
13
14
15
16
17
18
19
20
21
22

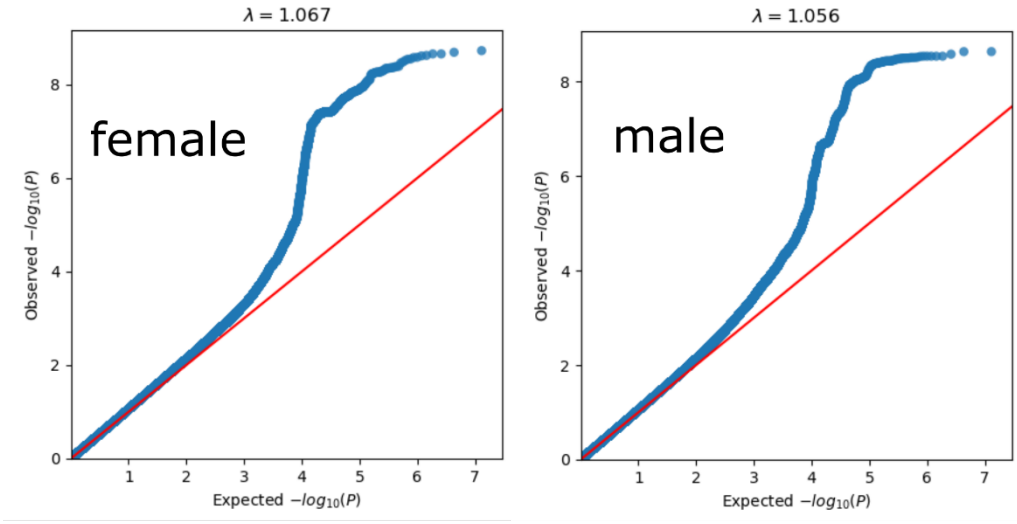
$\lambda = 1.067$
female
$\lambda = 1.056$
male
Observed $-log_{10}(P)$
Expected $-log_{10}(P)$

287

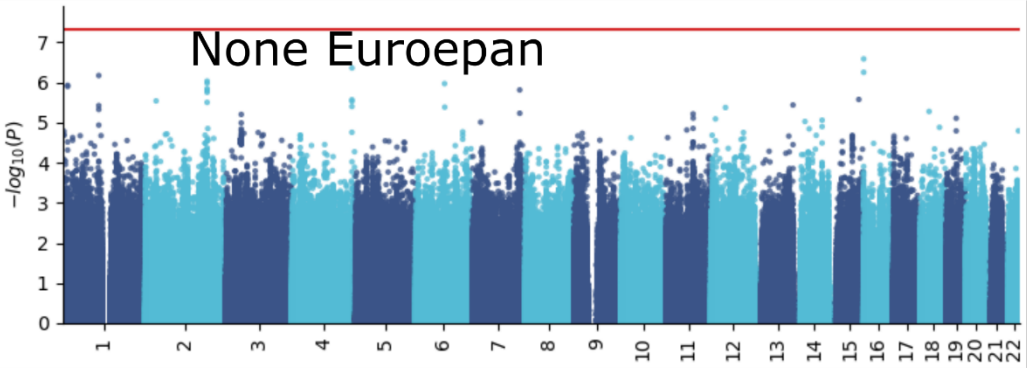

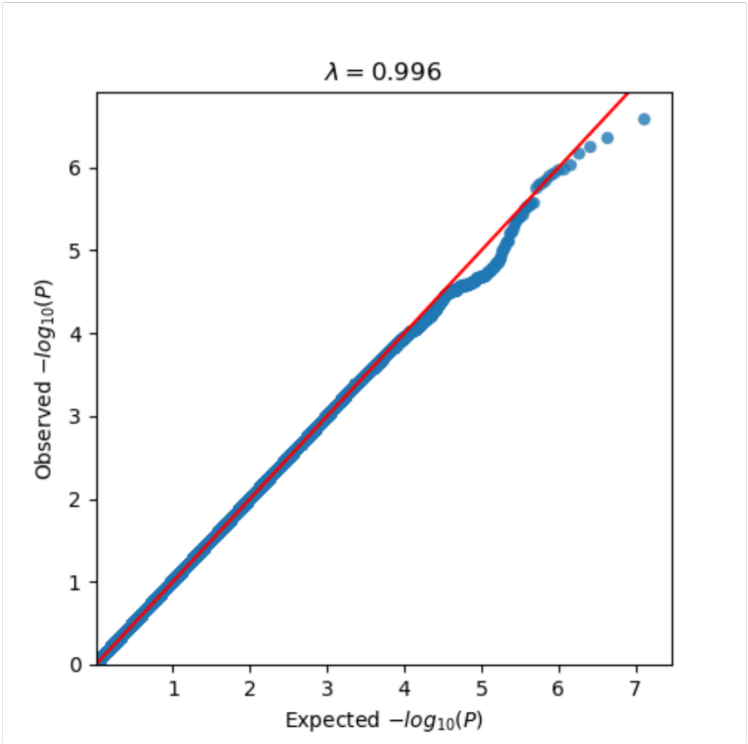

D

Manhattan and QQ plots, along with genomic inflation factors and LDSC intercepts, are displayed for the primary GWAS conducted on individuals of European ancestry (*N*=30,062) using PLINK and fastGWA (**A**). Additionally, results are presented for split-sample GWAS (split1 and split2, **B**), sex-stratified GWAS (female and male, **C**), and GWAS involving non-European ancestry populations (*N*=4465, **D**).

eFigure 2: GWAS Manhattan plots for the cardiovascular BAG

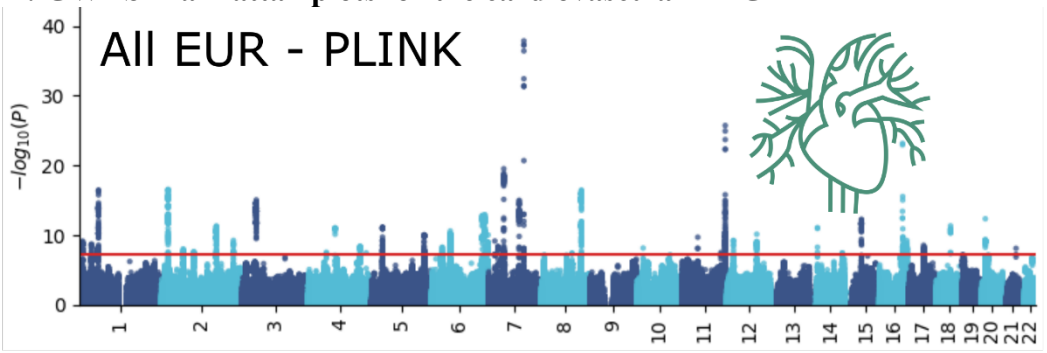

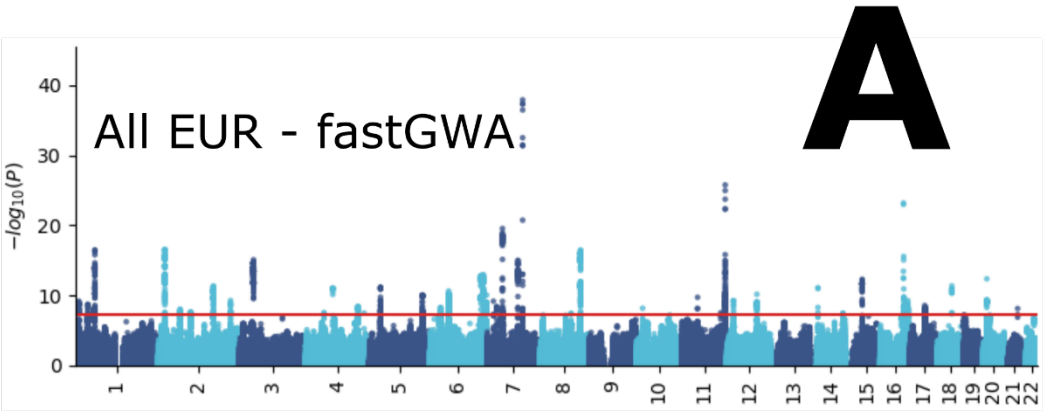

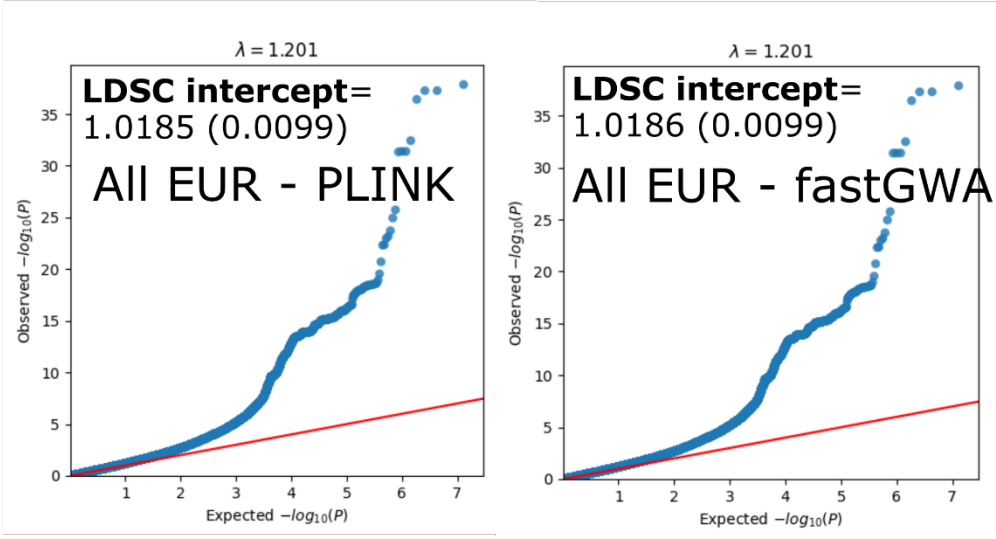

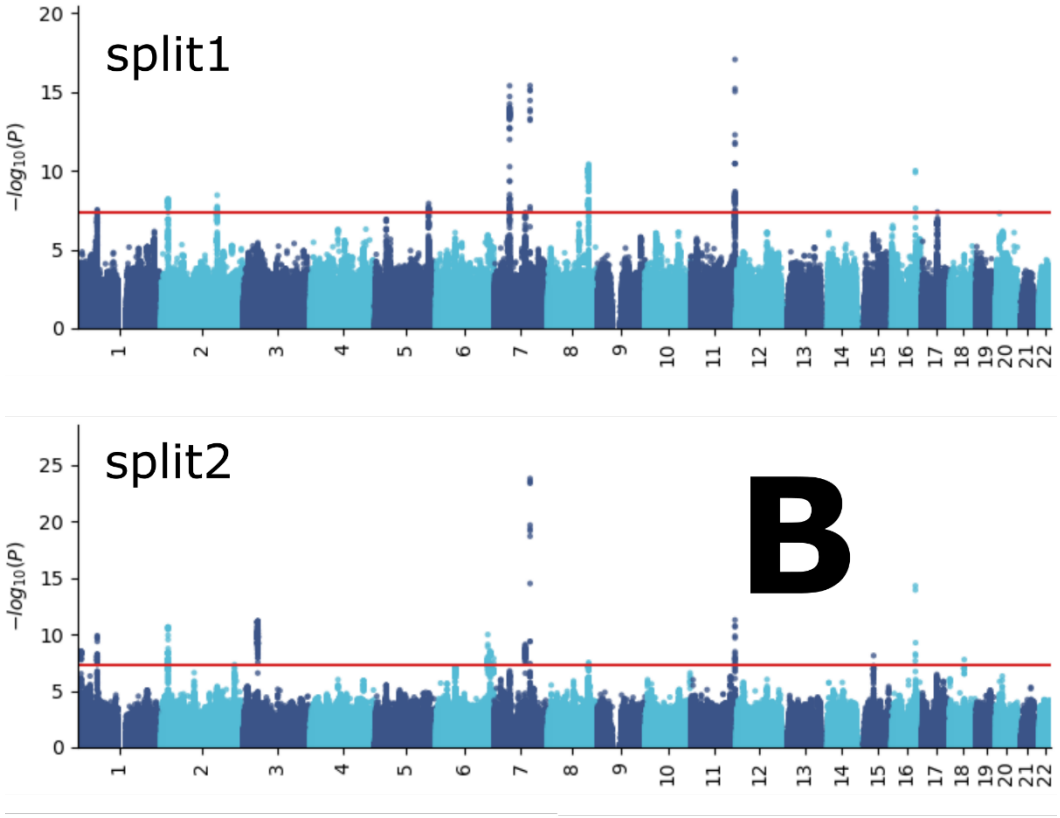
split1
split2
B
$-log_{10}(P)$
1
2
3
4
5
6
7
8
9
10
11
12
13
14
15
16
17
18
19
20
21
22

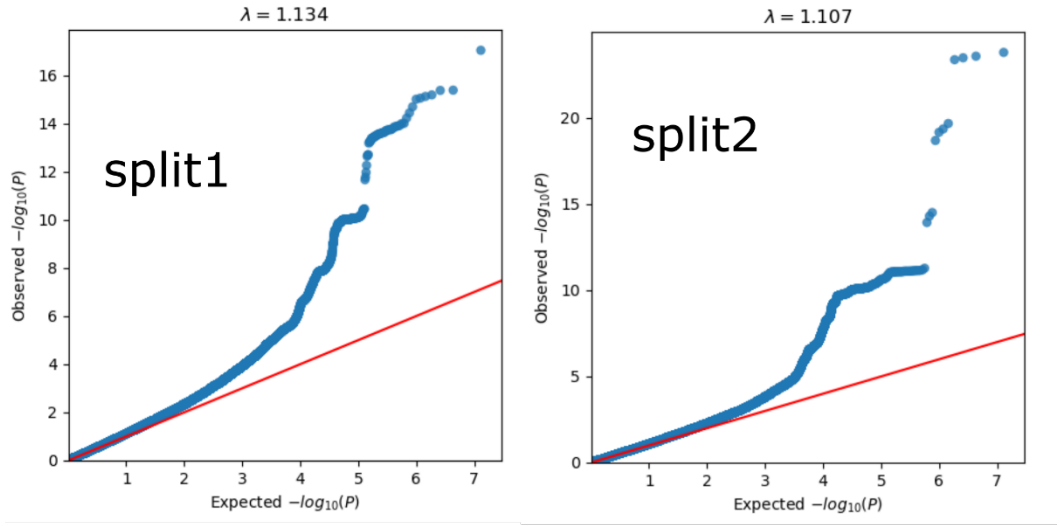
$\lambda = 1.134$
split1
$\lambda = 1.107$
split2
Observed $-log_{10}(P)$
Expected $-log_{10}(P)$

296

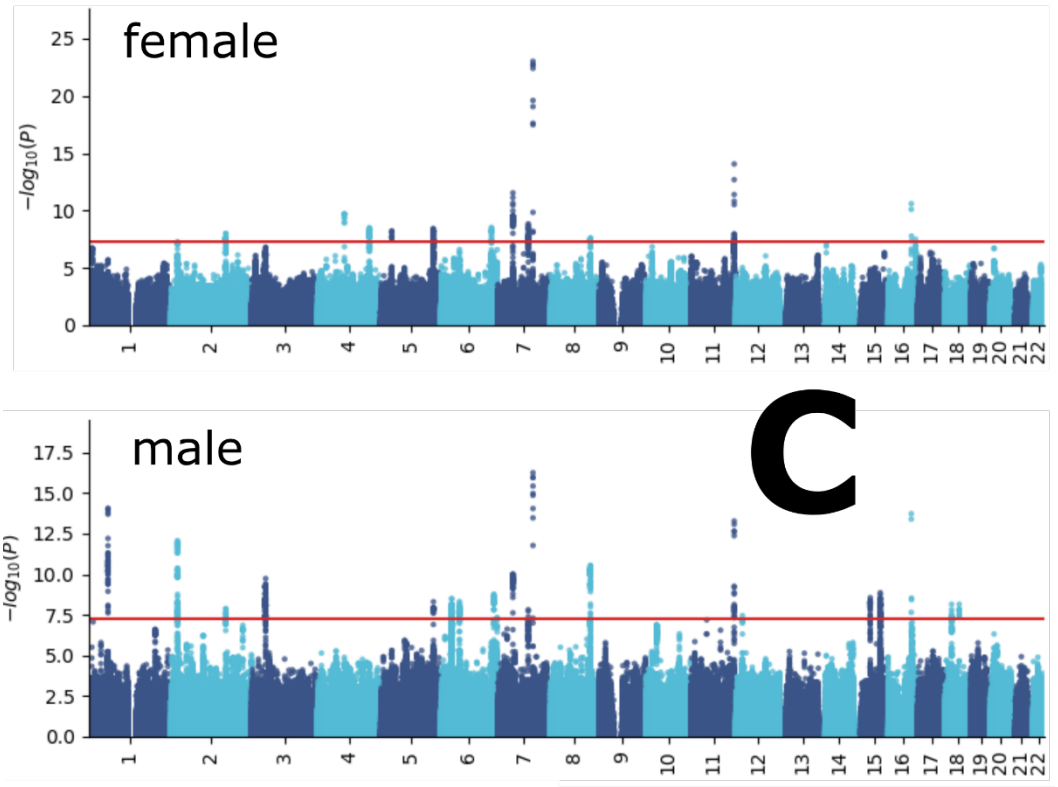
female
male
C
$-log_{10}(P)$
1 2 3 4 5 6 7 8 9 10 11 12 13 14 15 16 17 18 19 20 21 22

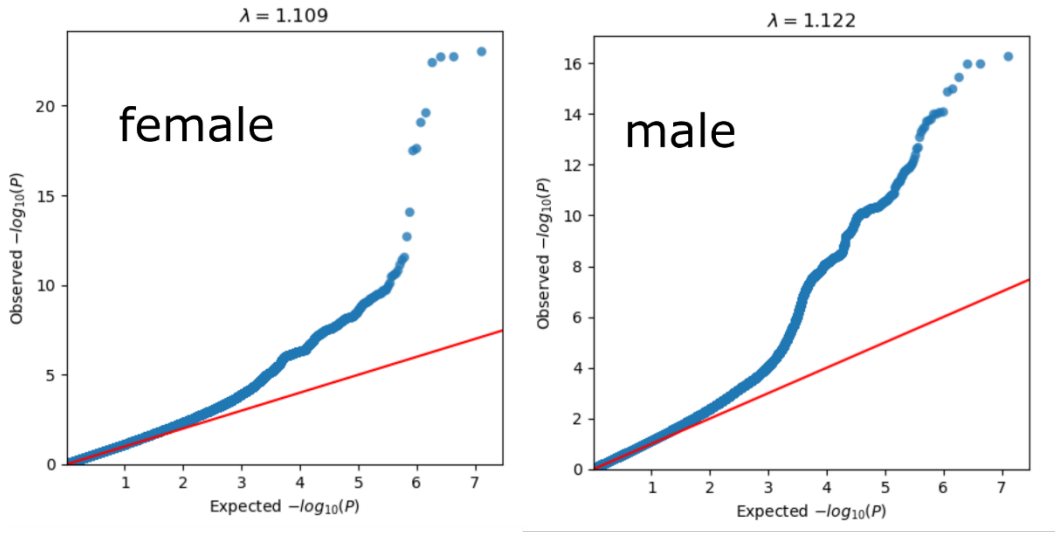
$\lambda = 1.109$
female
$\lambda = 1.122$
male
Observed $-log_{10}(P)$
Expected $-log_{10}(P)$

297

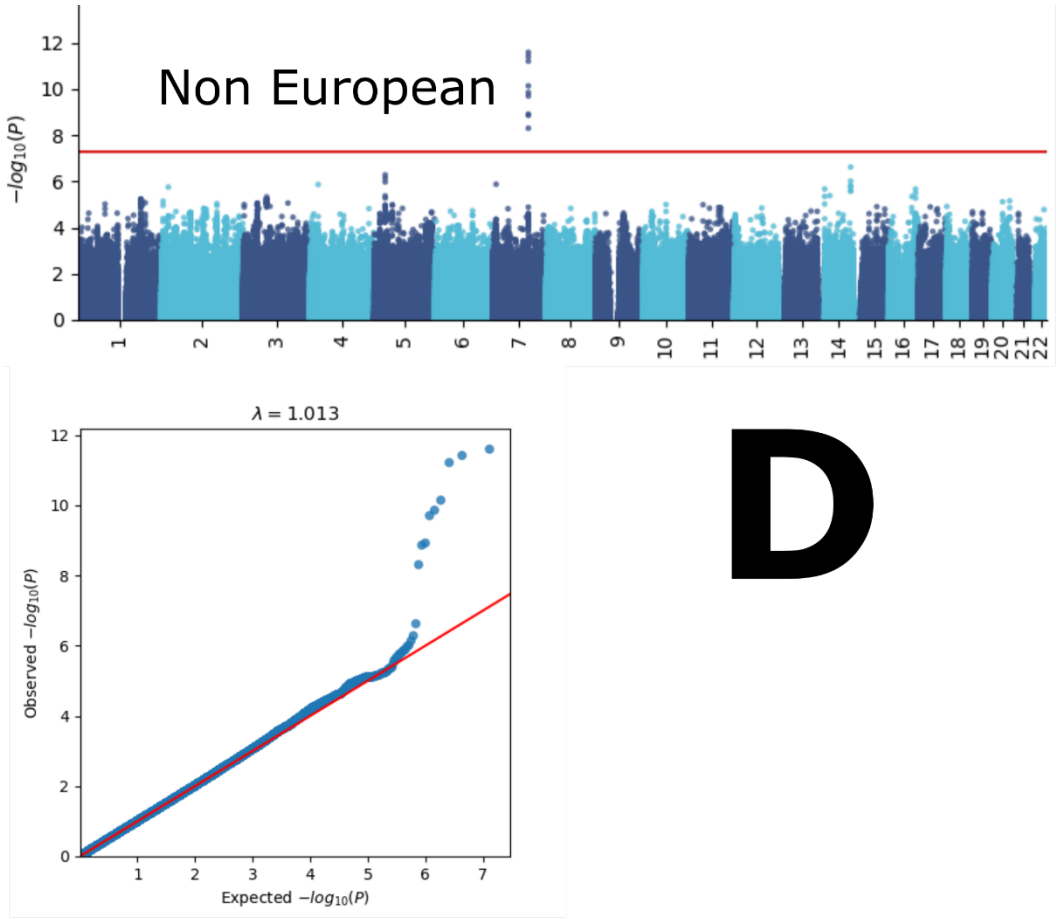

Manhattan and QQ plots, along with genomic inflation factors and LDSC intercepts, are displayed for the primary GWAS conducted on individuals of European ancestry (*N*=111,386) using PLINK and fastGWA (**A**). Additionally, results are presented for split-sample GWAS (split1 and split2, **B**), sex-stratified GWAS (female and male, **C**), and GWAS involving non-European ancestry populations (*N*=20,408, **D**).

eFigure 3: GWAS Manhattan plots for the eye BAG

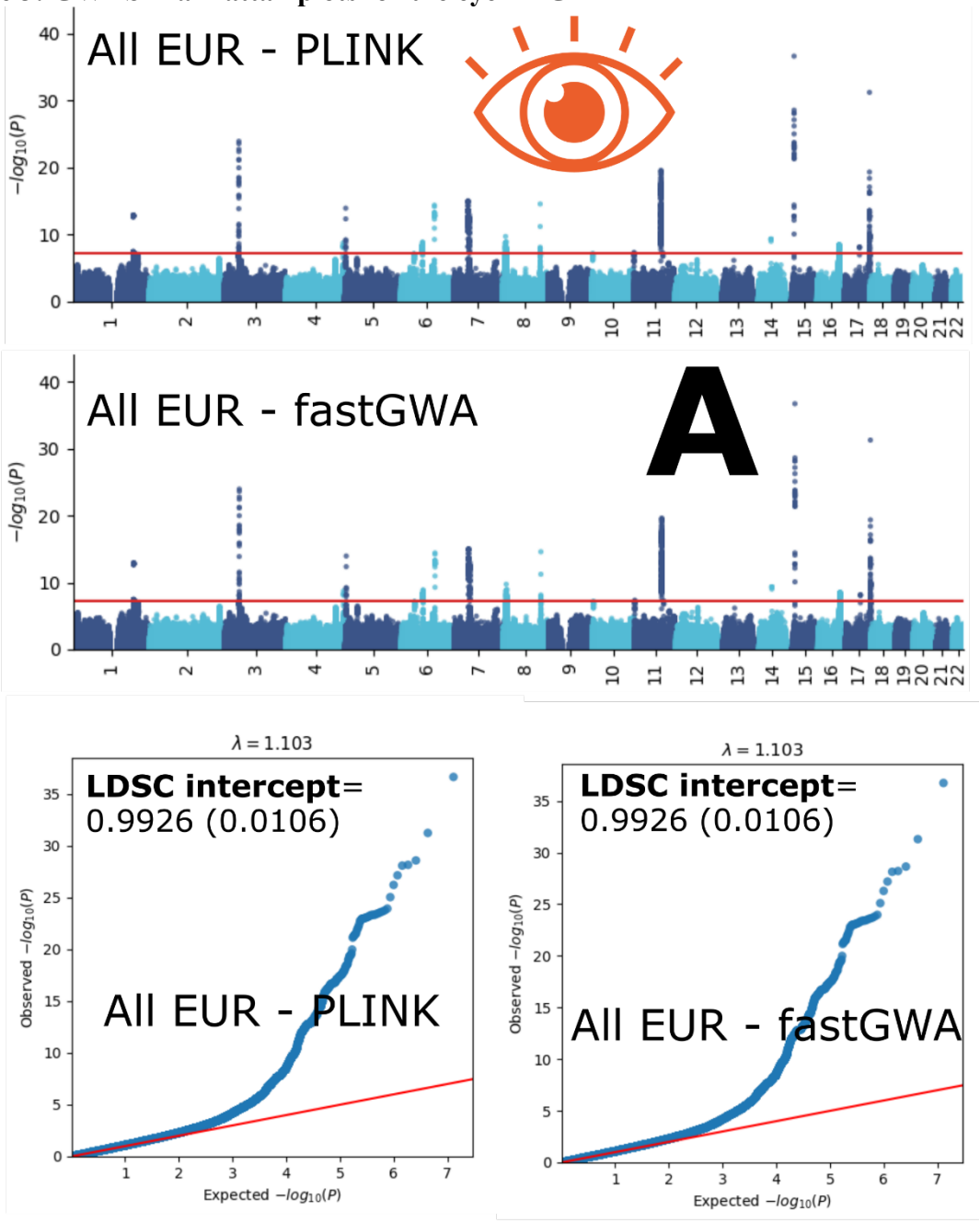

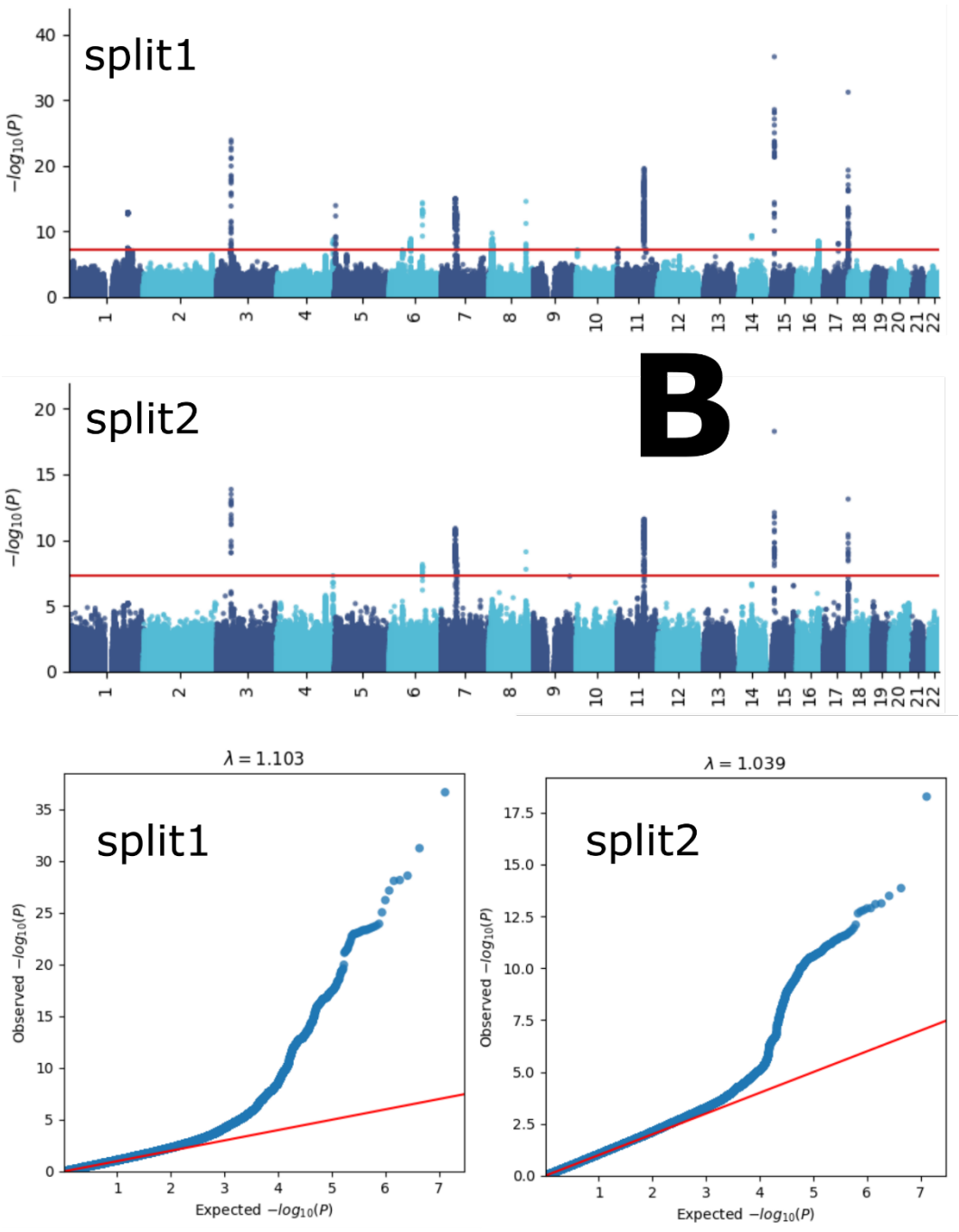
split1
split2
B
$-log_{10}(P)$
λ = 1.103
λ = 1.039
Observed $-log_{10}(P)$
Expected $-log_{10}(P)$

306

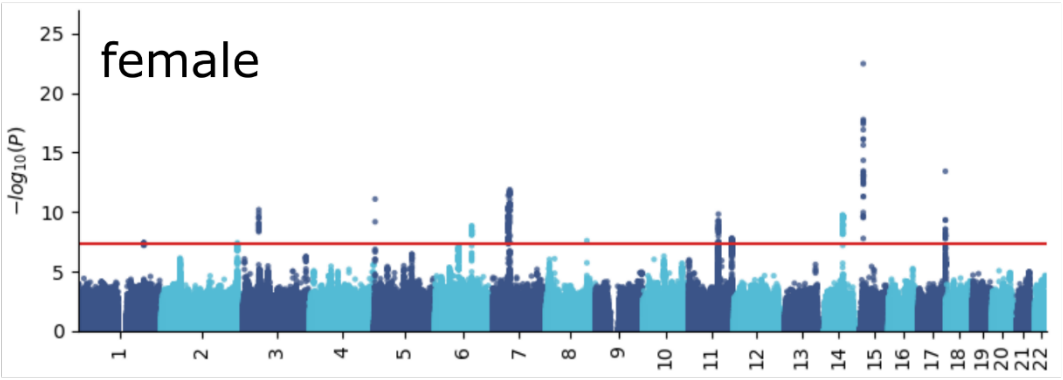
female
$-log_{10}(P)$
25
20
15
10
5
0
1
2
3
4
5
6
7
8
9
10
11
12
13
14
15
16
17
18
19
20
21
22

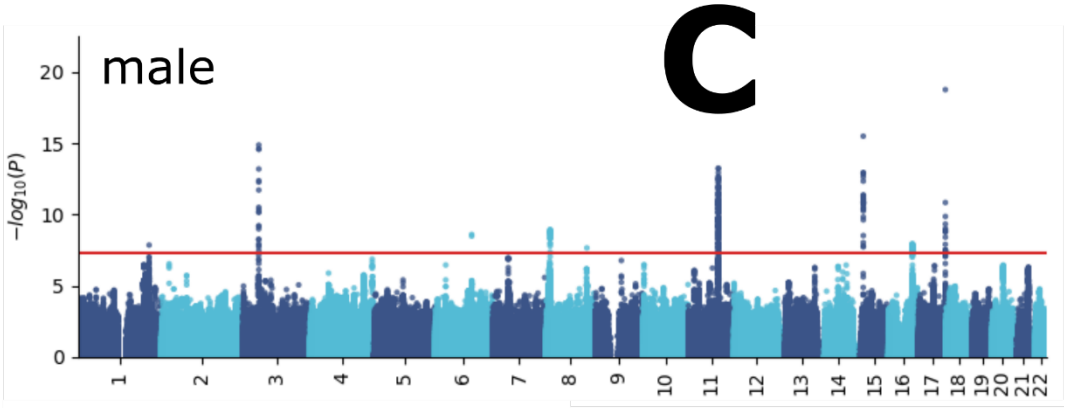
male
C
$-log_{10}(P)$
20
15
10
5
0
1
2
3
4
5
6
7
8
9
10
11
12
13
14
15
16
17
18
19
20
21
22

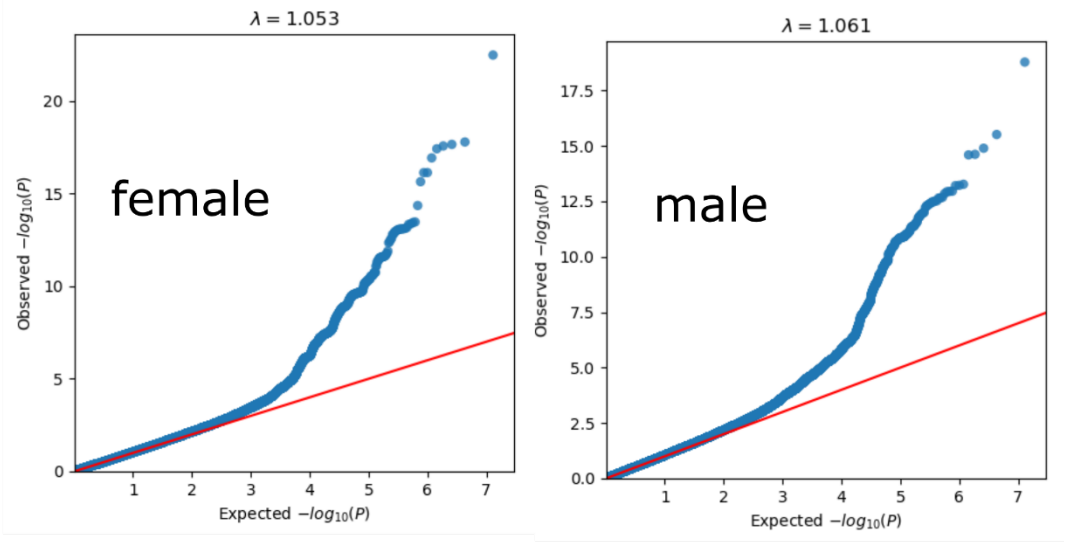
$\lambda = 1.053$
female
Observed $-log_{10}(P)$
Expected $-log_{10}(P)$
$\lambda = 1.061$
male
Observed $-log_{10}(P)$
Expected $-log_{10}(P)$

307

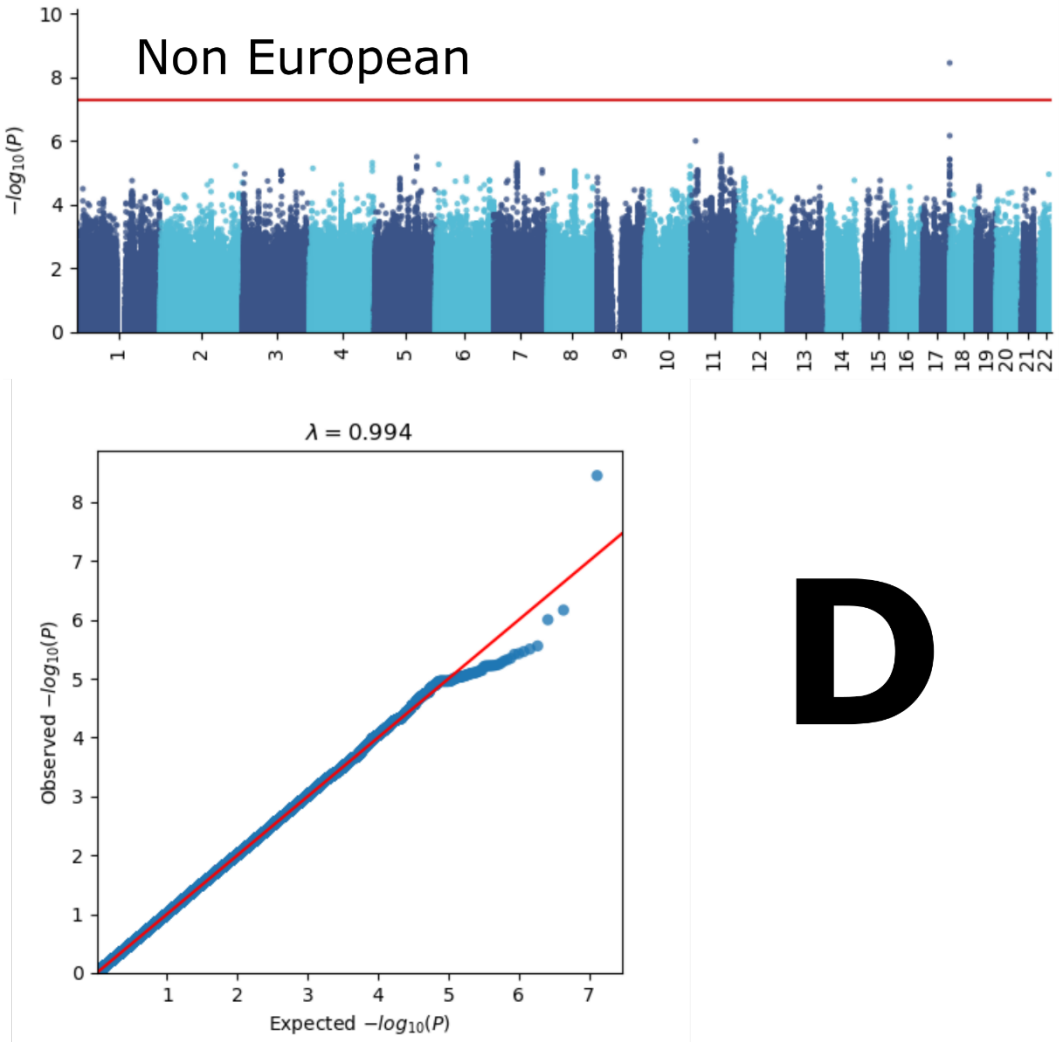

Manhattan and QQ plots, along with genomic inflation factors and LDSC intercepts, are displayed for the primary GWAS conducted on individuals of European ancestry (*N*=36,004) using PLINK and fastGWA (**A**). Additionally, results are presented for split-sample GWAS (split1 and split2, **B**), sex-stratified GWAS (female and male, **C**), and GWAS involving non-European ancestry populations (*N*=3407, **D**).

eFigure 4: GWAS Manhattan plots for the hepatic BAG

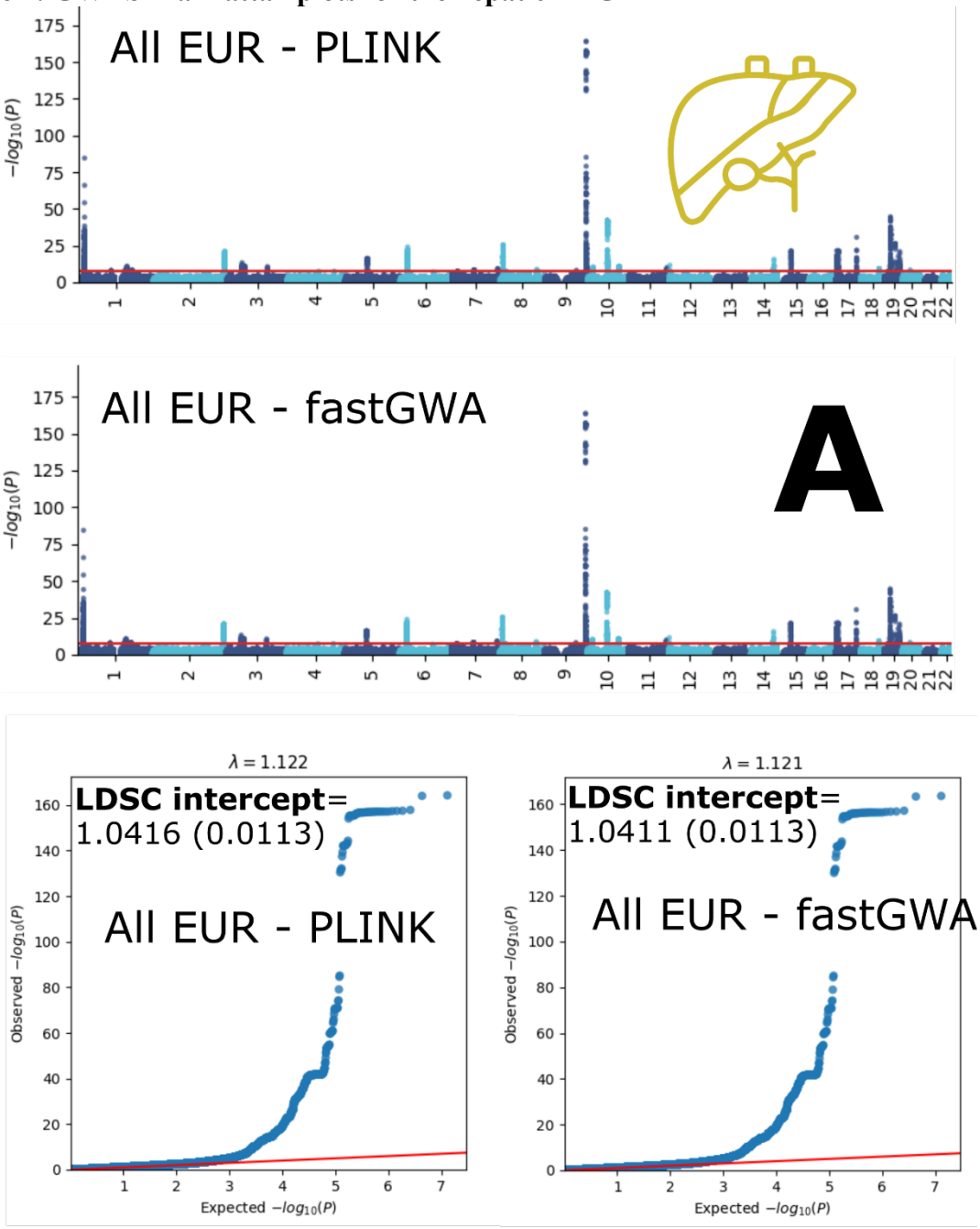

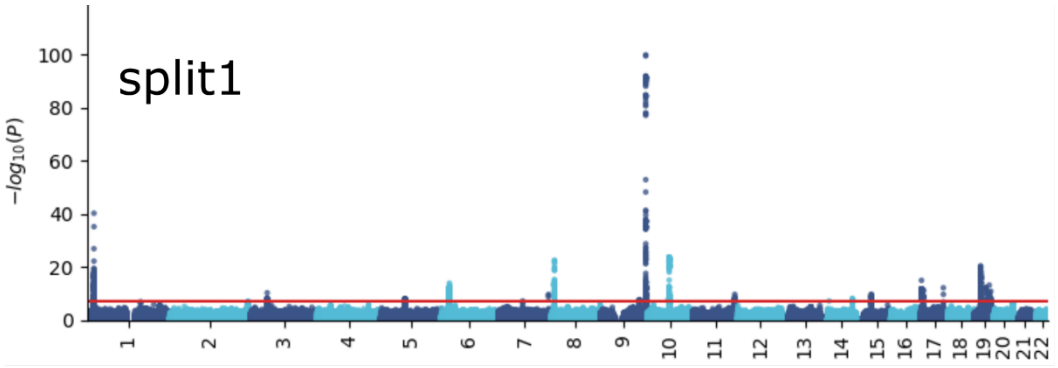
split1
$-log_{10}(P)$
100
80
60
40
20
0
1
2
3
4
5
6
7
8
9
10
11
12
13
14
15
16
17
18
19
20
21
22

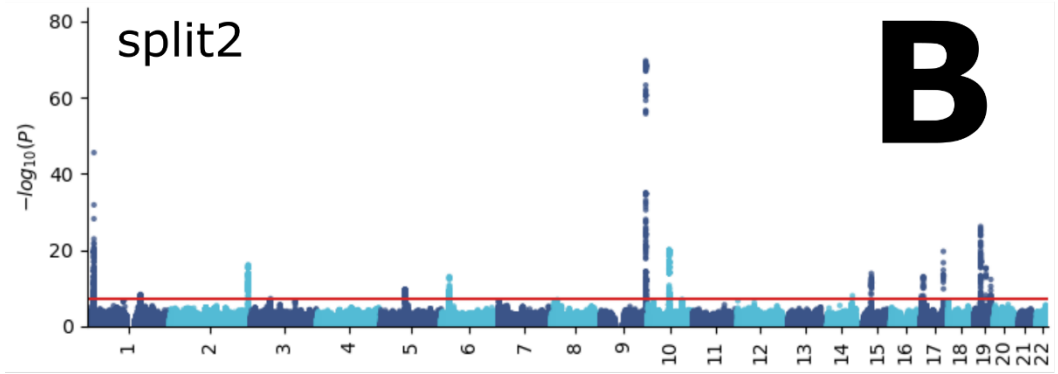
split2
B
$-log_{10}(P)$
80
60
40
20
0
1
2
3
4
5
6
7
8
9
10
11
12
13
14
15
16
17
18
19
20
21
22

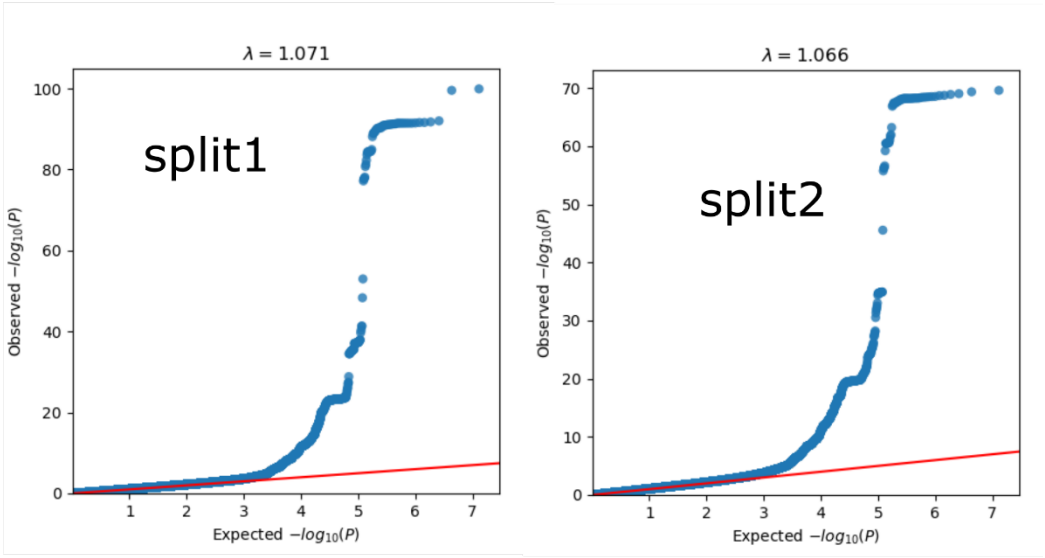
$\lambda = 1.071$
split1
Observed $-log_{10}(P)$
Expected $-log_{10}(P)$
$\lambda = 1.066$
split2
Observed $-log_{10}(P)$
Expected $-log_{10}(P)$

316

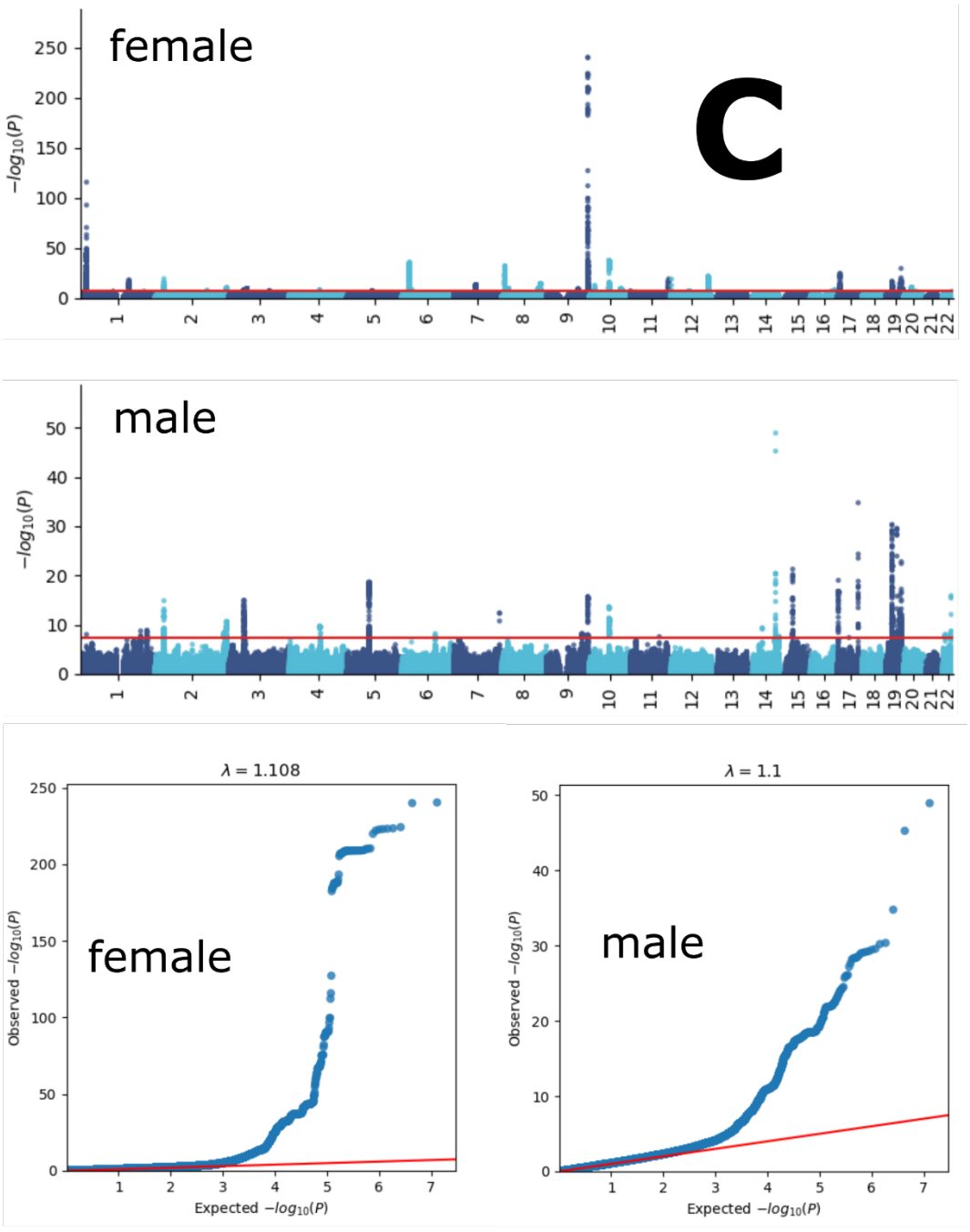
female
C
male
λ = 1.108
female
λ = 1.1
male
Observed −log10(P)
Expected −log10(P)

317

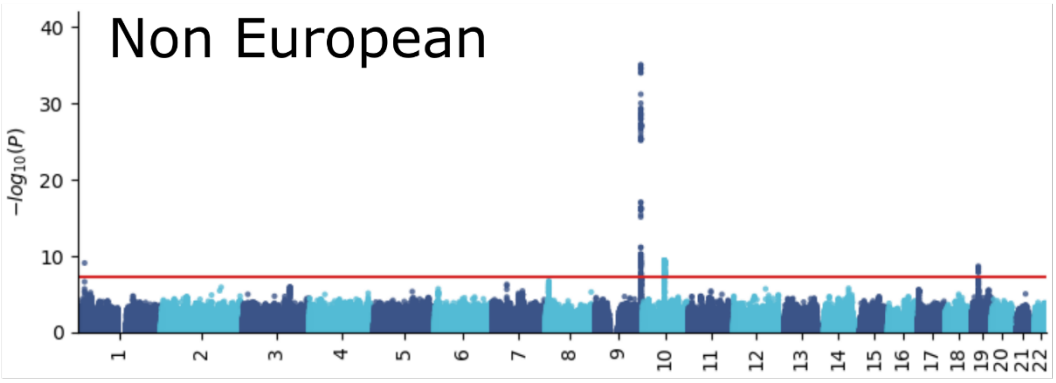

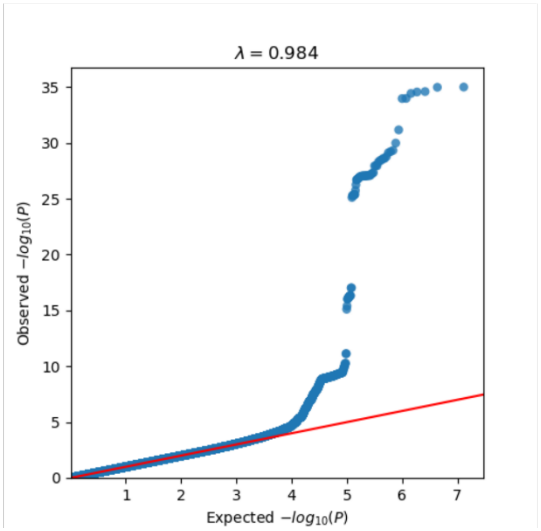

D

Manhattan and QQ plots, along with genomic inflation factors and LDSC intercepts, are displayed for the primary GWAS conducted on individuals of European ancestry (*N*=111,386) using PLINK and fastGWA (**A**). Additionally, results are presented for split-sample GWAS (split1 and split2, **B**), sex-stratified GWAS (female and male, **C**), and GWAS involving non-European ancestry populations (*N*=20,408, **D**).

eFigure 5: GWAS Manhattan plots for the immune BAG

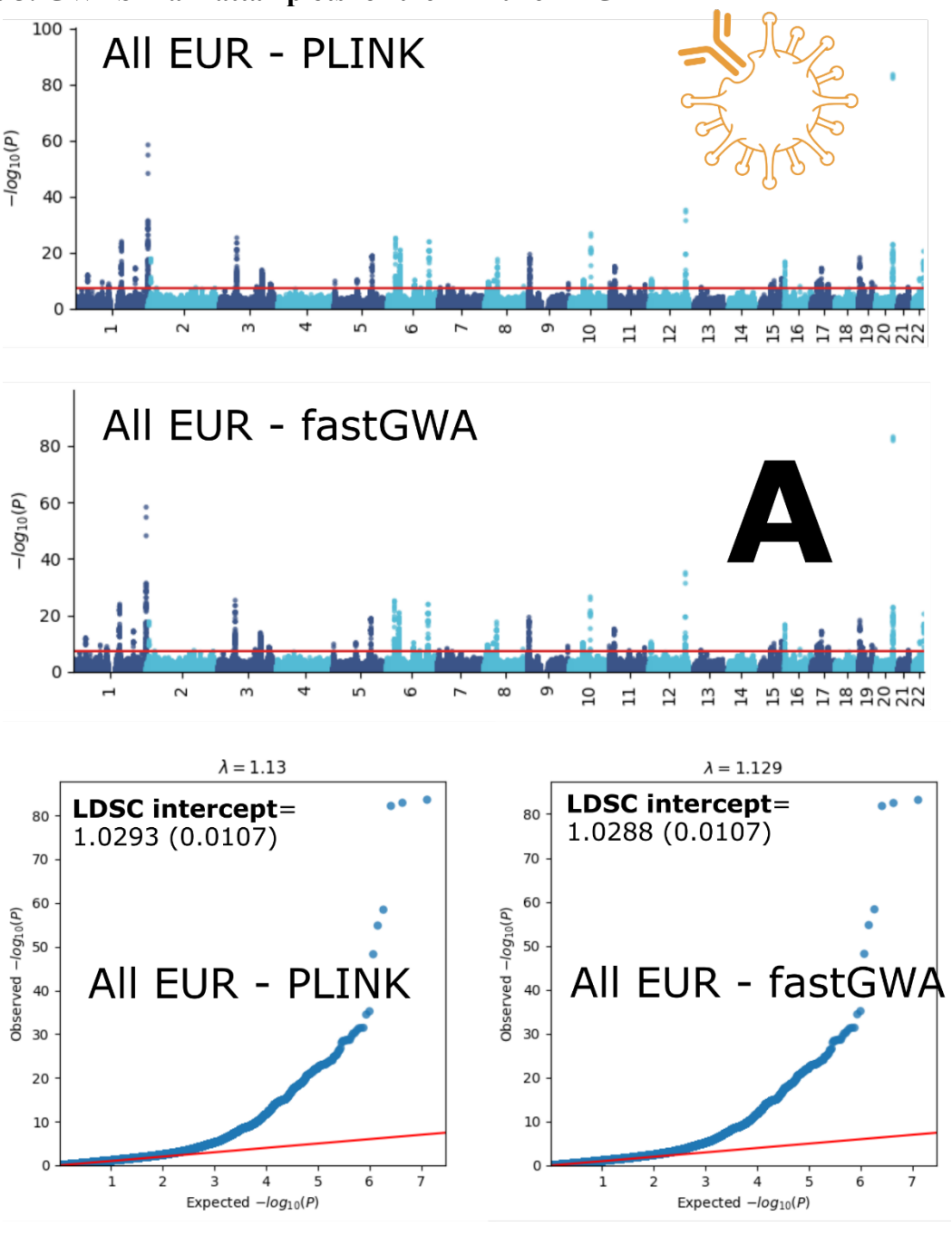

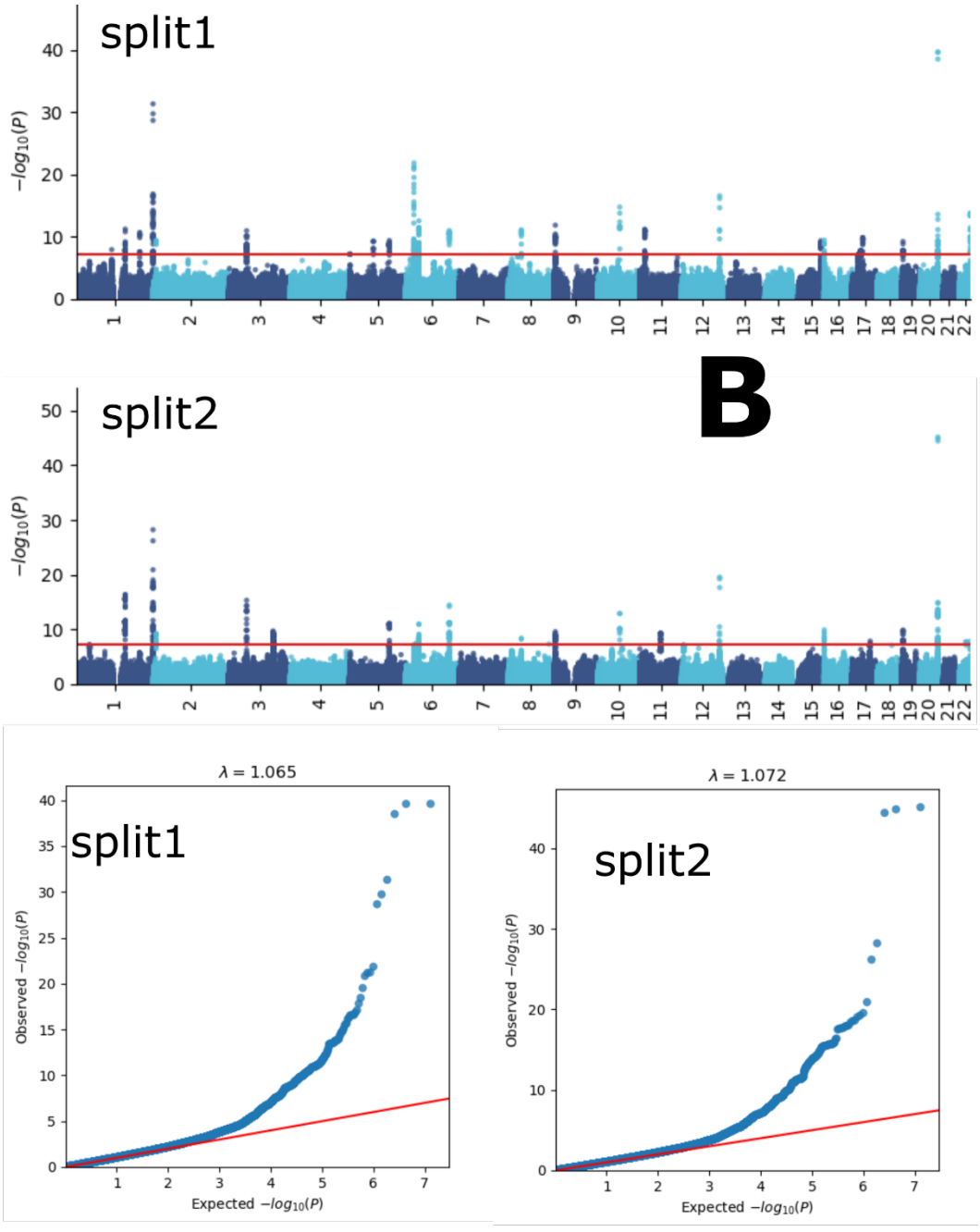
split1
split2
B
$-log_{10}(P)$
λ = 1.065
λ = 1.072
Observed $-log_{10}(P)$
Expected $-log_{10}(P)$

326

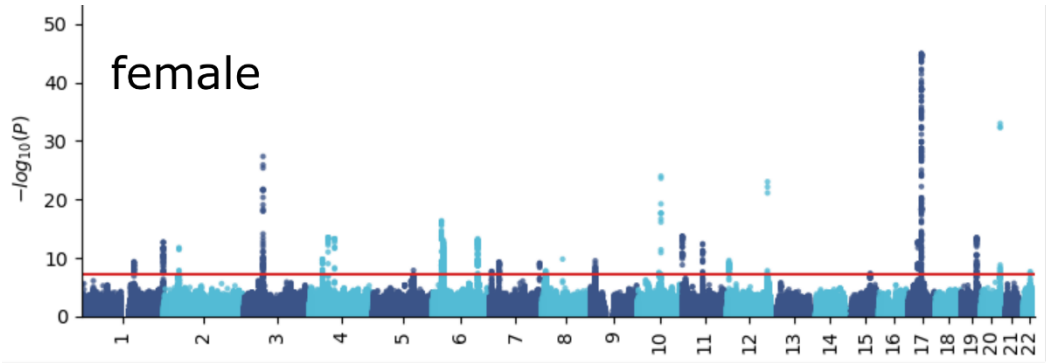
female
$-log_{10}(P)$
50
40
30
20
10
0
1
2
3
4
5
6
7
8
9
10
11
12
13
14
15
16
17
18
19
20
21
22

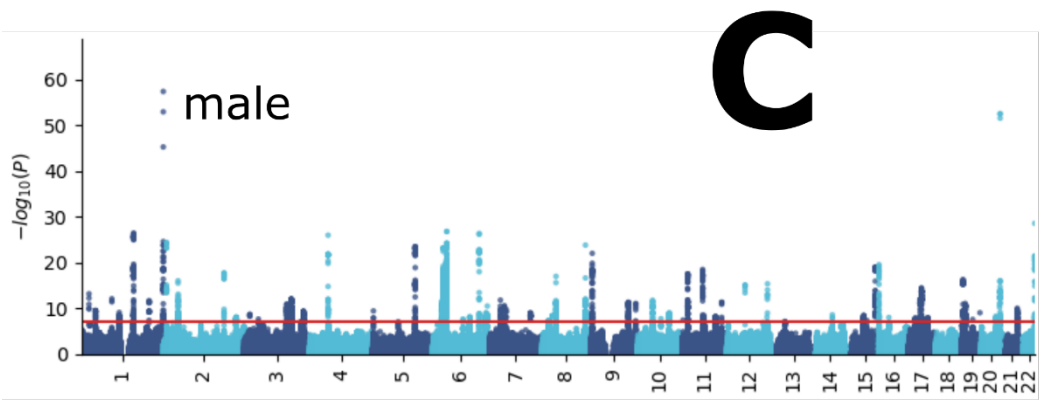
male
C
$-log_{10}(P)$
60
50
40
30
20
10
0
1
2
3
4
5
6
7
8
9
10
11
12
13
14
15
16
17
18
19
20
21
22

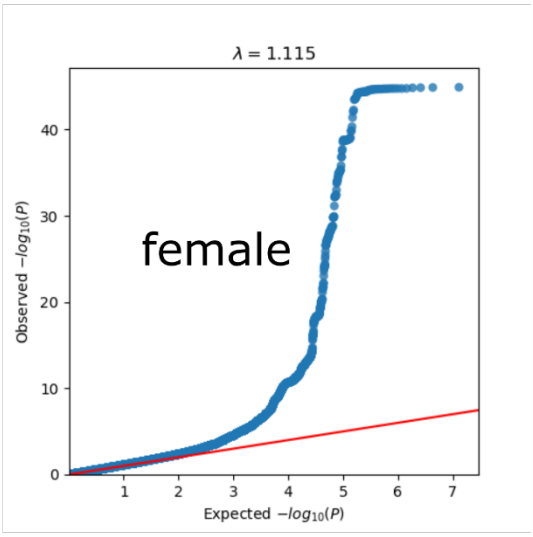
$\lambda = 1.115$
female
Observed $-log_{10}(P)$
Expected $-log_{10}(P)$
0
10
20
30
40
1
2
3
4
5
6
7

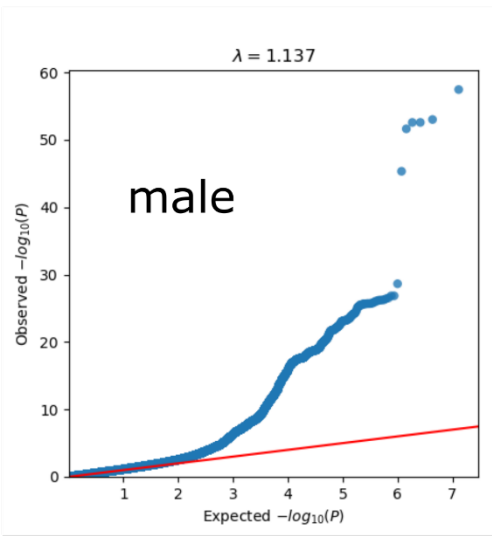
$\lambda = 1.137$
male
Observed $-log_{10}(P)$
Expected $-log_{10}(P)$
0
10
20
30
40
50
60
1
2
3
4
5
6
7

327

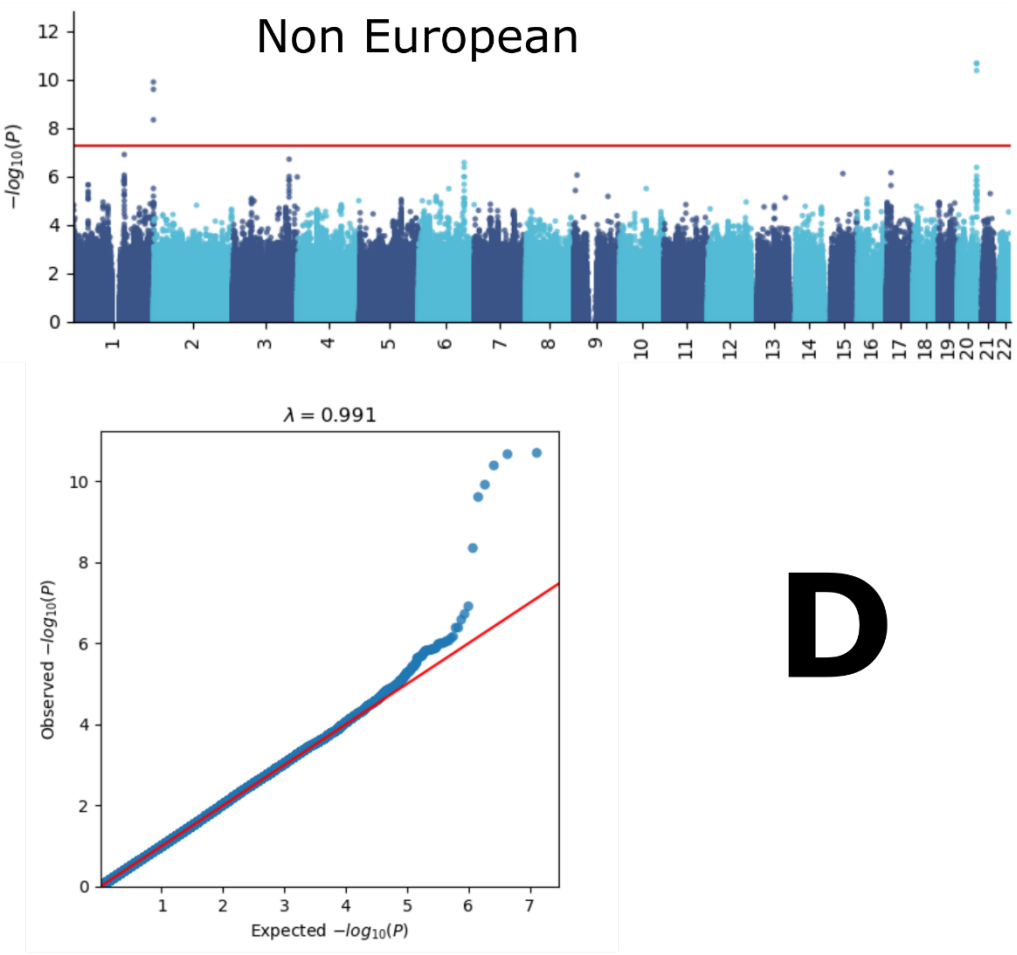

Manhattan and QQ plots, along with genomic inflation factors and LDSC intercepts, are displayed for the primary GWAS conducted on individuals of European ancestry (*N*=111,386) using PLINK and fastGWA (**A**). Additionally, results are presented for split-sample GWAS (split1 and split2, **B**), sex-stratified GWAS (female and male, **C**), and GWAS involving non-European ancestry populations (*N*=20,408, **D**).

eFigure 6: GWAS Manhattan plots for the metabolic BAG

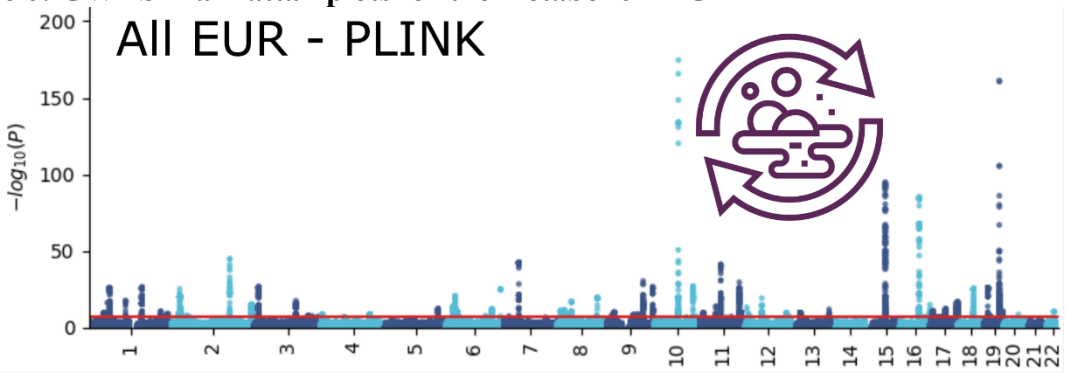

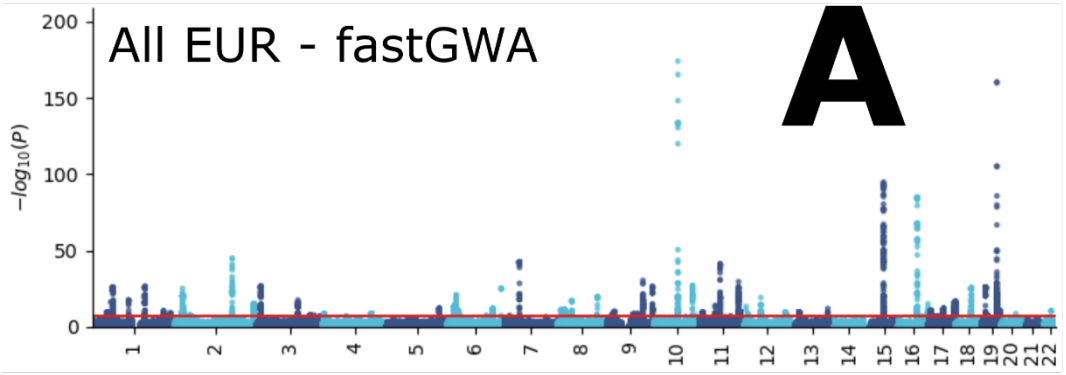

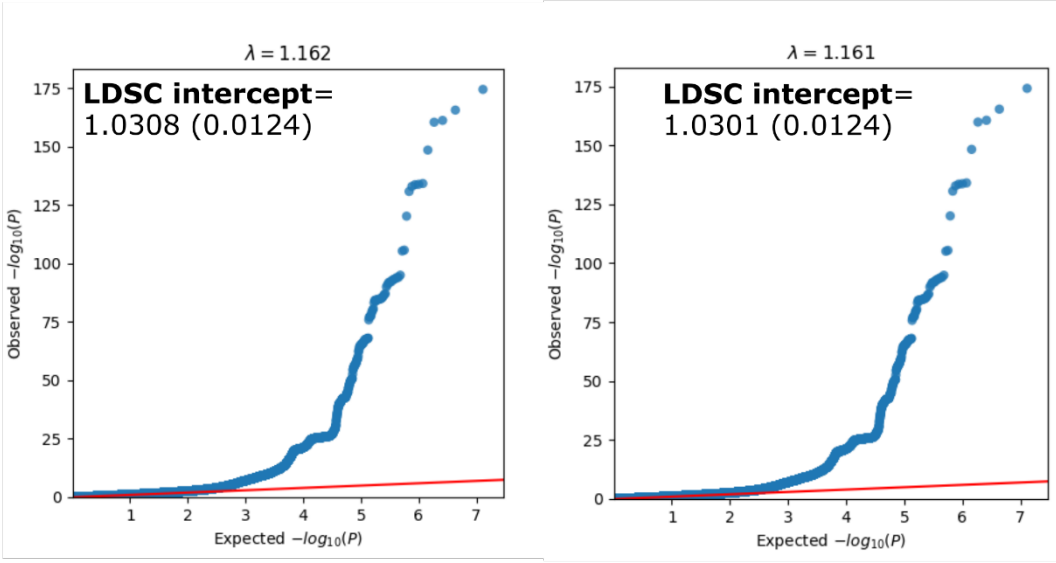

All EUR - PLINK

All EUR - fastGWA

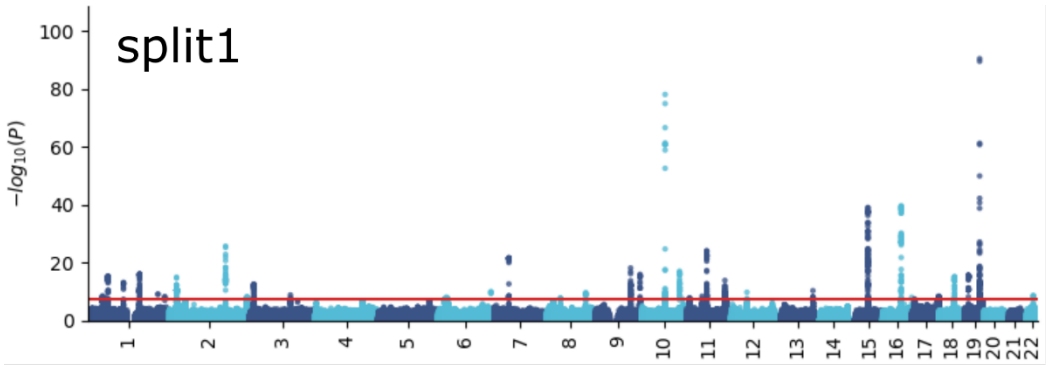
split1
$-log_{10}(P)$
100
80
60
40
20
0
1 2 3 4 5 6 7 8 9 10 11 12 13 14 15 16 17 18 19 20 21 22

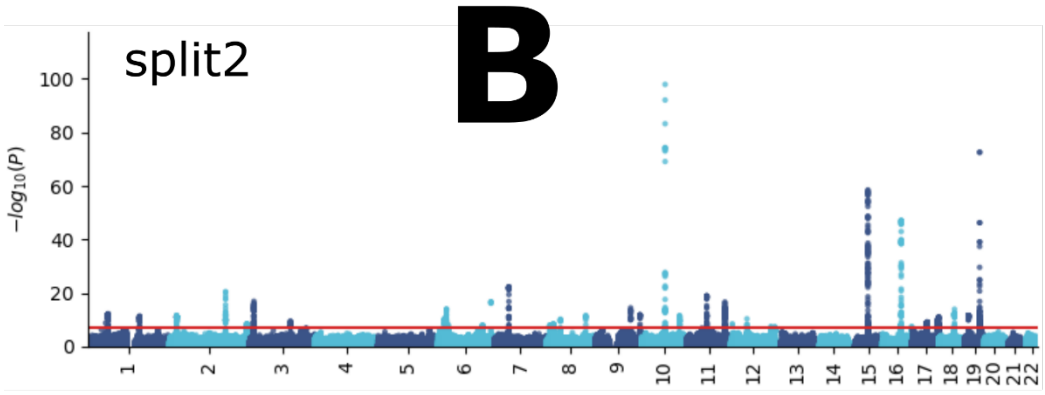
split2
B
$-log_{10}(P)$
100
80
60
40
20
0
1 2 3 4 5 6 7 8 9 10 11 12 13 14 15 16 17 18 19 20 21 22

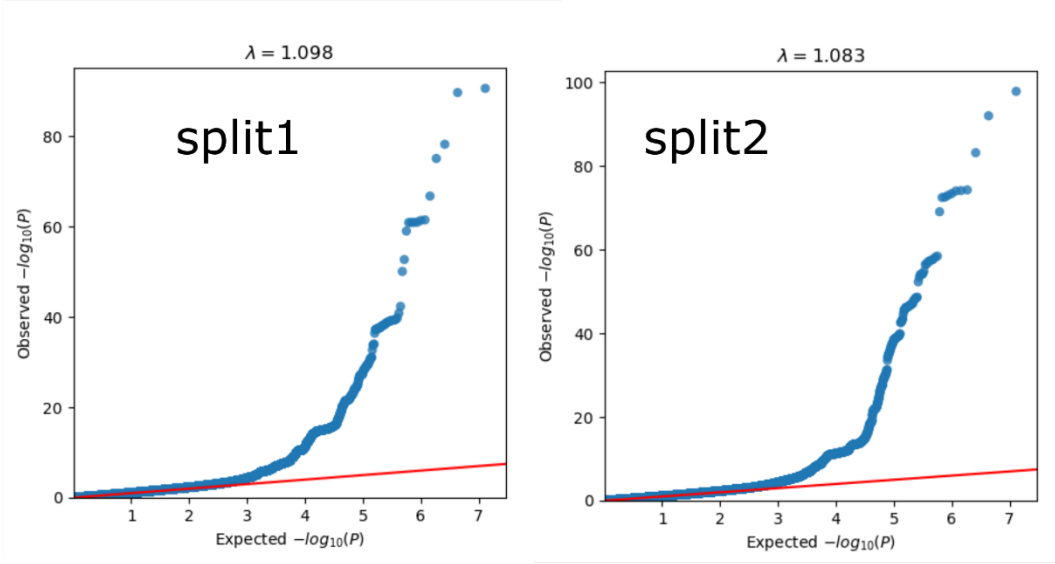
$\lambda = 1.098$
split1
Observed $-log_{10}(P)$
Expected $-log_{10}(P)$
$\lambda = 1.083$
split2
Observed $-log_{10}(P)$
Expected $-log_{10}(P)$

336

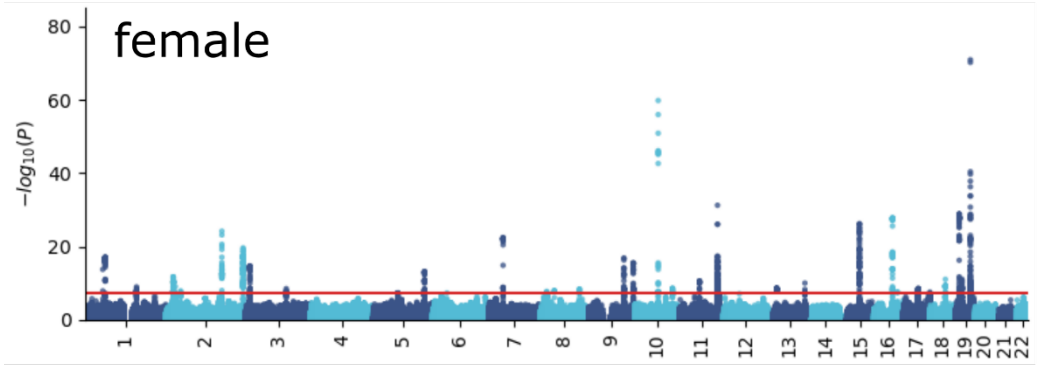
female
$-log_{10}(P)$
0
20
40
60
80
1
2
3
4
5
6
7
8
9
10
11
12
13
14
15
16
17
18
19
20
21
22

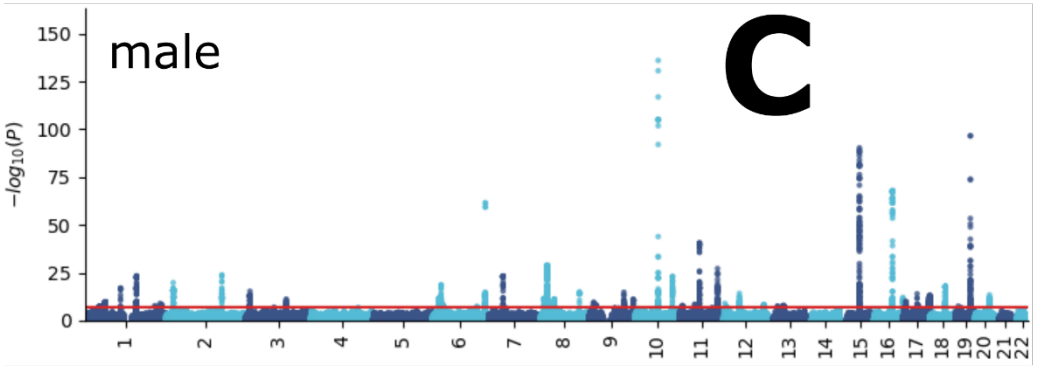
male
C
$-log_{10}(P)$
0
25
50
75
100
125
150
1
2
3
4
5
6
7
8
9
10
11
12
13
14
15
16
17
18
19
20
21
22

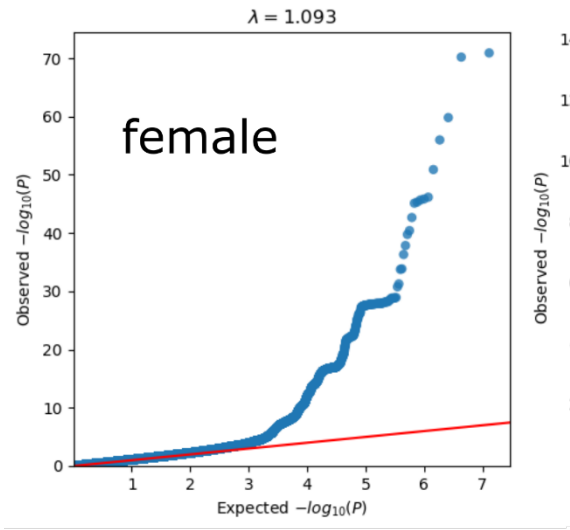
$\lambda = 1.093$
female
Observed $-log_{10}(P)$
Expected $-log_{10}(P)$
0
10
20
30
40
50
60
70
1
2
3
4
5
6
7

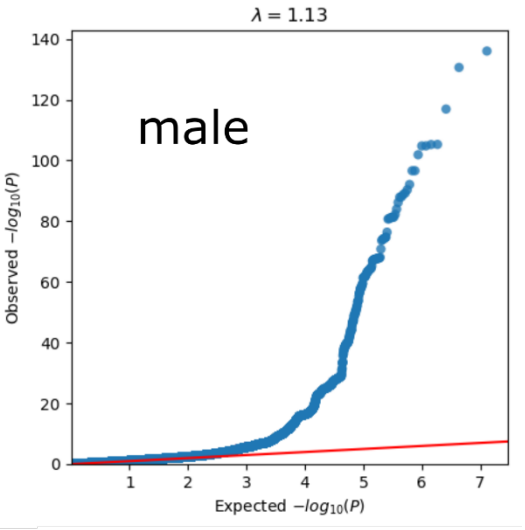
$\lambda = 1.13$
male
Observed $-log_{10}(P)$
Expected $-log_{10}(P)$
0
20
40
60
80
100
120
140
1
2
3
4
5
6
7

337

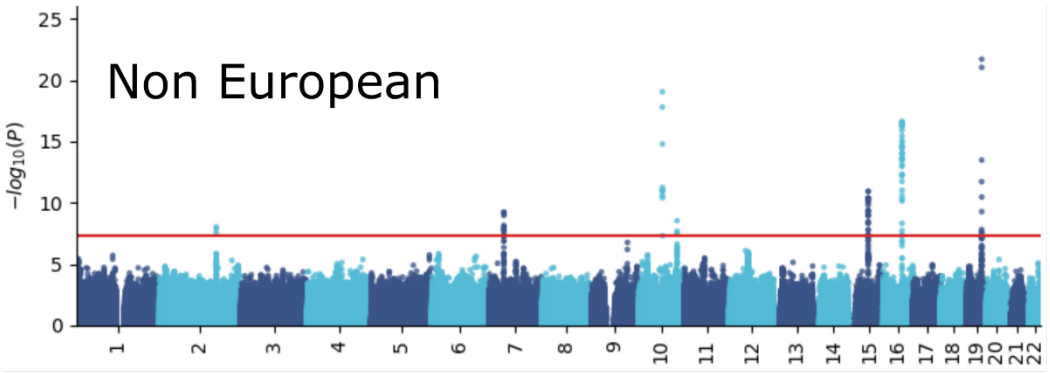

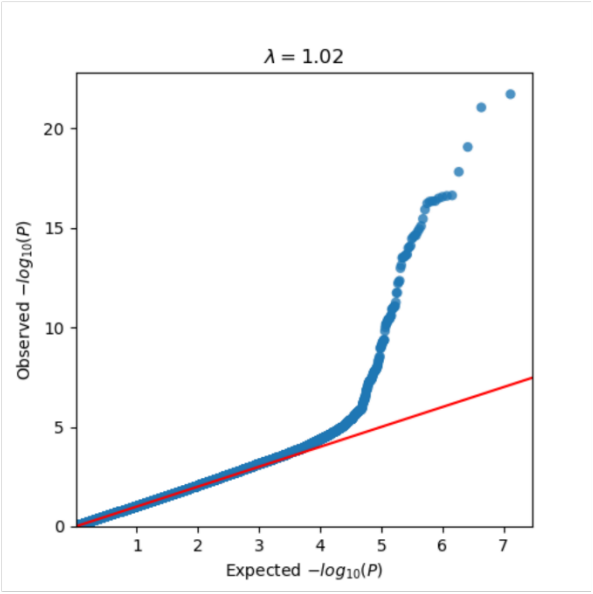

D

Manhattan and QQ plots, along with genomic inflation factors and LDSC intercepts, are displayed for the primary GWAS conducted on individuals of European ancestry (*N*=111,386) using PLINK and fastGWA (**A**). Additionally, results are presented for split-sample GWAS (split1 and split2, **B**), sex-stratified GWAS (female and male, **C**), and GWAS involving non-European ancestry populations (*N*=20,408, **D**).

eFigure 7: GWAS Manhattan plots for the musculoskeletal BAG

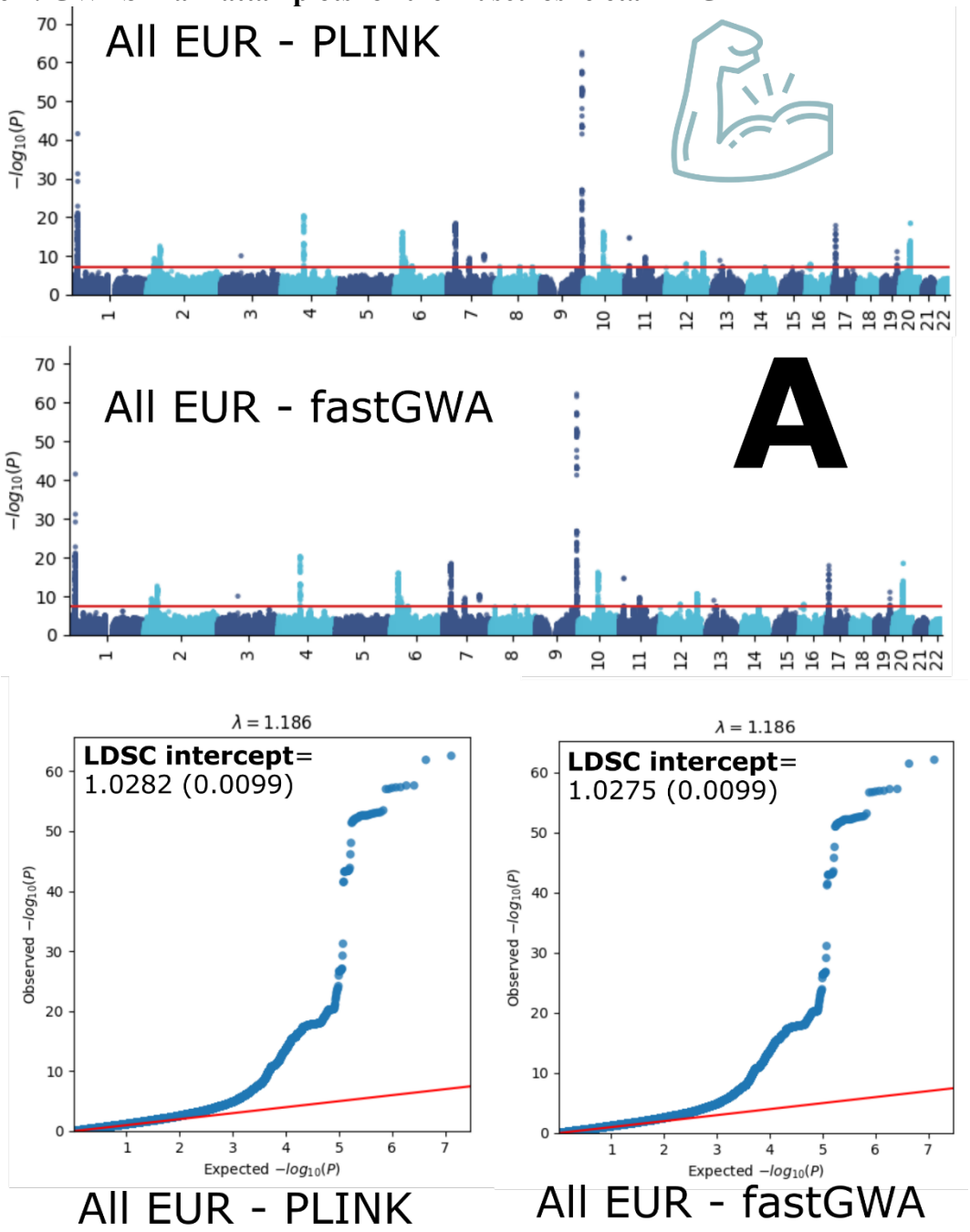

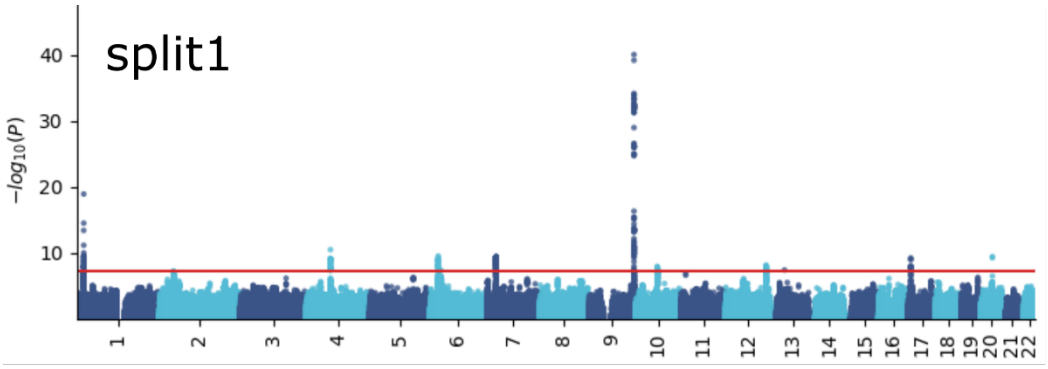
split1
$-log_{10}(P)$
40
30
20
10
1
2
3
4
5
6
7
8
9
10
11
12
13
14
15
16
17
18
19
20
21
22

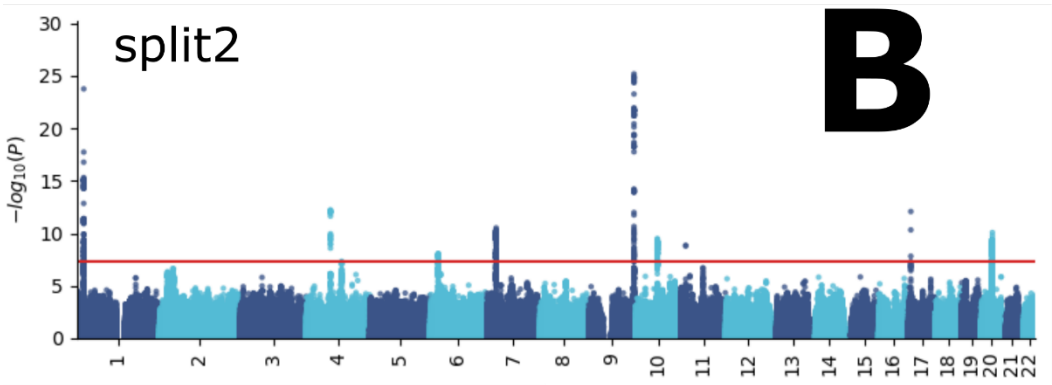
split2
B
$-log_{10}(P)$
30
25
20
15
10
5
0
1
2
3
4
5
6
7
8
9
10
11
12
13
14
15
16
17
18
19
20
21
22

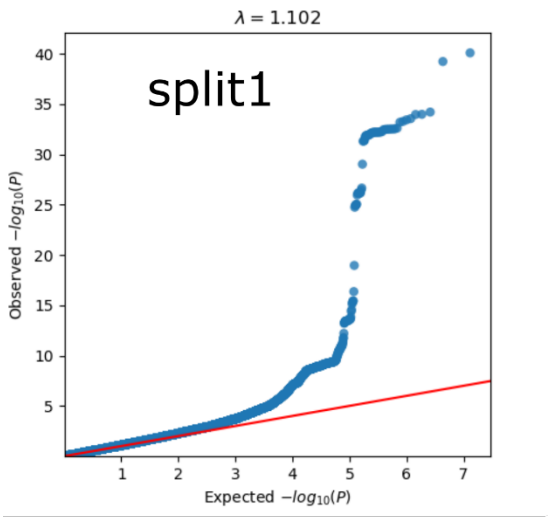
$\lambda = 1.102$
split1
Observed $-log_{10}(P)$
Expected $-log_{10}(P)$
40
35
30
25
20
15
10
5
1
2
3
4
5
6
7

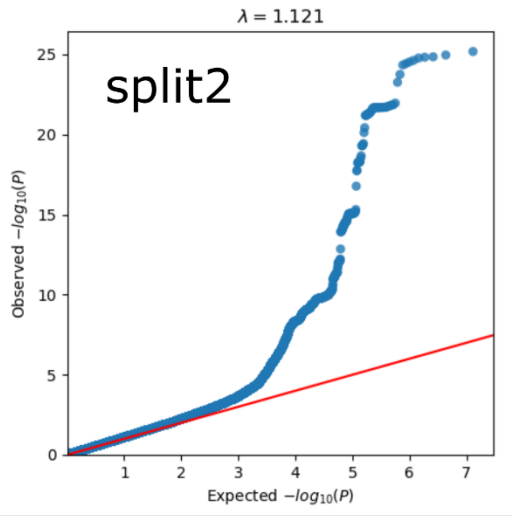
$\lambda = 1.121$
split2
Observed $-log_{10}(P)$
Expected $-log_{10}(P)$
25
20
15
10
5
0
1
2
3
4
5
6
7

346

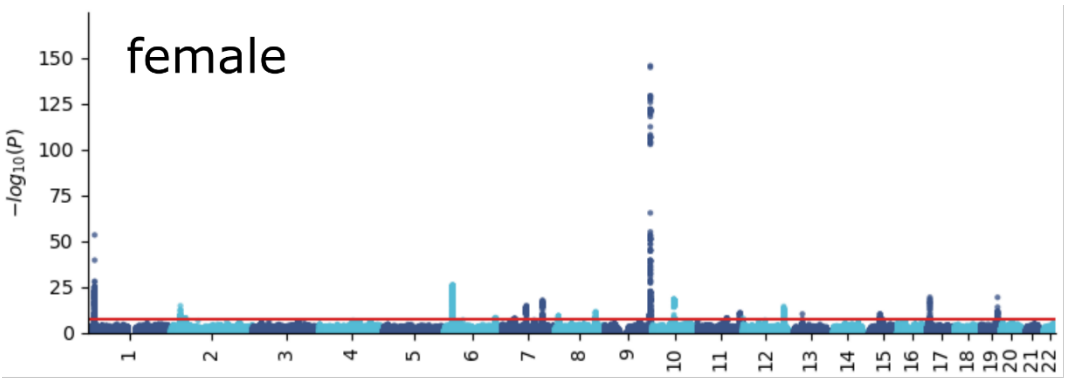
female
$-log_{10}(P)$
150
125
100
75
50
25
0
1
2
3
4
5
6
7
8
9
10
11
12
13
14
15
16
17
18
19
20
21
22

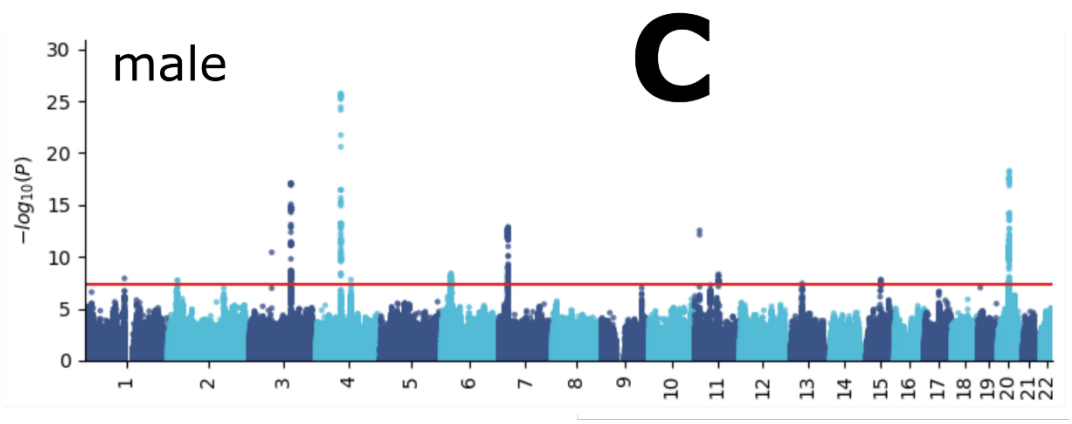
male
C
$-log_{10}(P)$
30
25
20
15
10
5
0
1
2
3
4
5
6
7
8
9
10
11
12
13
14
15
16
17
18
19
20
21
22

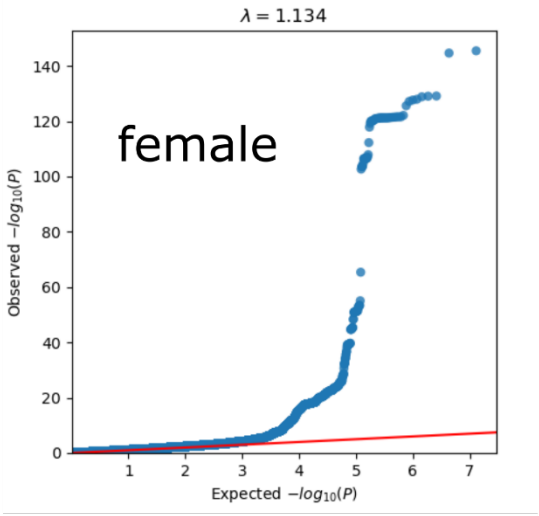
$\lambda = 1.134$
female
Observed $-log_{10}(P)$
Expected $-log_{10}(P)$
140
120
100
80
60
40
20
0
1
2
3
4
5
6
7

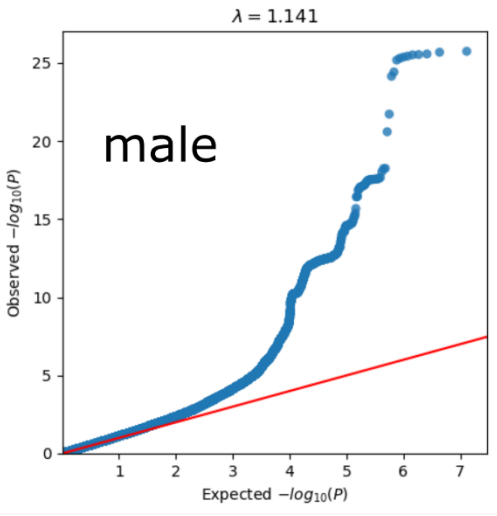
$\lambda = 1.141$
male
Observed $-log_{10}(P)$
Expected $-log_{10}(P)$
25
20
15
10
5
0
1
2
3
4
5
6
7

347

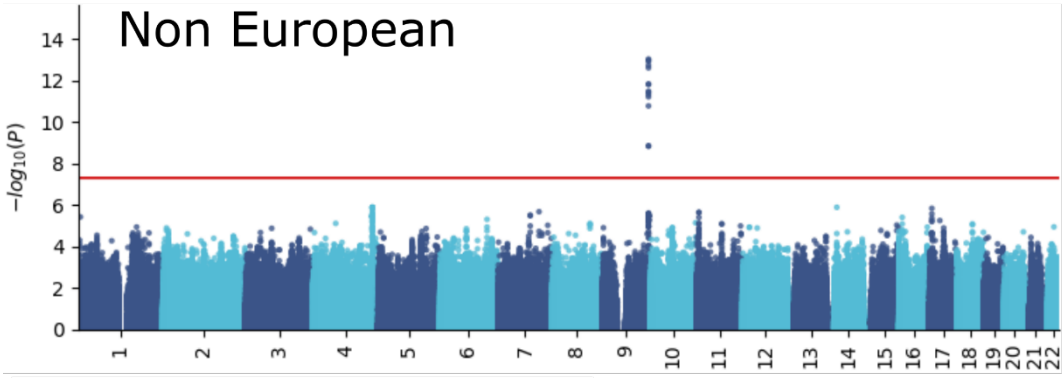

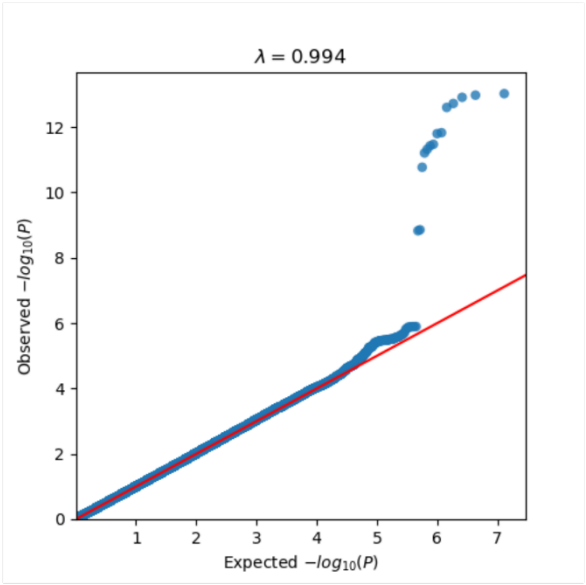

Manhattan and QQ plots, along with genomic inflation factors and LDSC intercepts, are displayed for the primary GWAS conducted on individuals of European ancestry (*N*=111,386) using PLINK and fastGWA (**A**). Additionally, results are presented for split-sample GWAS (split1 and split2, **B**), sex-stratified GWAS (female and male, **C**), and GWAS involving non-European ancestry populations (*N*=20,408, **D**).

354 **eFigure 8: GWAS Manhattan plots for the pulmonary BAG**

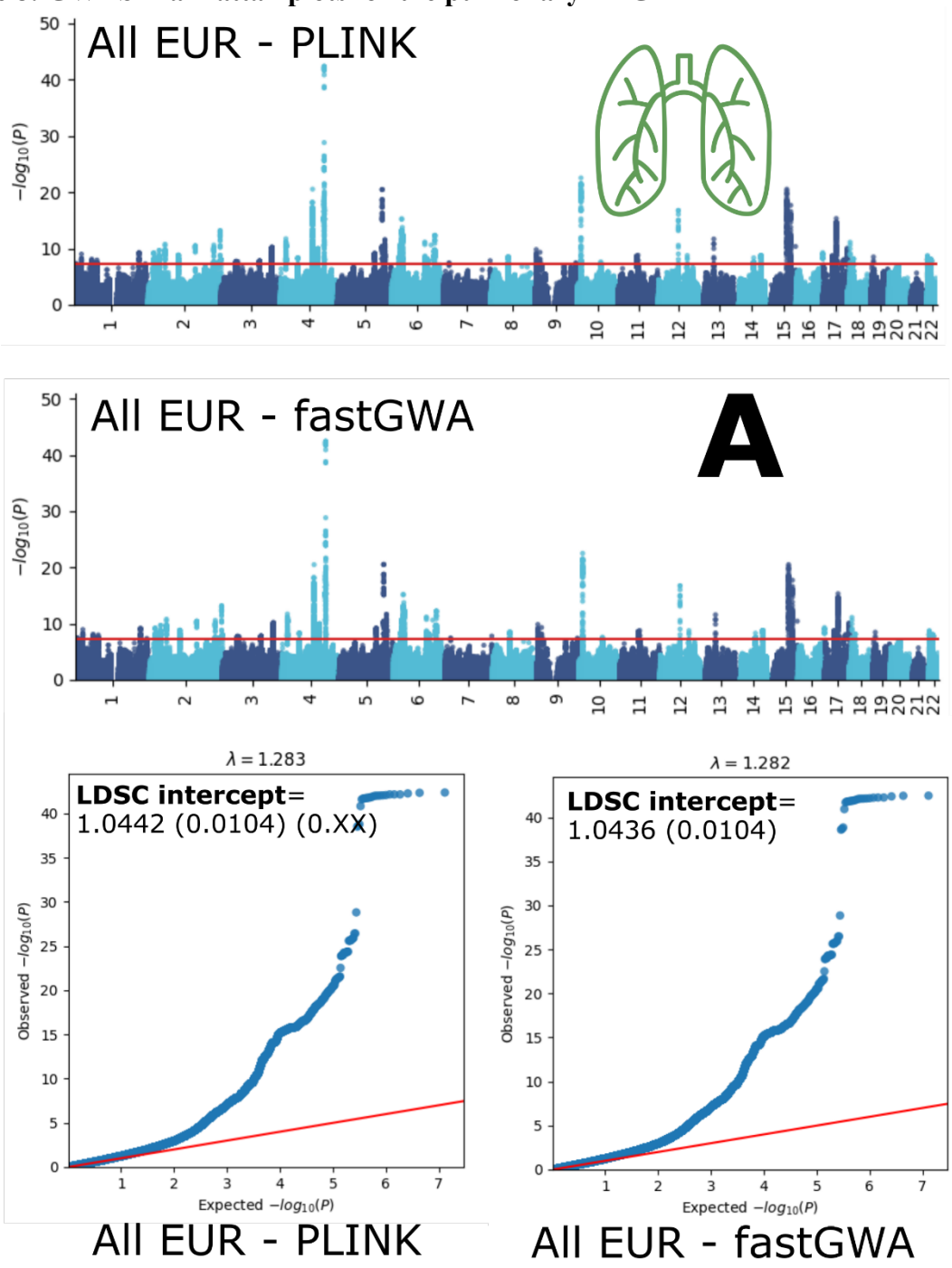

355

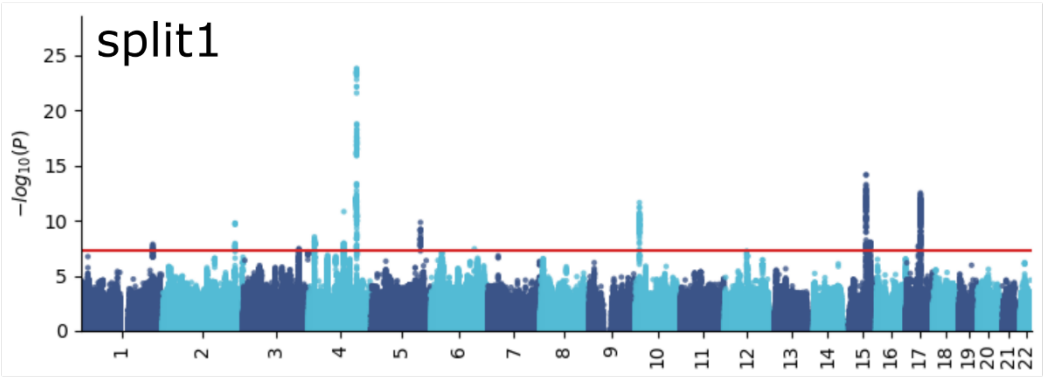
split1
$-log_{10}(P)$

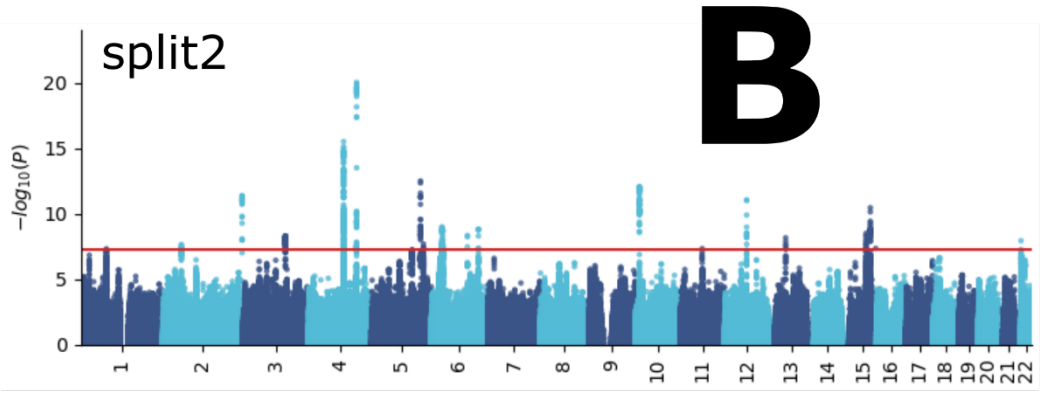
split2
B
$-log_{10}(P)$

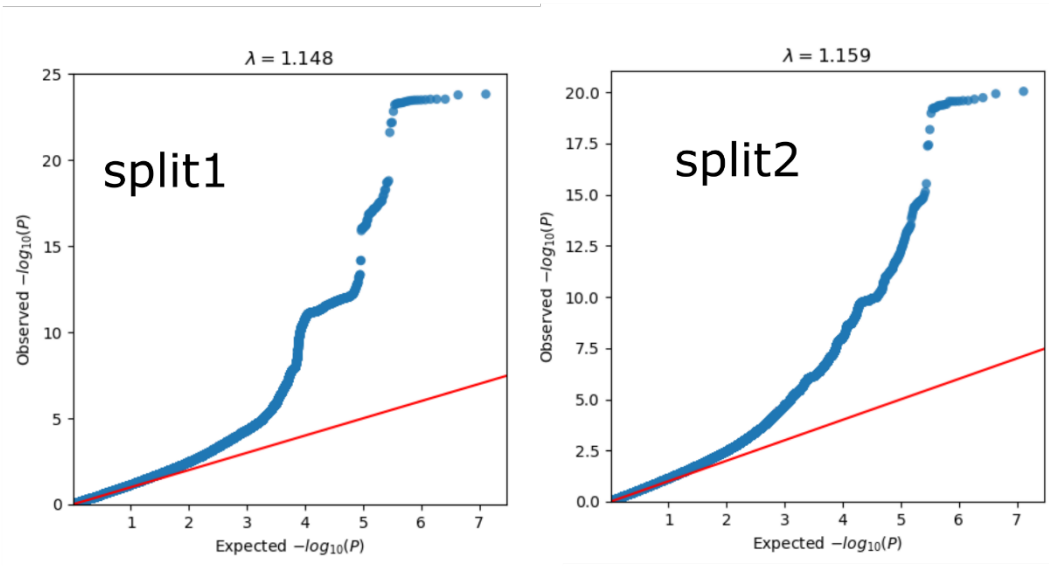
$\lambda = 1.148$
split1
Observed $-log_{10}(P)$
Expected $-log_{10}(P)$
$\lambda = 1.159$
split2
Observed $-log_{10}(P)$
Expected $-log_{10}(P)$

356

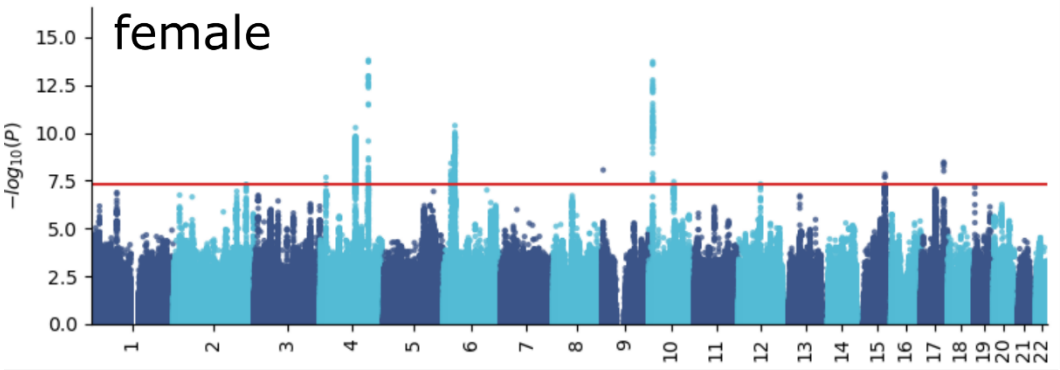
female
$-log_{10}(P)$
15.0
12.5
10.0
7.5
5.0
2.5
0.0
1 2 3 4 5 6 7 8 9 10 11 12 13 14 15 16 17 18 19 20 21 22

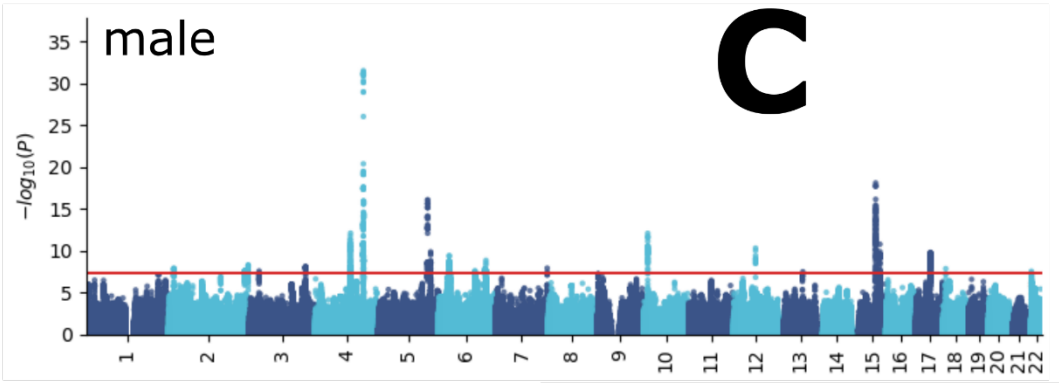
male
C
$-log_{10}(P)$
35
30
25
20
15
10
5
0
1 2 3 4 5 6 7 8 9 10 11 12 13 14 15 16 17 18 19 20 21 22

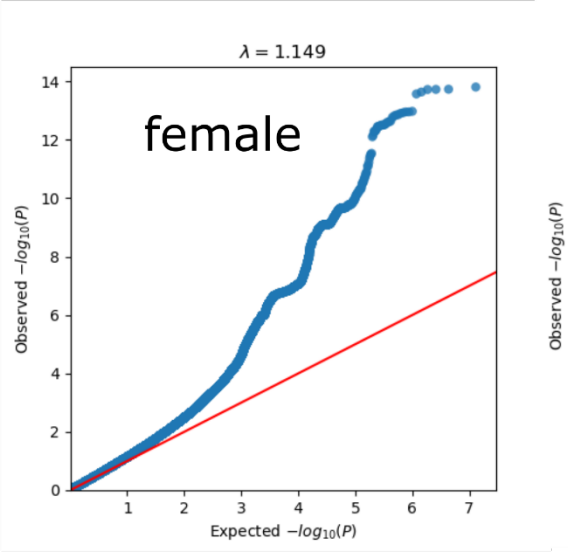
$\lambda = 1.149$
female
Observed $-log_{10}(P)$
Expected $-log_{10}(P)$
0 2 4 6 8 10 12 14
1 2 3 4 5 6 7

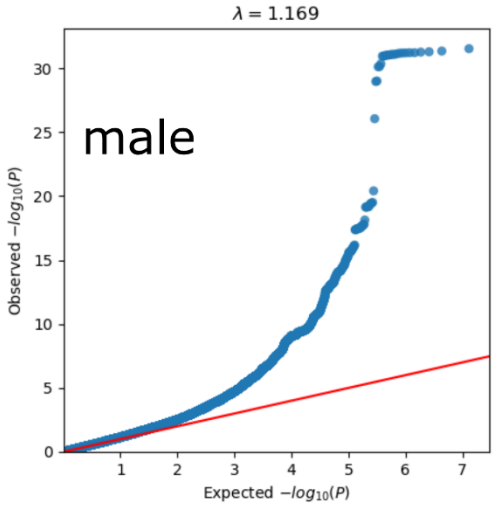
$\lambda = 1.169$
male
Observed $-log_{10}(P)$
Expected $-log_{10}(P)$
0 5 10 15 20 25 30
1 2 3 4 5 6 7

357

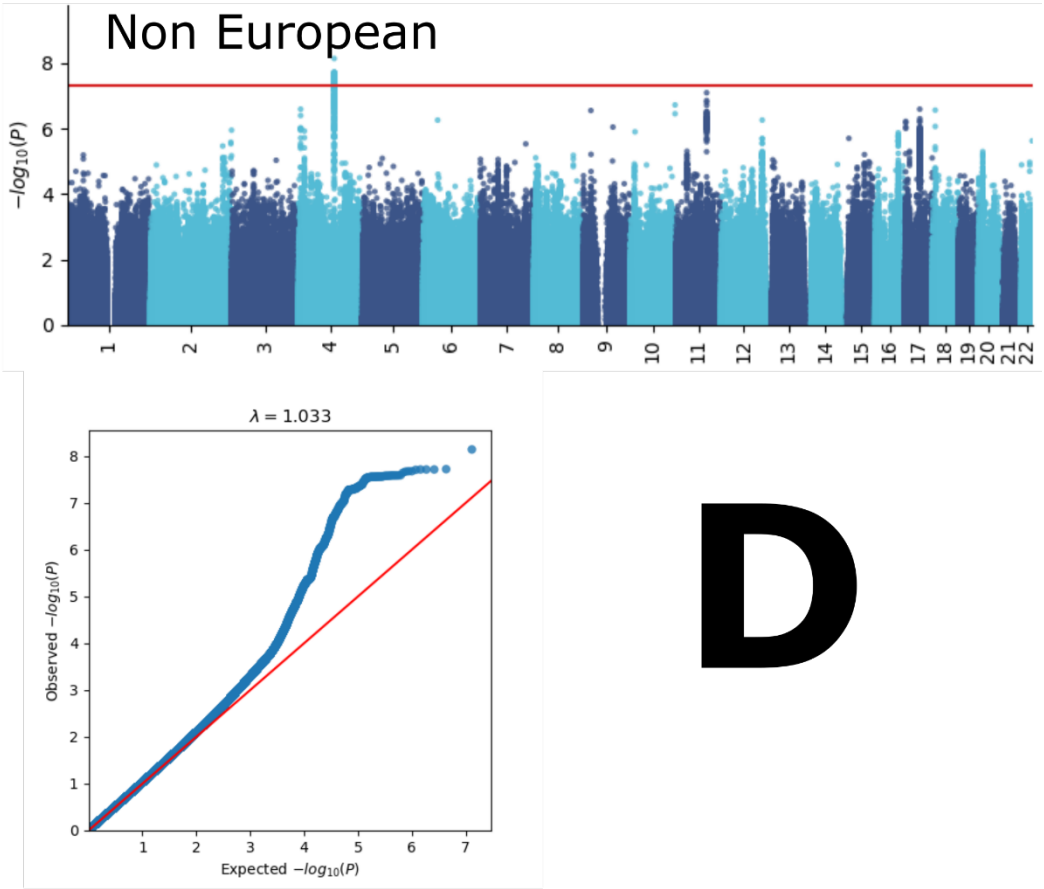

Manhattan and QQ plots, along with genomic inflation factors and LDSC intercepts, are displayed for the primary GWAS conducted on individuals of European ancestry (*N*=111,386) using PLINK and fastGWA (**A**). Additionally, results are presented for split-sample GWAS (split1 and split2, **B**), sex-stratified GWAS (female and male, **C**), and GWAS involving non-European ancestry populations (*N*=20,408, **D**).

364 **eFigure 9: GWAS Manhattan plots for the renal BAG**

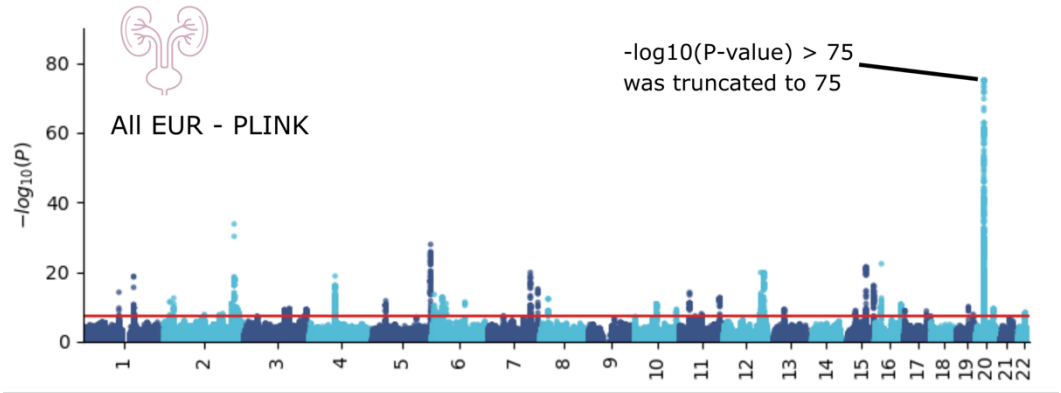

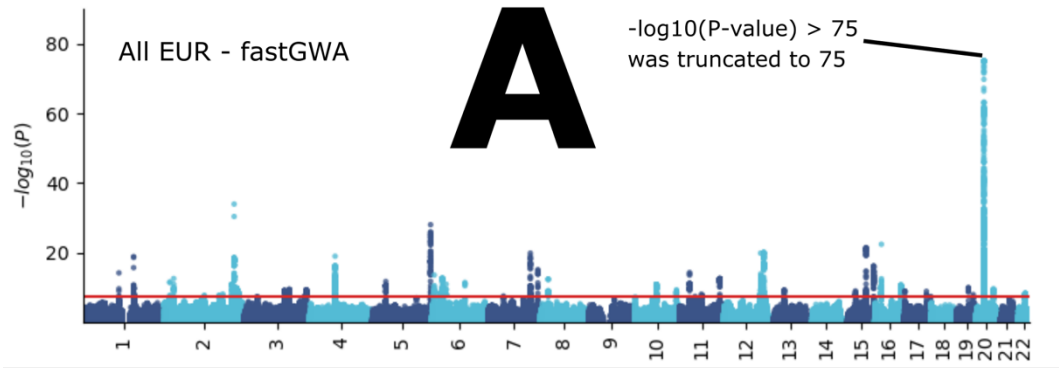

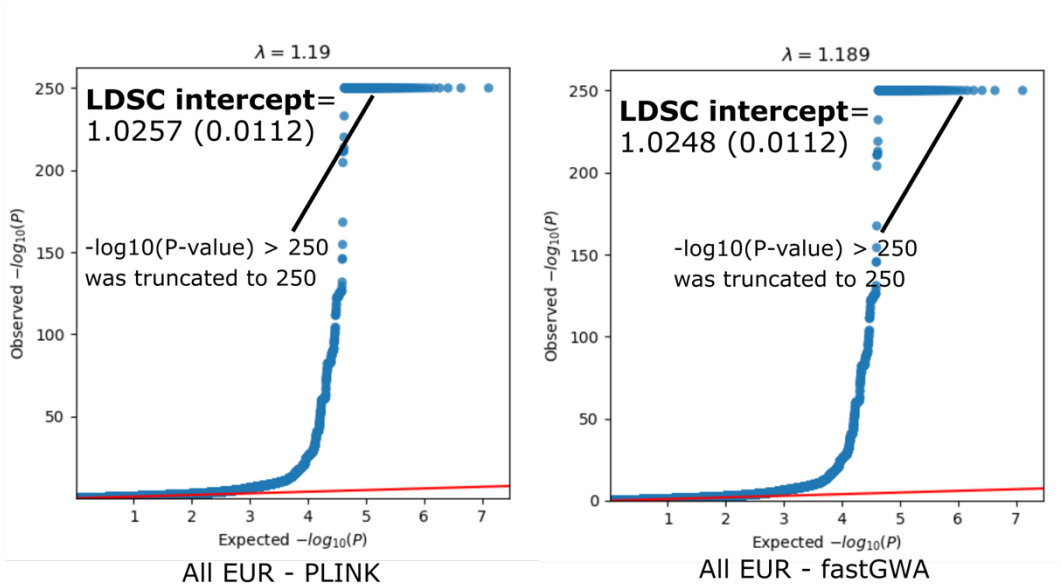

365

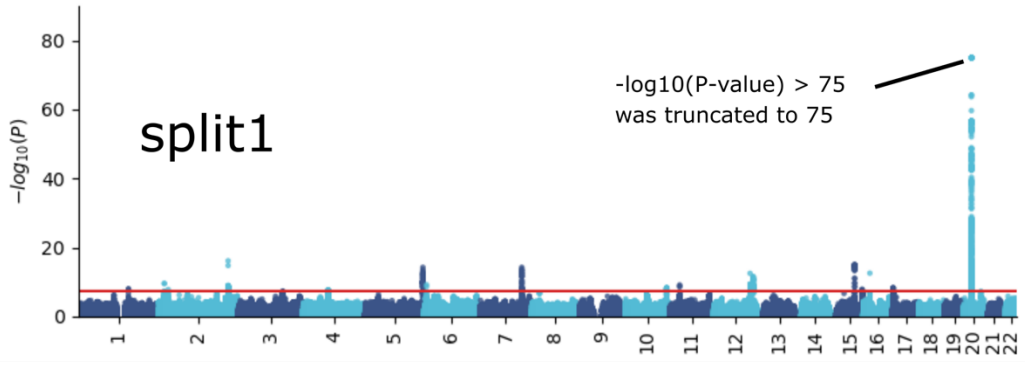
split1
-log10(P-value) > 75
was truncated to 75
$-log_{10}(P)$

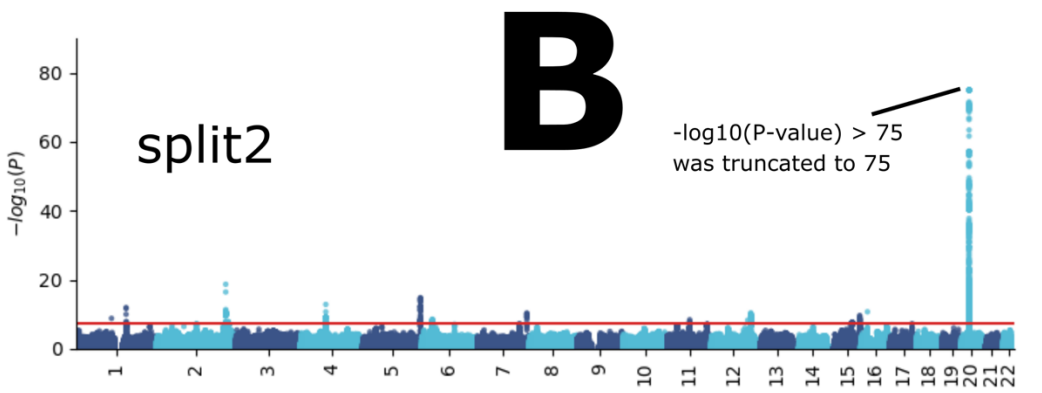
B
split2
-log10(P-value) > 75
was truncated to 75
$-log_{10}(P)$

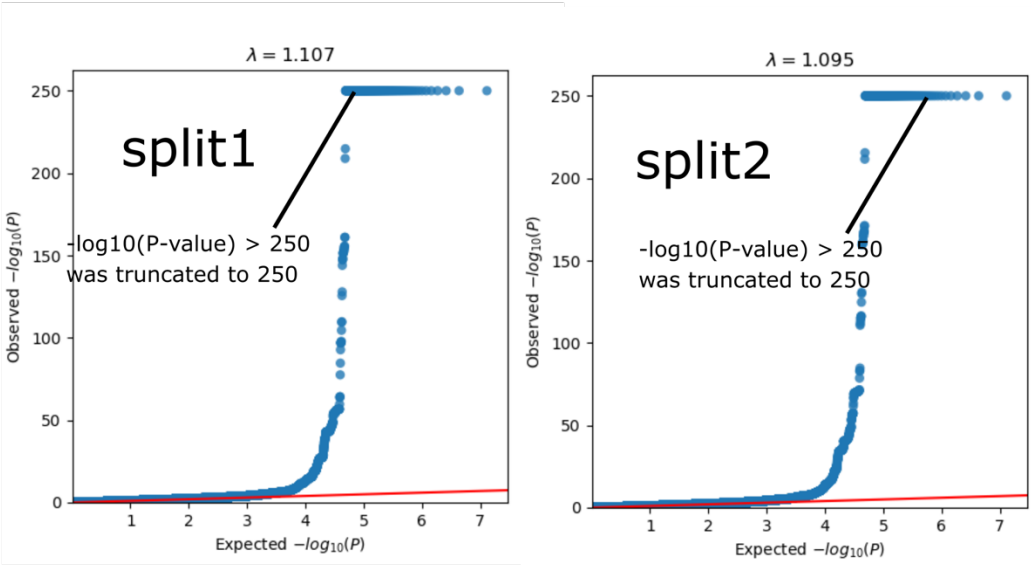
λ = 1.107
split1
-log10(P-value) > 250
was truncated to 250
Observed $-log_{10}(P)$
Expected $-log_{10}(P)$
λ = 1.095
split2
-log10(P-value) > 250
was truncated to 250
Observed $-log_{10}(P)$
Expected $-log_{10}(P)$

366

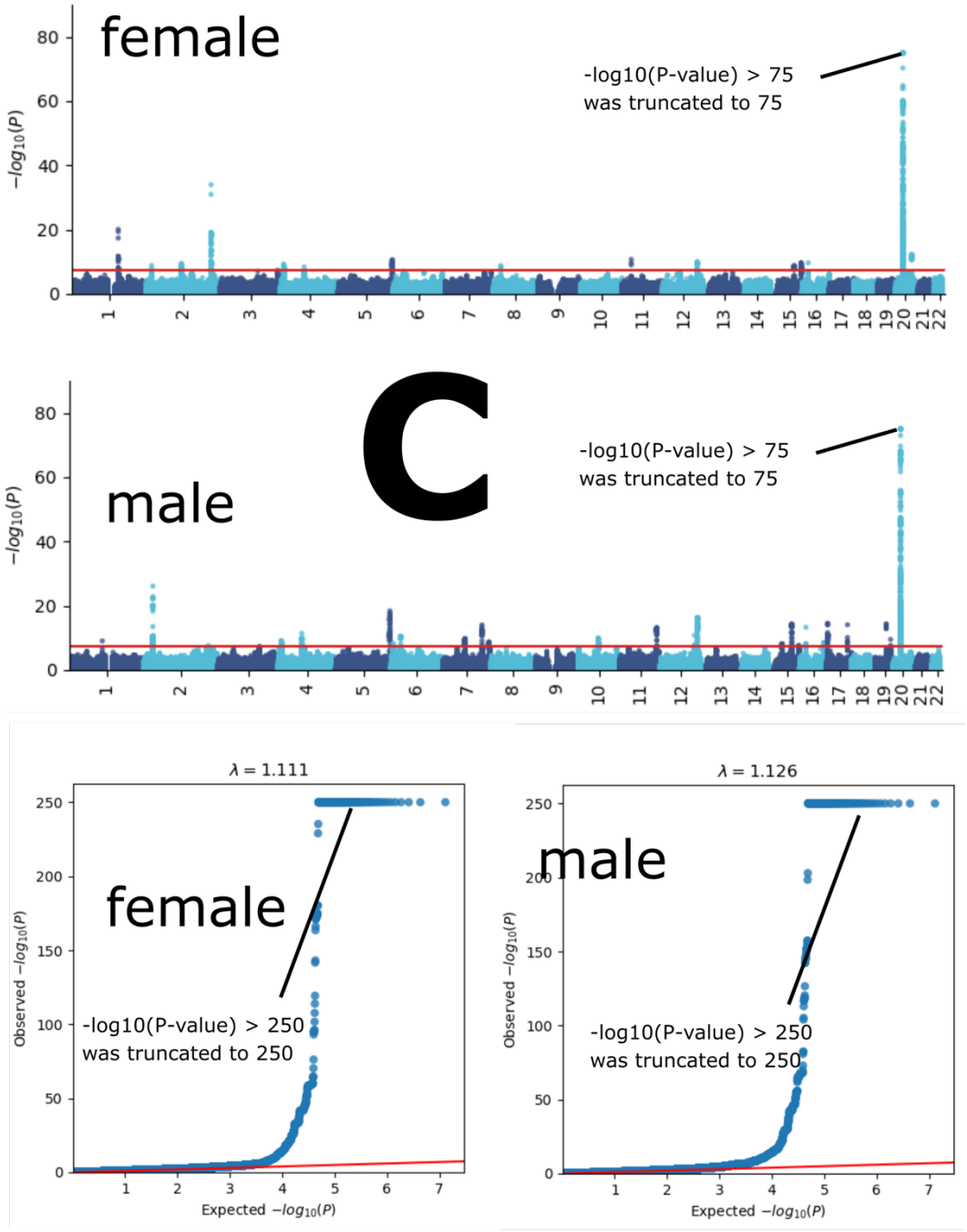
female
-log10(P-value) > 75
was truncated to 75
male
C
-log10(P-value) > 75
was truncated to 75
λ = 1.111
female
-log10(P-value) > 250
was truncated to 250
Observed −log10(P)
Expected −log10(P)
λ = 1.126
male
-log10(P-value) > 250
was truncated to 250
Observed −log10(P)
Expected −log10(P)

367

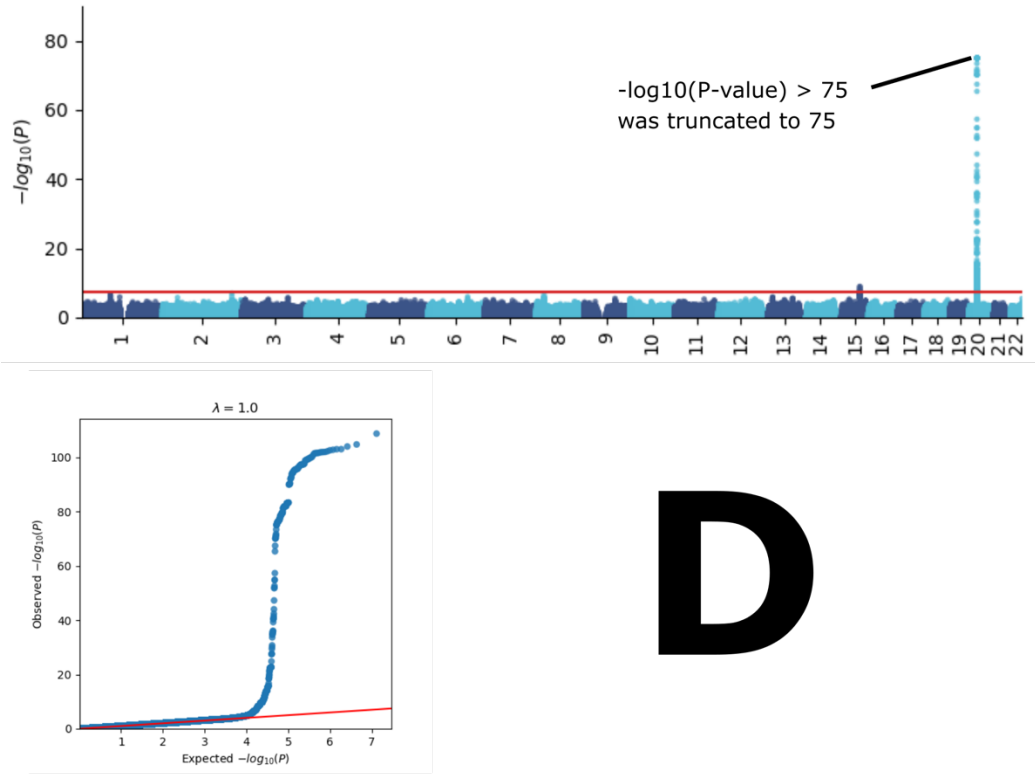

Manhattan and QQ plots, along with genomic inflation factors and LDSC intercepts, are displayed for the primary GWAS conducted on individuals of European ancestry (*N*=111,386) using PLINK and fastGWA (**A**). Additionally, results are presented for split-sample GWAS (split1 and split2, **B**), sex-stratified GWAS (female and male, **C**), and GWAS involving non-European ancestry populations (*N*=20,408, **D**). For visualization purposes, we chose to truncate the highly significant P-value (P-value<$1x10^{-300}$) to a lower P-value ($1x10^{-75}$ for Manhattan plots and $1x10^{-250}$ for QQ plots).

eFigure 10: Bayesian colocalization analysis for the locus on chromosome 6 between the hepatic and musculoskeletal BAGs

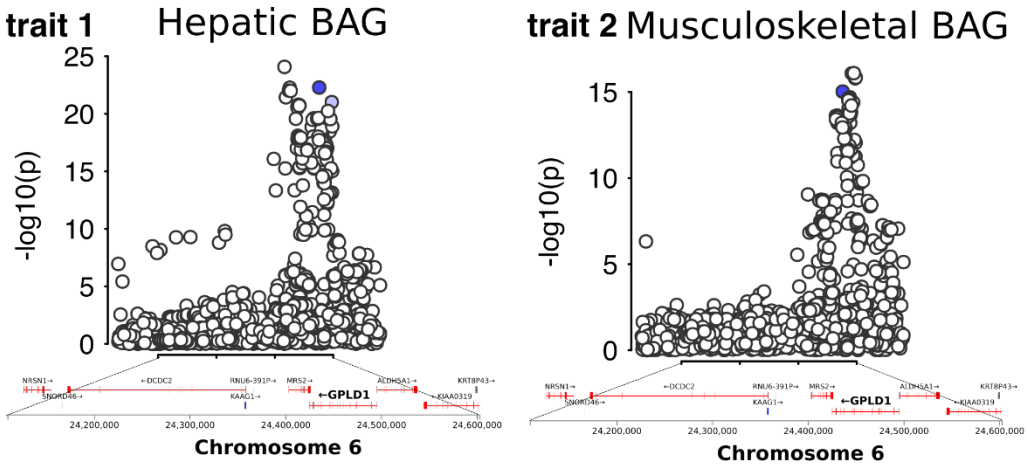

We conducted a Bayesian colocalization analysis using Bayes factors to investigate shared causal variants in a specific locus on chromosome 6 for the hepatic and musculoskeletal BAGs. The analysis tested five hypotheses, denoted by their posterior probabilities: H0 (no association with either trait), H1 (association with trait 1 but not trait 2), H2 (association with trait 2 but not trait 1), H3 (association with both traits but with separate causal variants), and H4 (association with both traits with a shared causal variant). The potential causal variants for both traits are indicated by blue-colored SNPs, assuming each locus contains at most one causal variant. The gene mapped to this locus (*GPLD1*) is shown in bold based on physical positions.

eFigure 11: Exemplary genomic locus for each BAG in the nine human organ systems

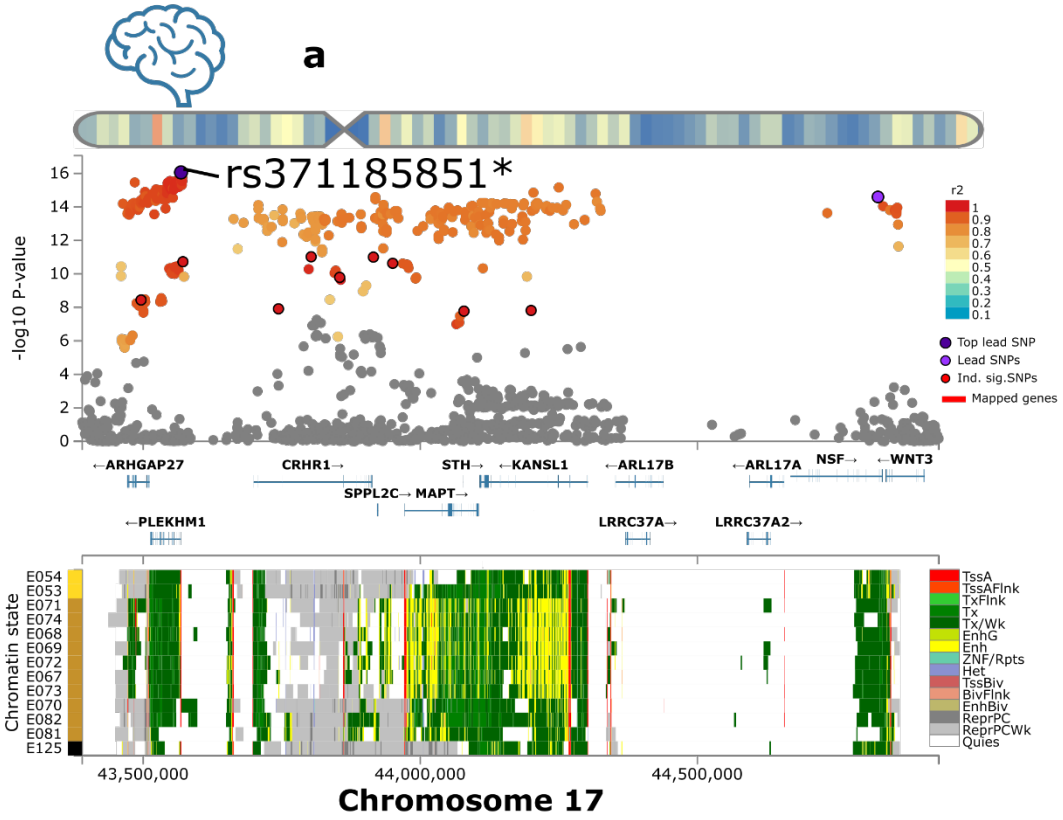

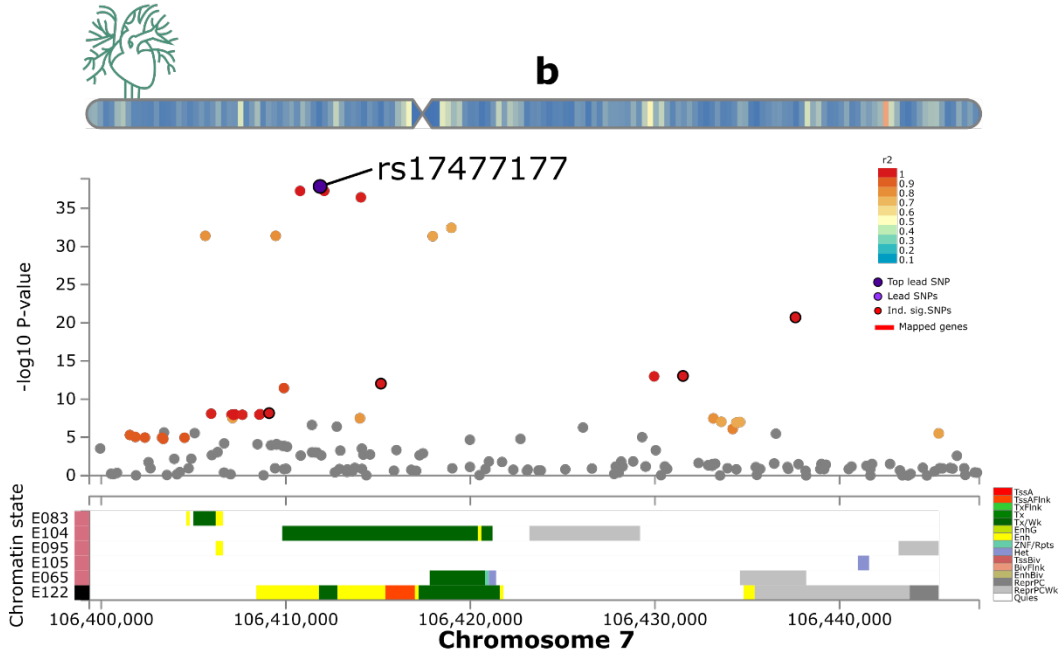

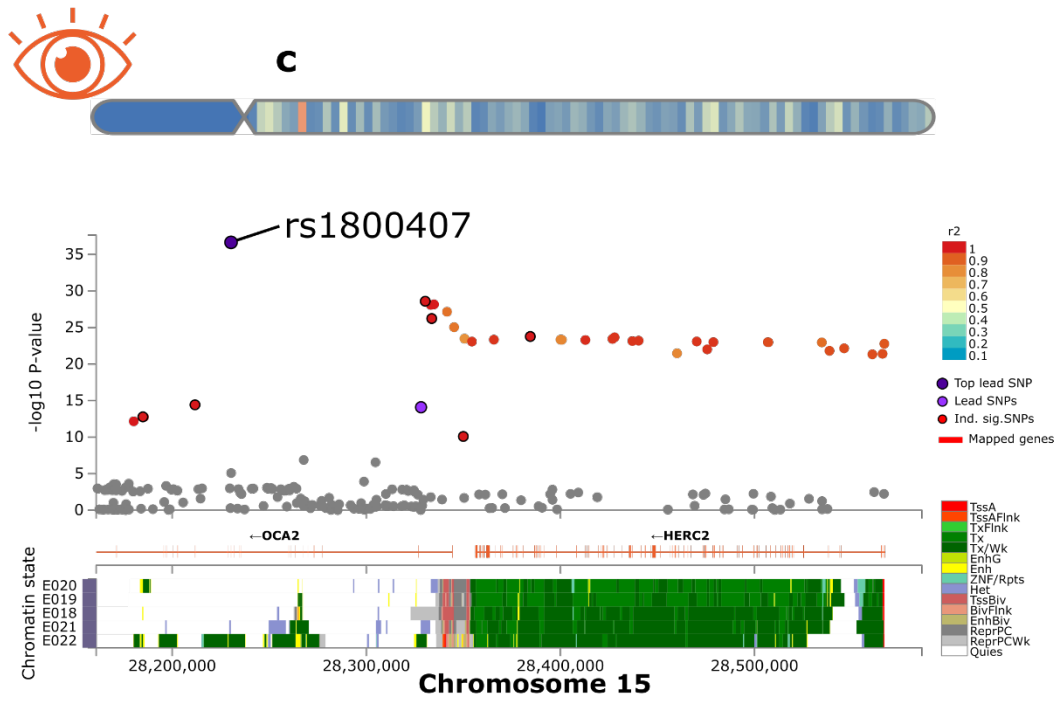
c
rs1800407
-log10 P-value
r2
Top lead SNP
Lead SNPs
Ind. sig.SNPs
Mapped genes
←OCA2
←HERC2
Chromatin state
E020
E019
E018
E021
E022
TssA
TssAFlnk
TxFlnk
Tx
Tx/Wk
EnhG
Enh
ZNF/Rpts
Het
TssBiv
BivFlnk
EnhBiv
ReprPC
ReprPCWk
Quies
28,200,000
28,300,000
28,400,000
28,500,000
Chromosome 15

391

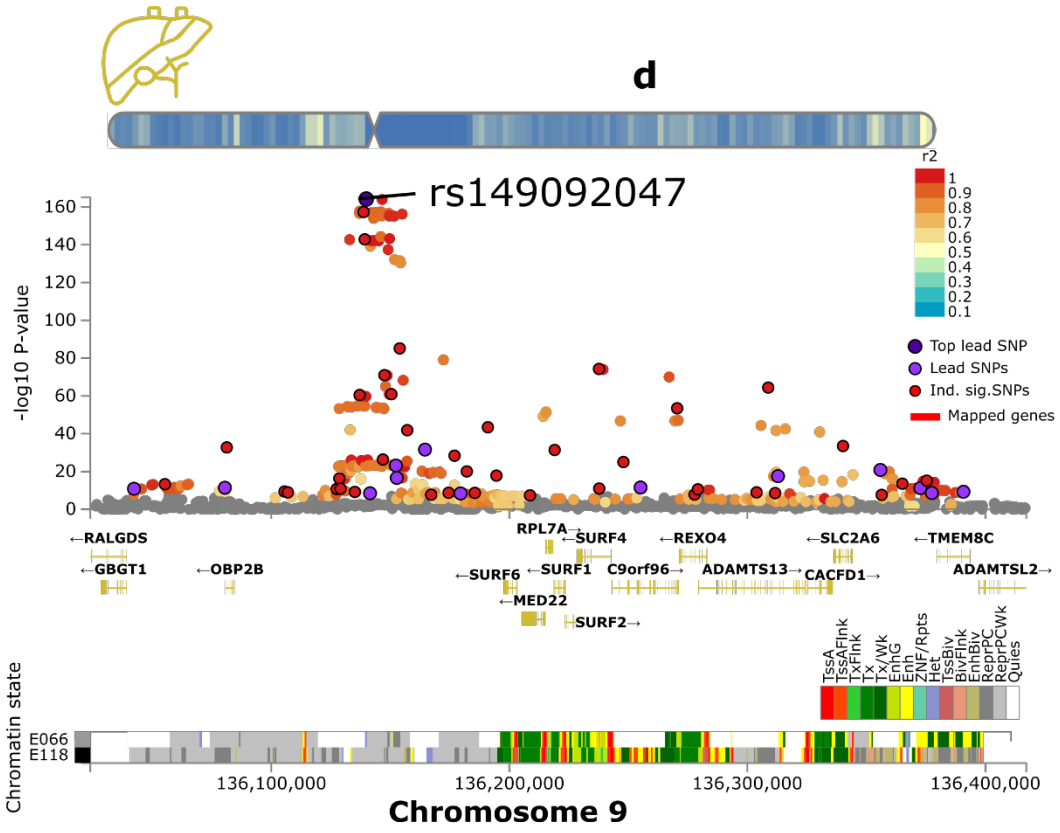
d
rs149092047
-log10 P-value
r2
Top lead SNP
Lead SNPs
Ind. sig.SNPs
Mapped genes
←RALGDS
←GBGT1
←OBP2B
RPL7A→
←SURF4
←REXO4
←SLC2A6
←TMEM8C
←SURF6
←SURF1
C9orf96→
ADAMTS13→
CACFD1→
ADAMTSL2→
←MED22
SURF2→
Chromatin state
E066
E118
136,100,000
136,200,000
136,300,000
136,400,000
Chromosome 9

392

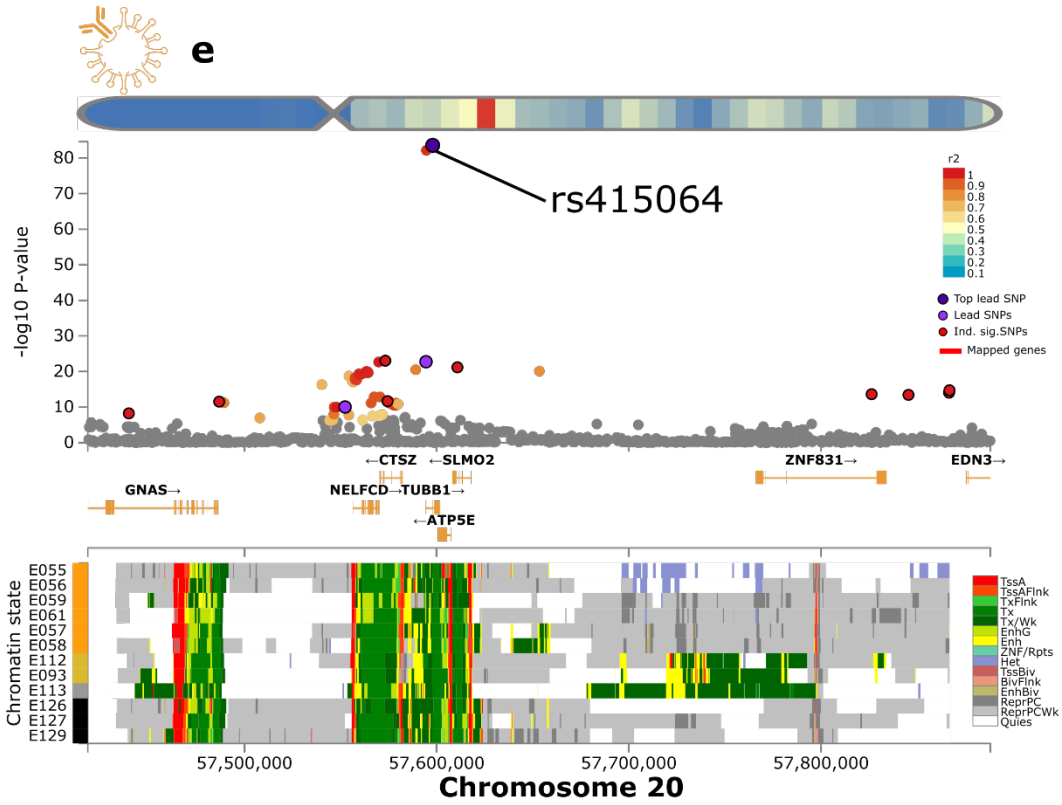
e
rs415064
-log10 P-value
r2
Top lead SNP
Lead SNPs
Ind. sig.SNPs
Mapped genes
←CTSZ
←SLMO2
ZNF831→
EDN3→
GNAS→
NELFCD→TUBB1→
←ATP5E
Chromatin state
E055
E056
E059
E061
E057
E058
E112
E093
E113
E126
E127
E129
TssA
TssAFlnk
TxFlnk
Tx
Tx/Wk
EnhG
Enh
ZNF/Rpts
Het
TssBiv
BivFlnk
EnhBiv
ReprPC
ReprPCWk
Quies
57,500,000
57,600,000
57,700,000
57,800,000
Chromosome 20

393

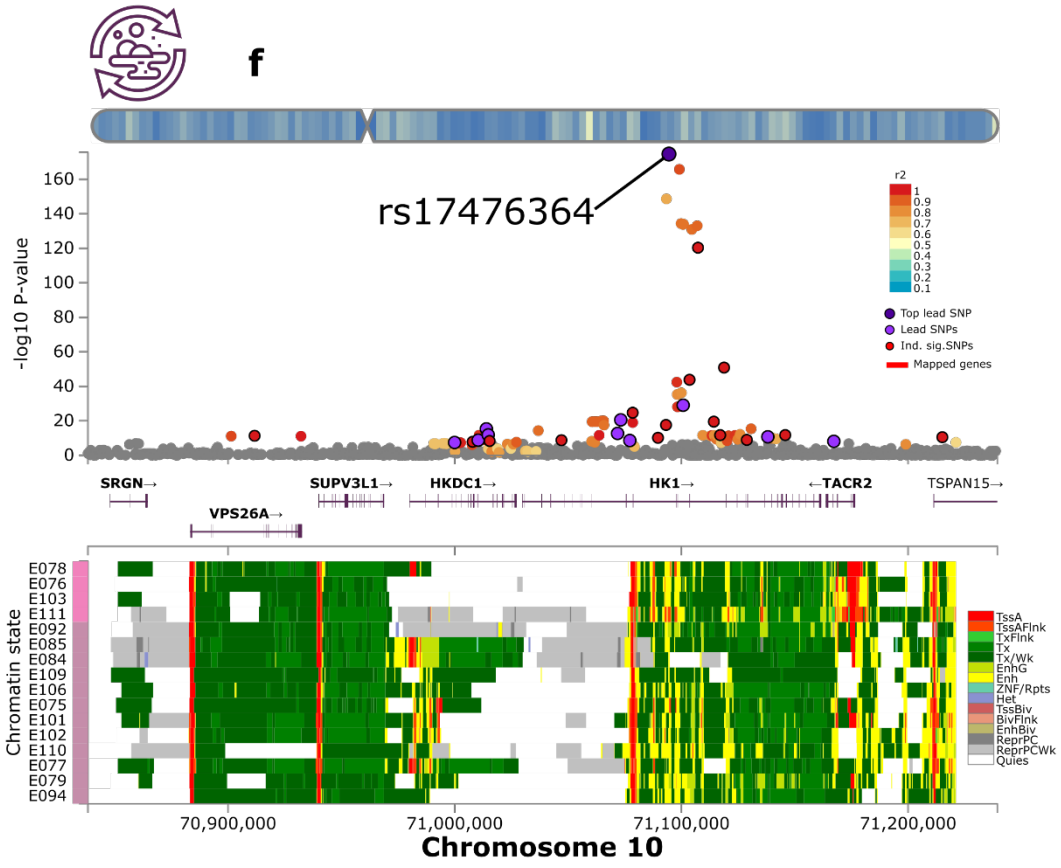
f
rs17476364
-log10 P-value
r2
Top lead SNP
Lead SNPs
Ind. sig.SNPs
Mapped genes
SRGN→
SUPV3L1→
HKDC1→
HK1→
←TACR2
TSPAN15→
VPS26A→
Chromatin state
E078
E076
E103
E111
E092
E085
E084
E109
E106
E075
E101
E102
E110
E077
E079
E094
TssA
TssAFlnk
TxFlnk
Tx
Tx/Wk
EnhG
Enh
ZNF/Rpts
Het
TssBiv
BivFlnk
EnhBiv
ReprPC
ReprPCWk
Quies
70,900,000
71,000,000
71,100,000
71,200,000
Chromosome 10

394

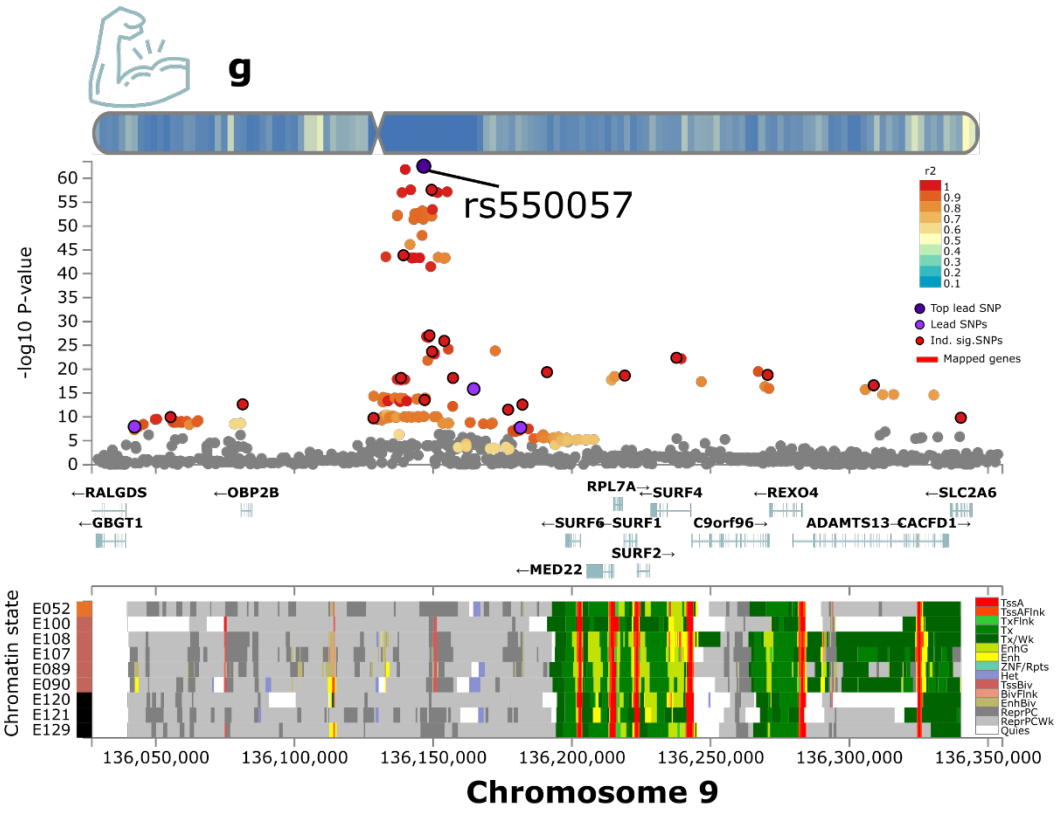
g
rs550057
-log10 P-value
r2
Top lead SNP
Lead SNPs
Ind. sig.SNPs
Mapped genes
←RALGDS
←OBP2B
←GBGT1
RPL7A→
←SURF4
←REXO4
←SLC2A6
←SURF6
SURF1
C9orf96→
ADAMTS13
CACFD1→
SURF2→
←MED22
Chromatin state
E052
E100
E108
E107
E089
E090
E120
E121
E129
TssA
TssAFlnk
TxFlnk
Tx
Tx/Wk
EnhG
Enh
ZNF/Rpts
Het
TssBiv
BivFlnk
EnhBiv
ReprPC
ReprPCWk
Quies
136,050,000
136,100,000
136,150,000
136,200,000
136,250,000
136,300,000
136,350,000
Chromosome 9

395

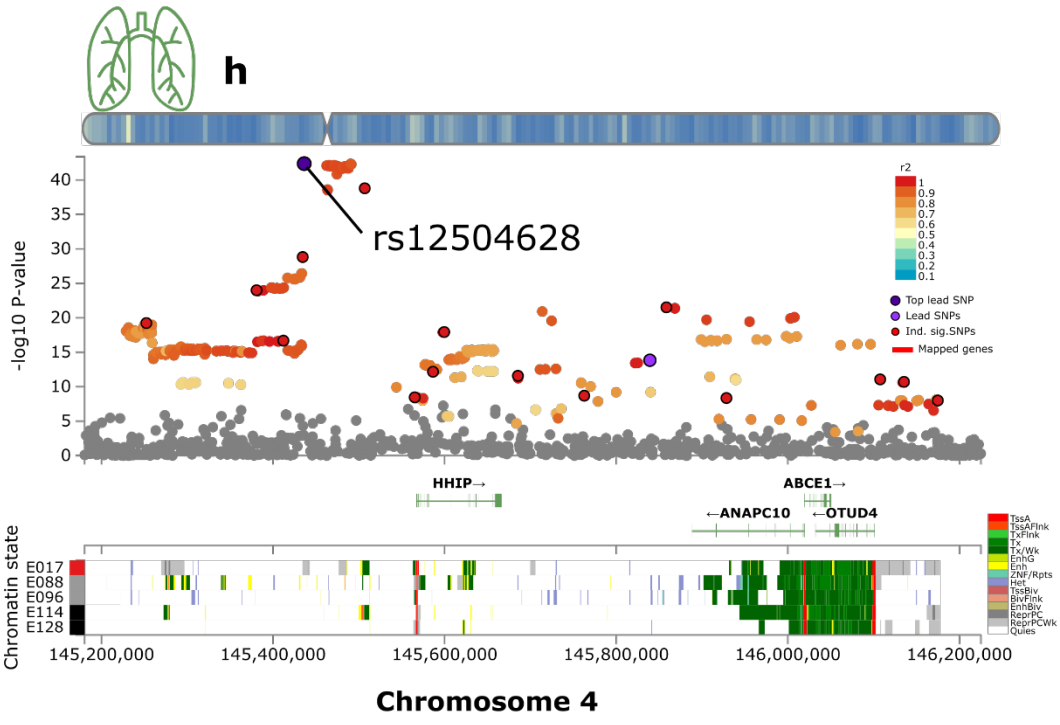
h
rs12504628
-log10 P-value
r2
Top lead SNP
Lead SNPs
Ind. sig.SNPs
Mapped genes
HHIP→
ABCE1→
←ANAPC10
←OTUD4
Chromatin state
E017
E088
E096
E114
E128
TssA
TssAFlnk
TxFlnk
Tx
Tx/Wk
EnhG
Enh
ZNF/Rpts
Het
TssBiv
BivFlnk
EnhBiv
ReprPC
ReprPCWk
Quies
145,200,000
145,400,000
145,600,000
145,800,000
146,000,000
146,200,000
Chromosome 4

396

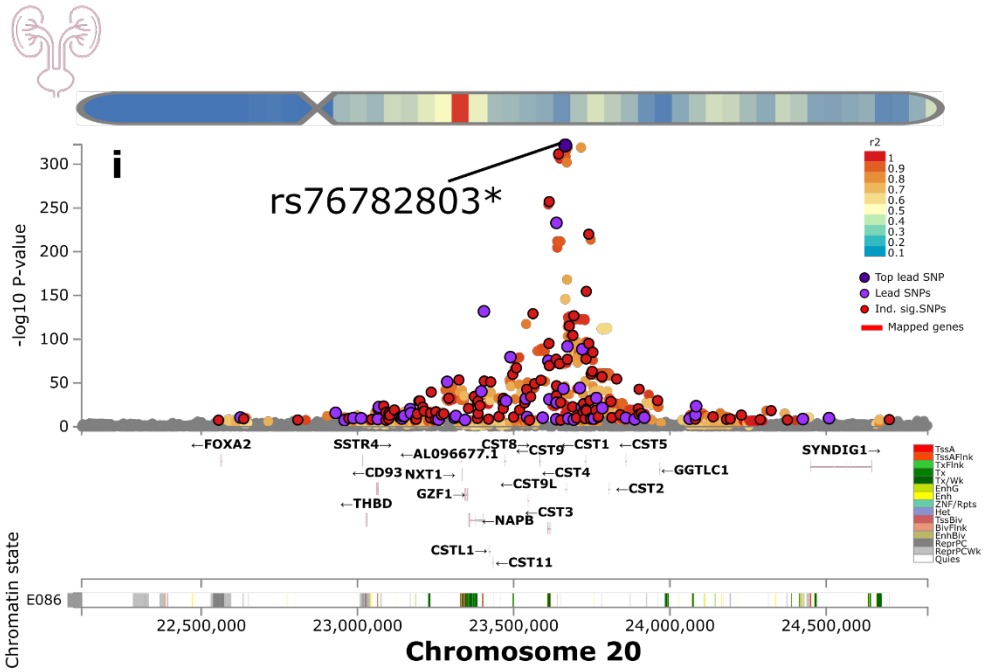

a-i) The exemplary genomic locus with the most significant signals for the brain, cardiovascular, eye, hepatic, immune, metabolic, musculoskeletal, pulmonary, and renal BAGs. The top lead SNP, lead SNPs, and independent significant SNPs are annotated within each locus. We mapped the SNPs to the genes and predicted their chromatin states in specific tissues, including the brain for the brain BAG, the heart and vascular tissues for the cardiovascular BAG, the iPSC for the eye BAG, the liver for the hepatic BAG, the spleen, bone, skin, and thymus tissues for the immune BAG, the gastrointestinal tissue for the metabolic BAG, the muscle and bone tissues for the musculoskeletal BAG, the lung tissue for the pulmonary BAG, and the kidney for the renal BAG, respectively.

eFigure 12: SNP-based heritability, beta coefficients, and alternative allele frequency using the brain-BAG comparable populations and different inclusion criteria for the SNPs

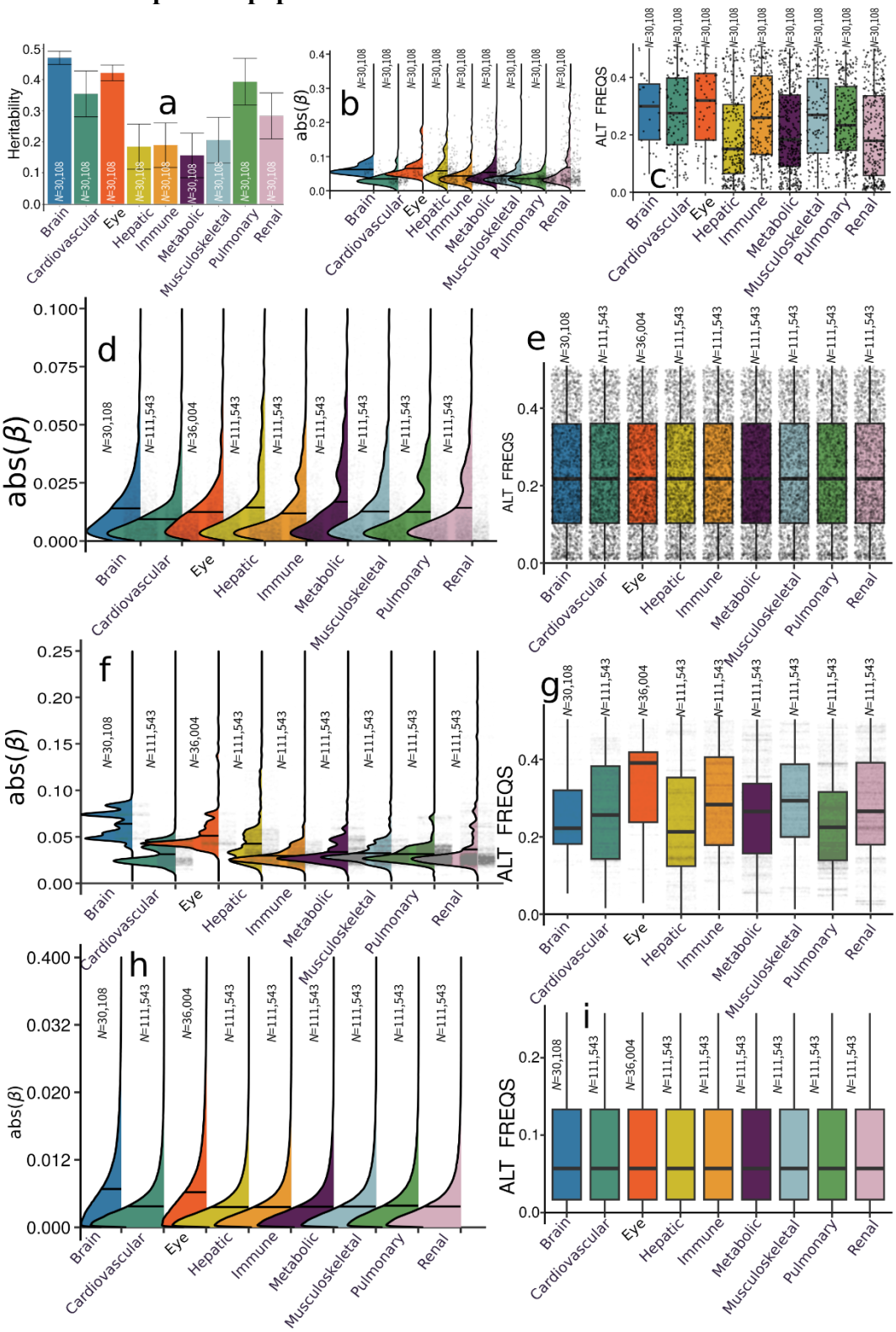

a) The SNP-based heritability of the nine BAGs using populations from downsampling to the brain BAG population. Error bars represent the standard error of the estimated parameters. **b**)

The absolute value of the beta coefficients of the independent significant SNPs of the nine BAG GWASs using populations from downsampling to the brain BAG population (*N*=30,108); the independent significant SNPs are shown separately for each BAG. **c**) The alternative (effective) allele frequency of the independent significant SNPs from the nine BAG GWASs using populations from downsampling to the brain BAG population (*N*=30,108). **d**) The beta coefficients of the independent significant SNPs using the original full samples but with all identified independent significant SNPs across the nine BAG GWASs (with the same number of SNPs tested), where we see no difference regarding allele frequency in Figure **e**). **f**) The absolute value of the beta coefficients of the independent significant SNPs plus the candidate SNPs in LD of the nine BAG GWASs using the original full samples; the SNPs are shown separately for each BAG. **g**) The alternative allele frequency for the setting in Figure **f**). **h**) The absolute beta coefficients of the nine BAGs using all genome-wide SNPs (the y-axis was truncated to 0.1 for visualization purposes). **i**) the alternative allele frequency did not differ for Figure h) including all genome-wide SNPs.

eFigure 13: Trumpet plots of the alternative allele frequency vs. the beta coefficient of the nine BAG GWASs

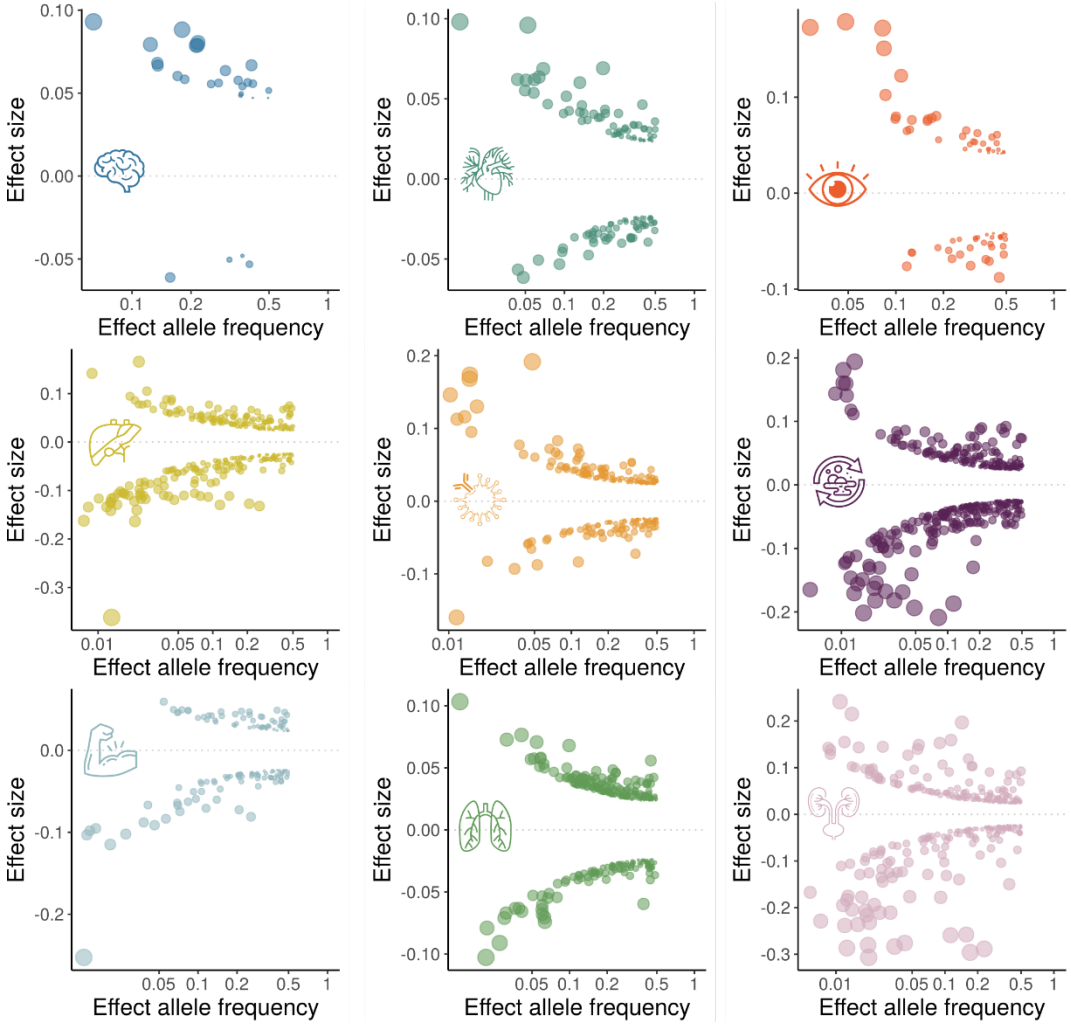

The trumpet plots display the inverse relationship between the alternative (effect) allele frequency and the effect size (beta coefficient) for the brain, cardiovascular, eye, hepatic, immune, metabolic, musculoskeletal, pulmonary, and renal BAGs. Only the independent significant SNPs were considered. The dot size corresponds to the effect size, while the transparency of the dot is proportional to its statistical significance.

eFigure 14: Manhattan and QQ plots for the four pulmonary features used to compute the pulmonary BAG

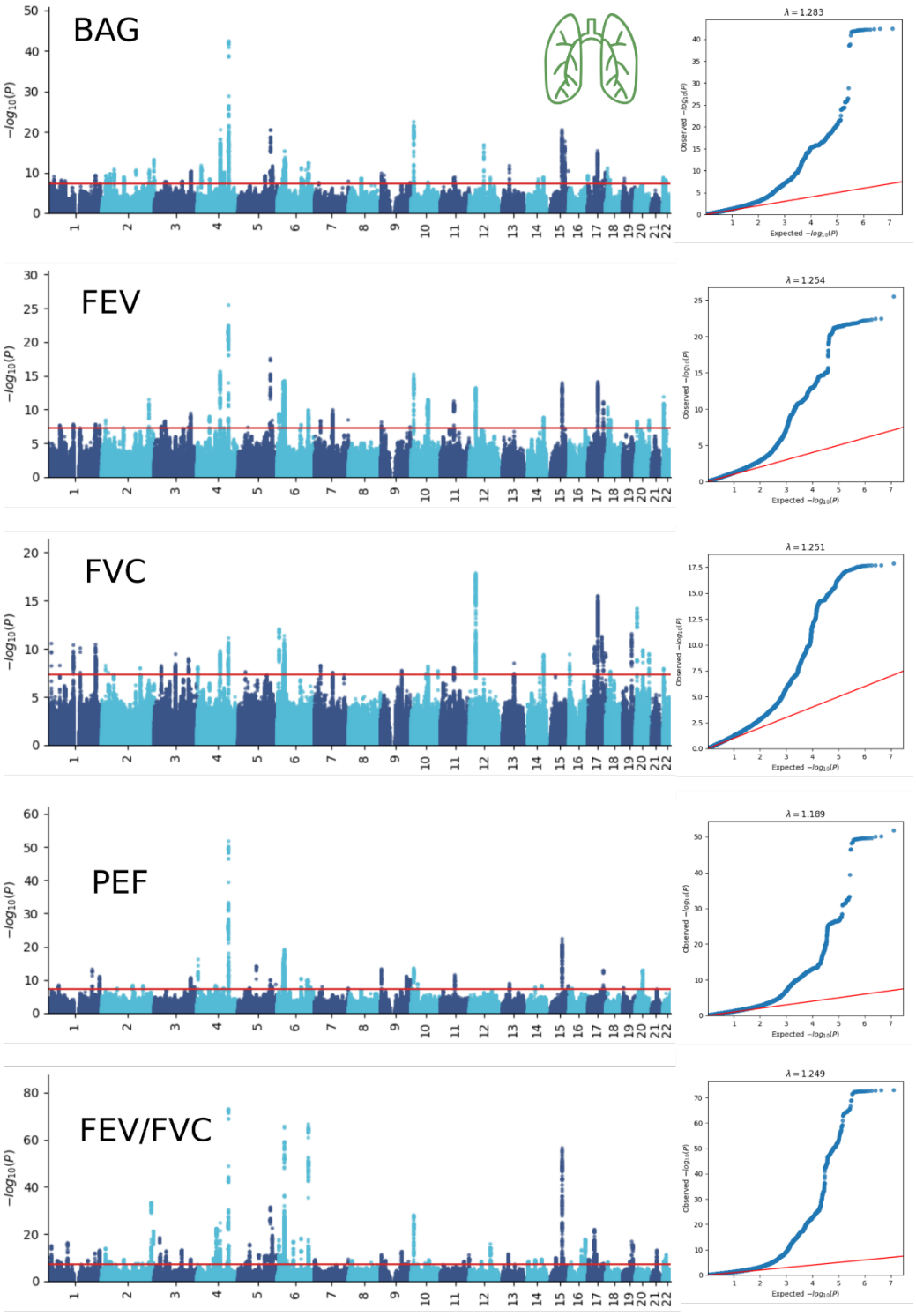

The Manhattan and QQ plots for the pulmonary BAG vs. its four features used to compute the BAG: forced vital capacity (FVC), forced expiratory volume (FEV), peak expiratory flow (PEF), and the ratio of forced expiratory volume to forced vital capacity (FEV/FVC).

eFigure 15: Bayesian colocalization signal between the pulmonary BAG and FEV/FVC

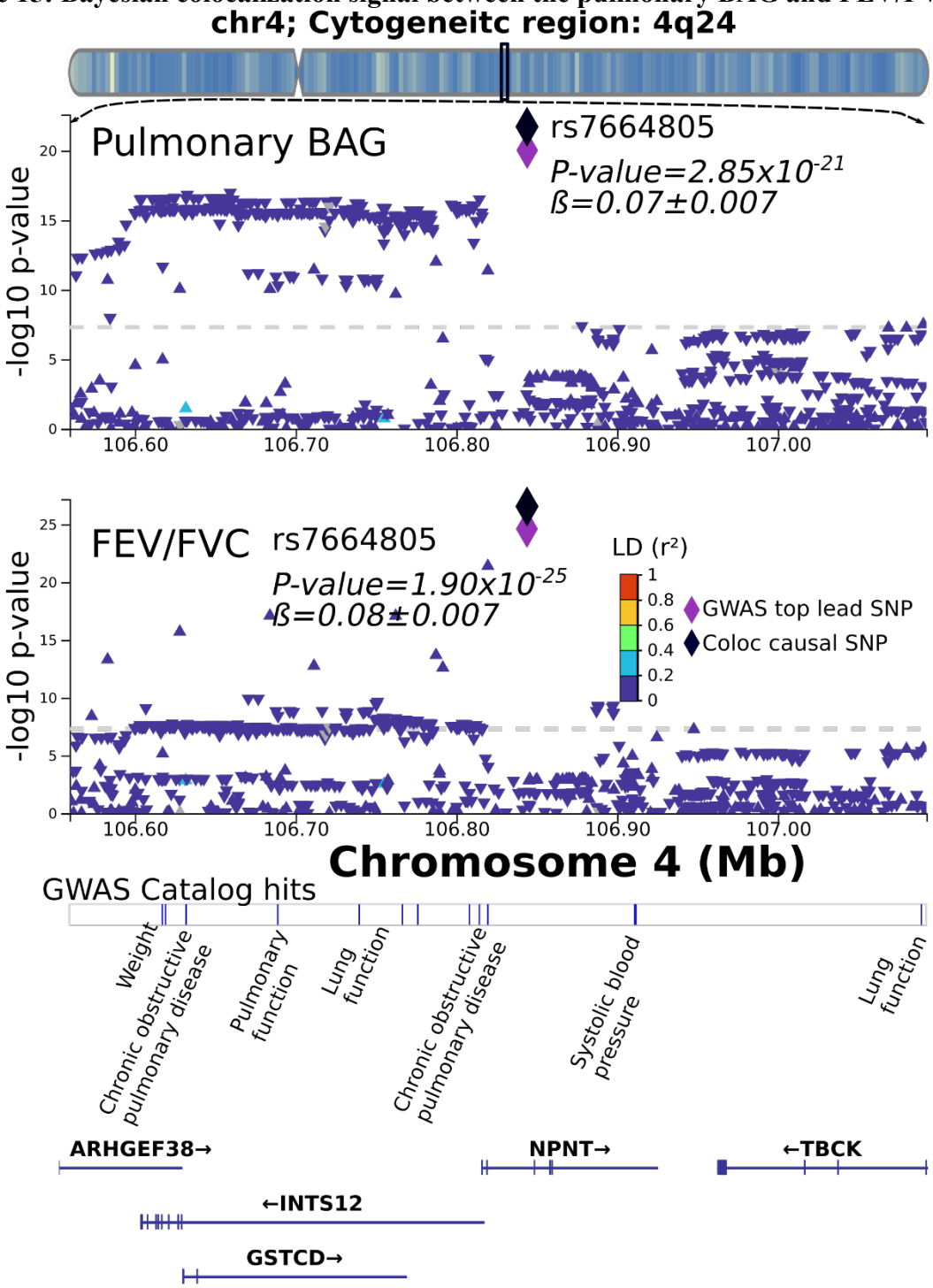

We illustrate here the colocalization signal between the pulmonary BAG and the FEV/FCV feature at the genomic locus: 4q24 with the top lead SNP (causal SNP: rs7664805). Genetic colocalization was evidenced at one locus (4q24) between the pulmonary BAG and the FEV/FCV feature. The signed PP.H4.ABF (0.99) denotes the posterior probability (PP) of hypothesis H4, which suggests that both traits share the same causal SNP (rs7664805).

eFigure 16: Beta coefficients of the significant colocalization signal between the pulmonary BAG and the four pulmonary features

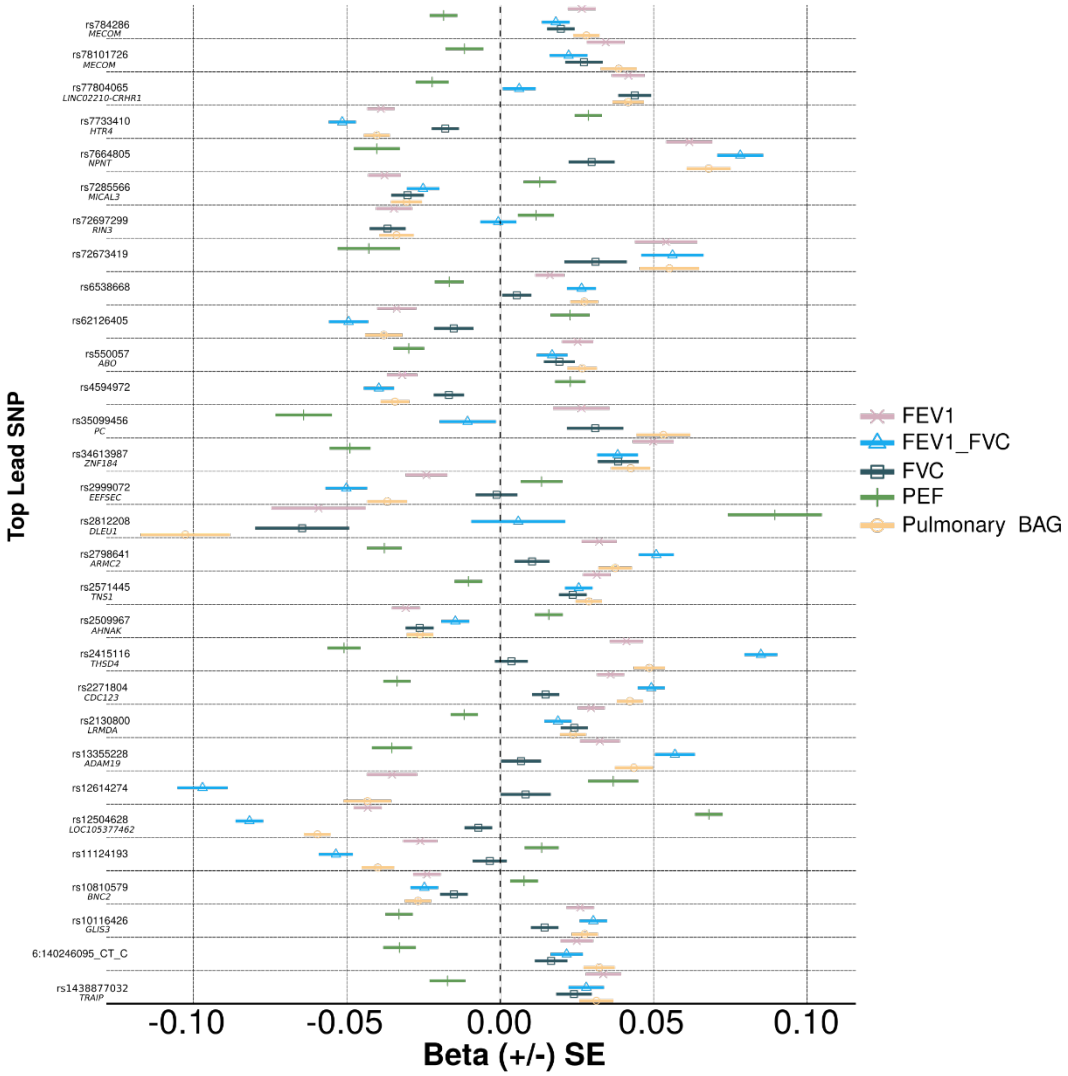

We show the beta coefficients of the significant colocalization signals between the pulmonary BAG and its underlying four pulmonary features. We ensured that at least one of the four pulmonary features achieved the genome-wide P-value threshold, totaling 48 loci (represented by its top lead SNP). We also showed the mapped gene when available.

eFigure 17: GSEA using sex-stratified GWAS results

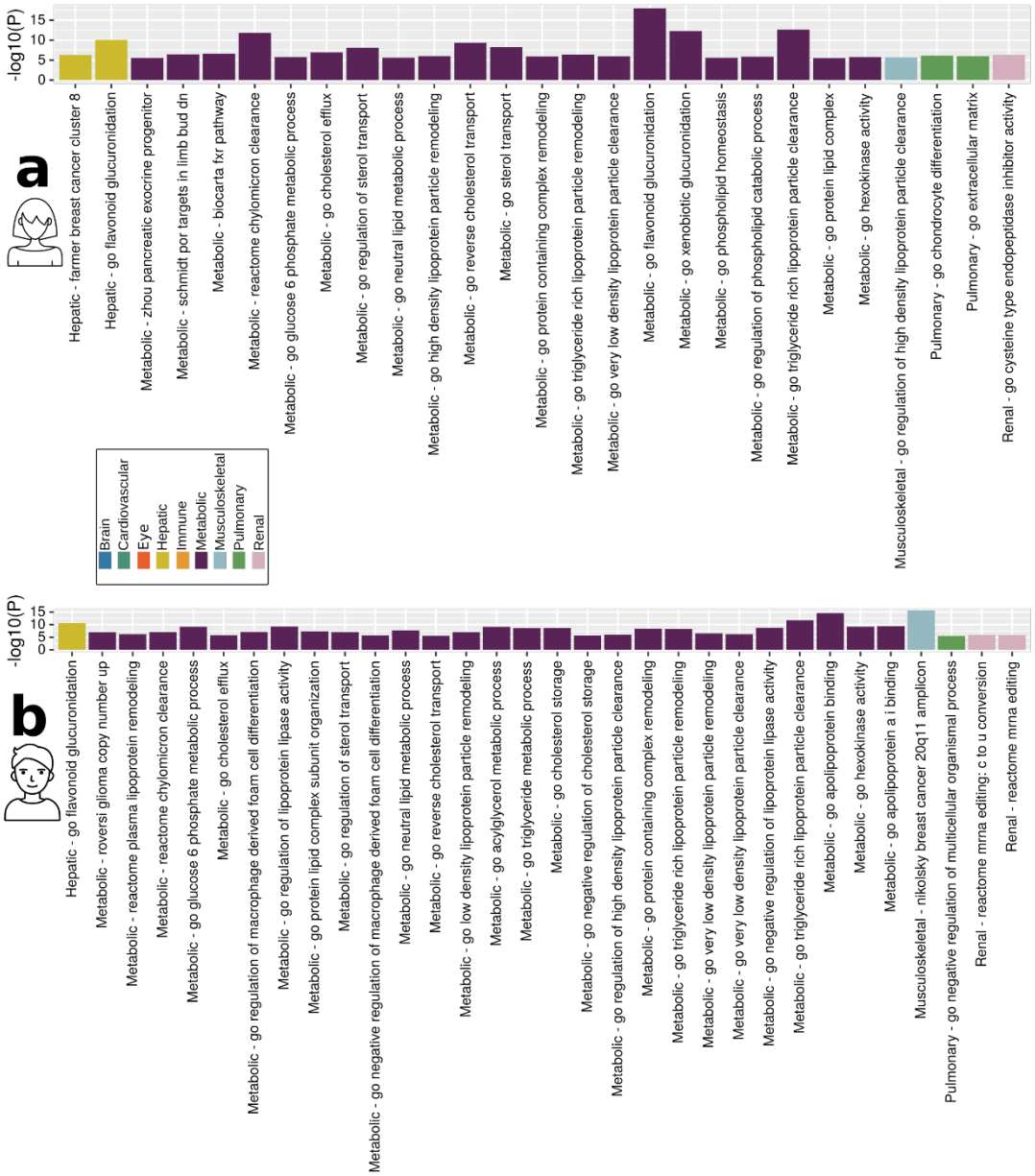

Gene-set enrichment analysis was performed using the GWAS summary statistics specific to females (**a**) and males (**b**).

eFigure 18: TEA correlations using sex-stratified GWAS results

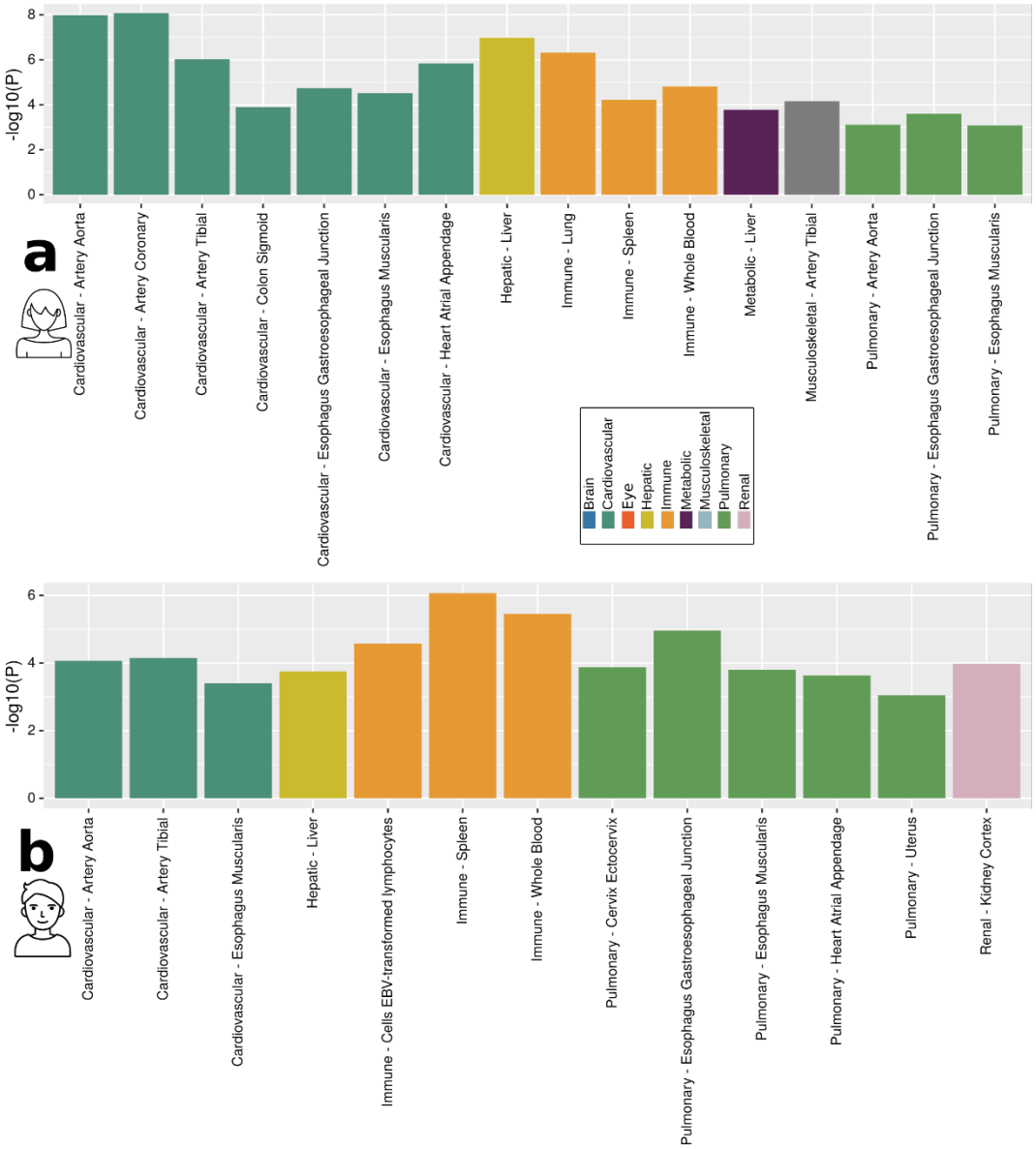

Tissue-specific enrichment analysis was performed using the GWAS summary statistics specific to females (**a**) and males (**b**).

eFigure 19: Genetic correlations using sex-stratified GWAS results

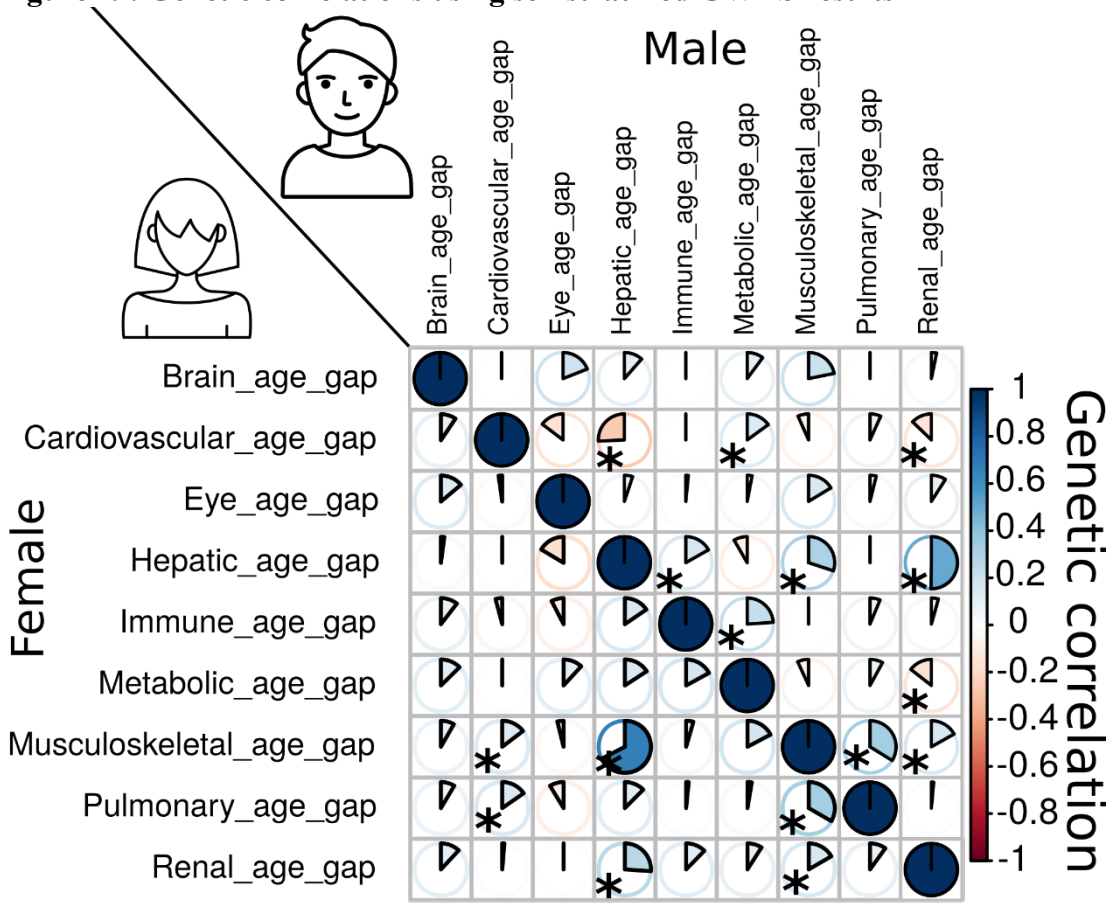

The Genetic correlation between each pair of BAGs using sex-stratified GWAS summary statistics from our analyses. Most of the genetic correlations showed consistency between females and males, albeit sex differences are evident in certain BAGs, particularly in the cardiovascular BAG results. Specifically, males exhibit dominant correlations between cardiovascular BAGs and hepatic and renal BAGs, while females demonstrate specific correlations with musculoskeletal and pulmonary BAGs.

eFigure 20: Mendelian randomization sensitivity check for the hepatic BAG on the musculoskeletal BAG

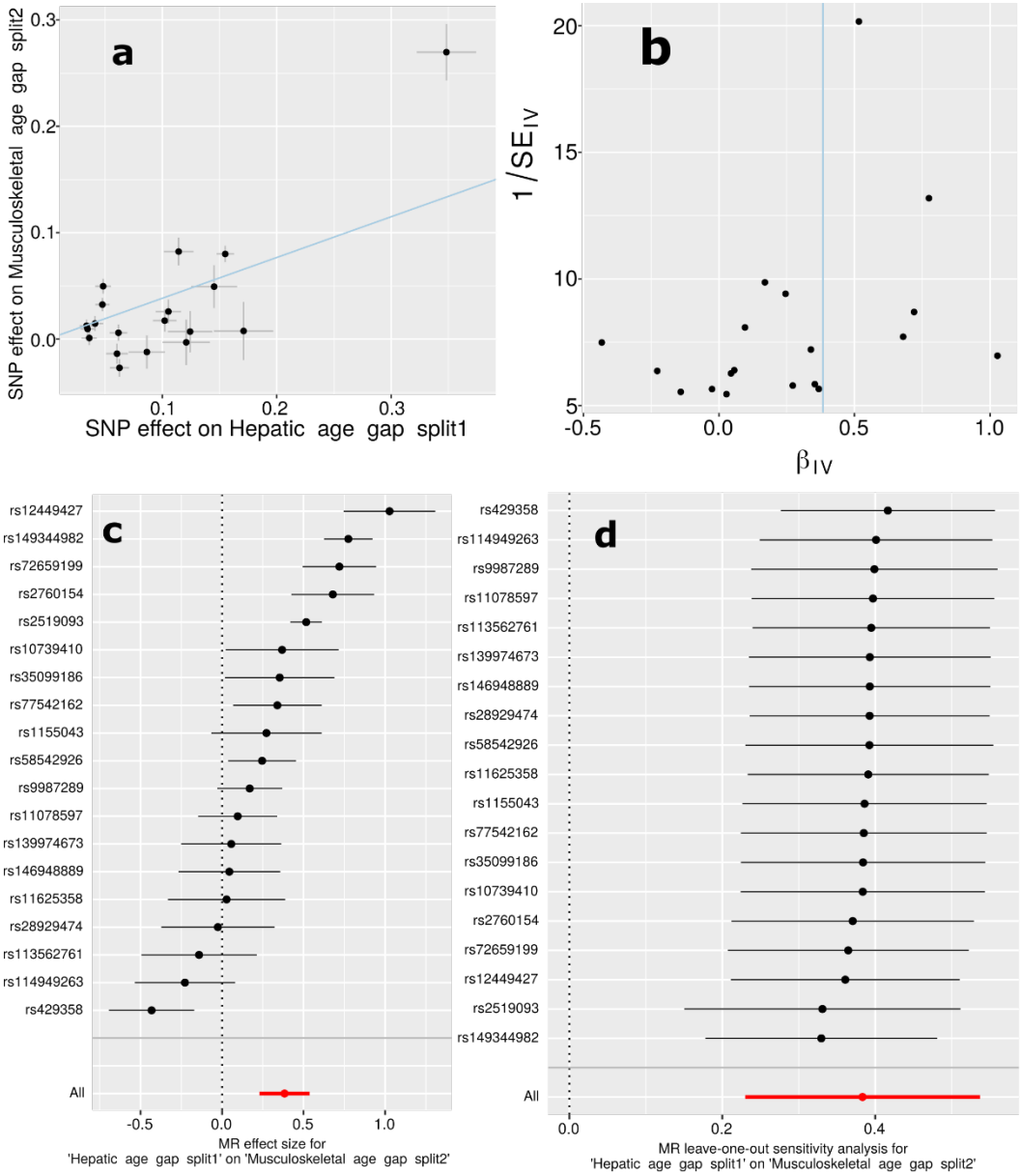

a) Scatter plot for the MR effect sizes of the exposure variable (hepatic BAG, *x*-axis, SD units) and the outcome variable (musculoskeletal BAG, *y*-axis, log OR) with standard error bars. The slopes of the regression line correspond to the causal effect sizes estimated by the IVW estimator. **b**) Funnel plot for the relationship between the causal effect of the exposure variable on the outcome variable. Each dot represents MR effect sizes estimated using each SNP as a separate instrument against the inverse of the standard error of the causal estimate. The vertical red line shows the MR estimates using all SNPs. **c**) Forest plot for the single-SNP MR results. Each line represents the MR effect (log OR) for the exposure variable on the outcome variable using only one SNP; the red line shows the MR effect using all SNPs together. **d**) Leave-one-out analysis of the exposure variable on the outcome variable. Each row represents the MR effect

(log OR) and the 95% CI by excluding that SNP from the analysis. The red line depicts the IVW estimator using all SNPs.

eFigure 21: Mendelian randomization sensitivity check for the musculoskeletal BAG on the hepatic BAG

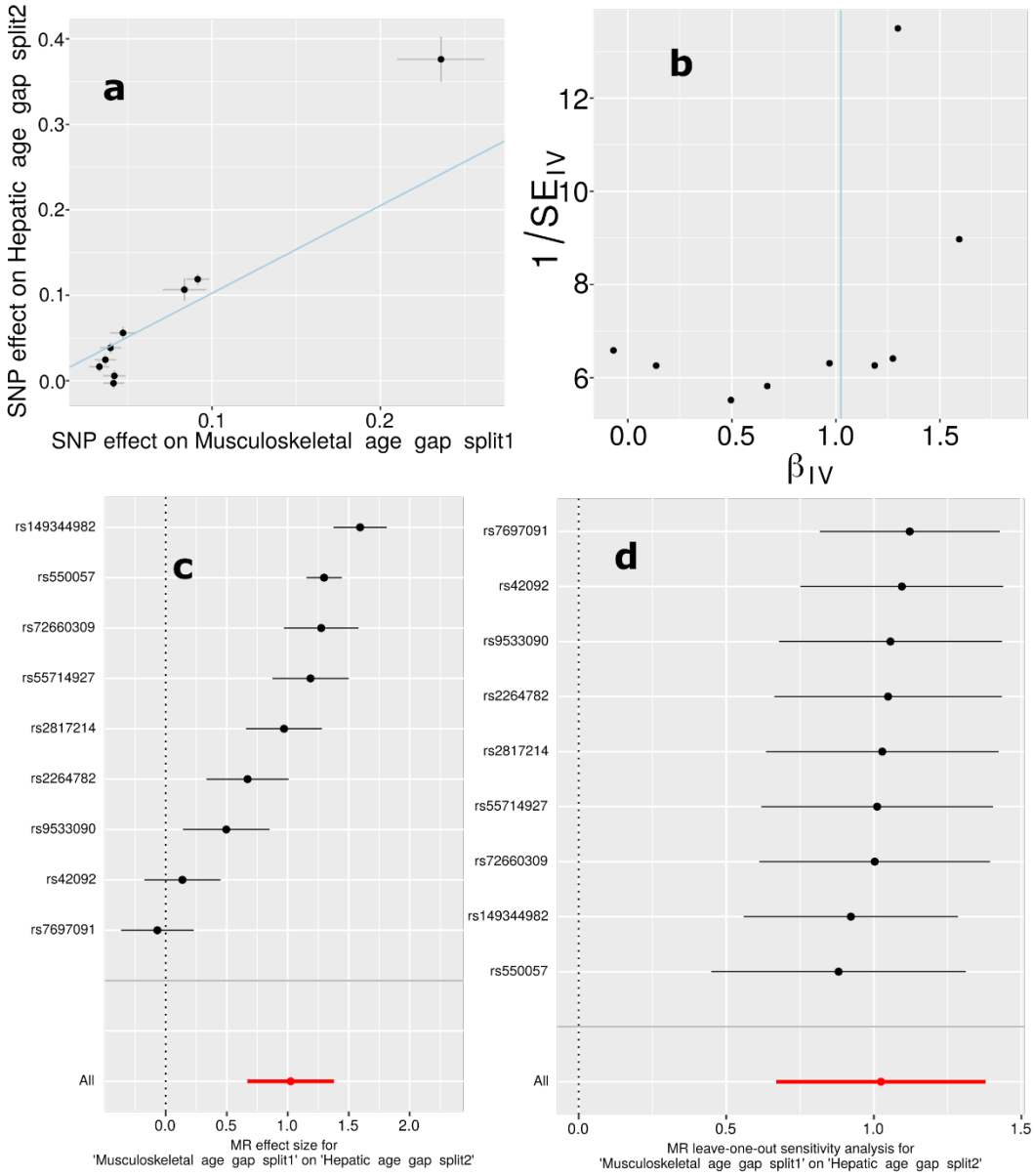

a) Scatter plot for the MR effect sizes of the exposure variable (musculoskeletal BAG, *x*-axis, SD units) and the outcome variable (hepatic BAG, *y*-axis, log OR) with standard error bars. The slopes of the regression line correspond to the causal effect sizes estimated by the IVW estimator. **b**) Funnel plot for the relationship between the causal effect of the exposure variable on the outcome variable. Each dot represents MR effect sizes estimated using each SNP as a separate instrument against the inverse of the standard error of the causal estimate. The vertical red line shows the MR estimates using all SNPs. **c**) Forest plot for the single-SNP MR results. Each line represents the MR effect (log OR) for the exposure variable on the outcome variable using only one SNP; the red line shows the MR effect using all SNPs together. **d**) Leave-one-out analysis of the exposure variable on the outcome variable. Each row represents the MR effect

(log OR) and the 95% CI by excluding that SNP from the analysis. The red line depicts the IVW estimator using all SNPs.

eFigure 22: Mendelian randomization sensitivity check for AD on the brain BAG

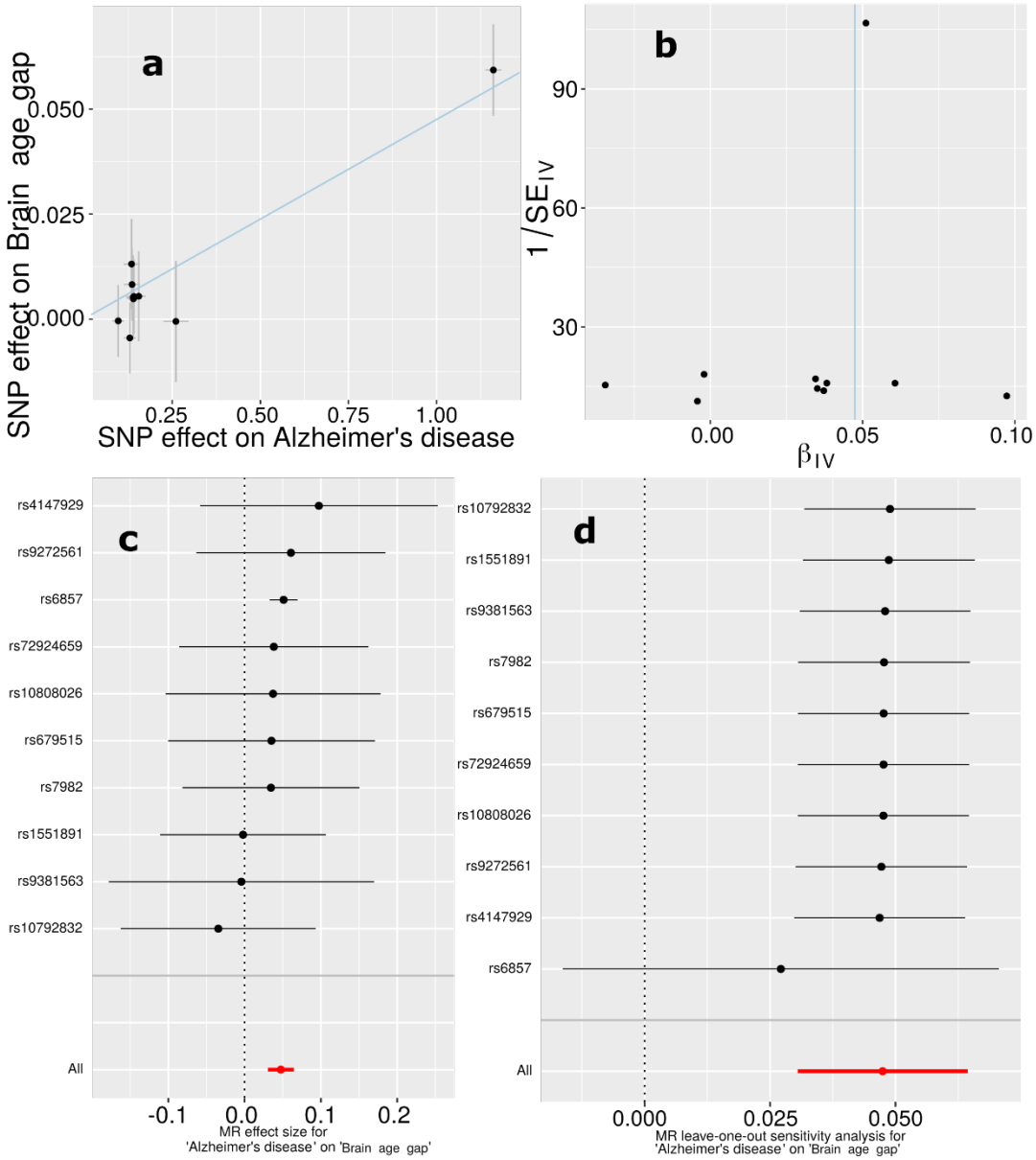

a) Scatter plot for the MR effect sizes of the exposure variable (AD, *x*-axis, SD units) and the outcome variable (brain BAG, *y*-axis, log OR) with standard error bars. The slopes of the regression line correspond to the causal effect sizes estimated by the IVW estimator. **b**) Funnel plot for the relationship between the causal effect of the exposure variable on the outcome variable. Each dot represents MR effect sizes estimated using each SNP as a separate instrument against the inverse of the standard error of the causal estimate. The vertical red line shows the MR estimates using all SNPs. **c**) Forest plot for the single-SNP MR results. Each line represents the MR effect (log OR) for the exposure variable on the outcome variable using only one SNP; the red line shows the MR effect using all SNPs together. **d**) Leave-one-out analysis of the exposure variable on the outcome variable. Each row represents the MR effect (log OR) and the 95% CI by excluding that SNP from the analysis. The red line depicts the IVW estimator using all SNPs.

eFigure 23: Mendelian randomization sensitivity check for AD on the hepatic BAG

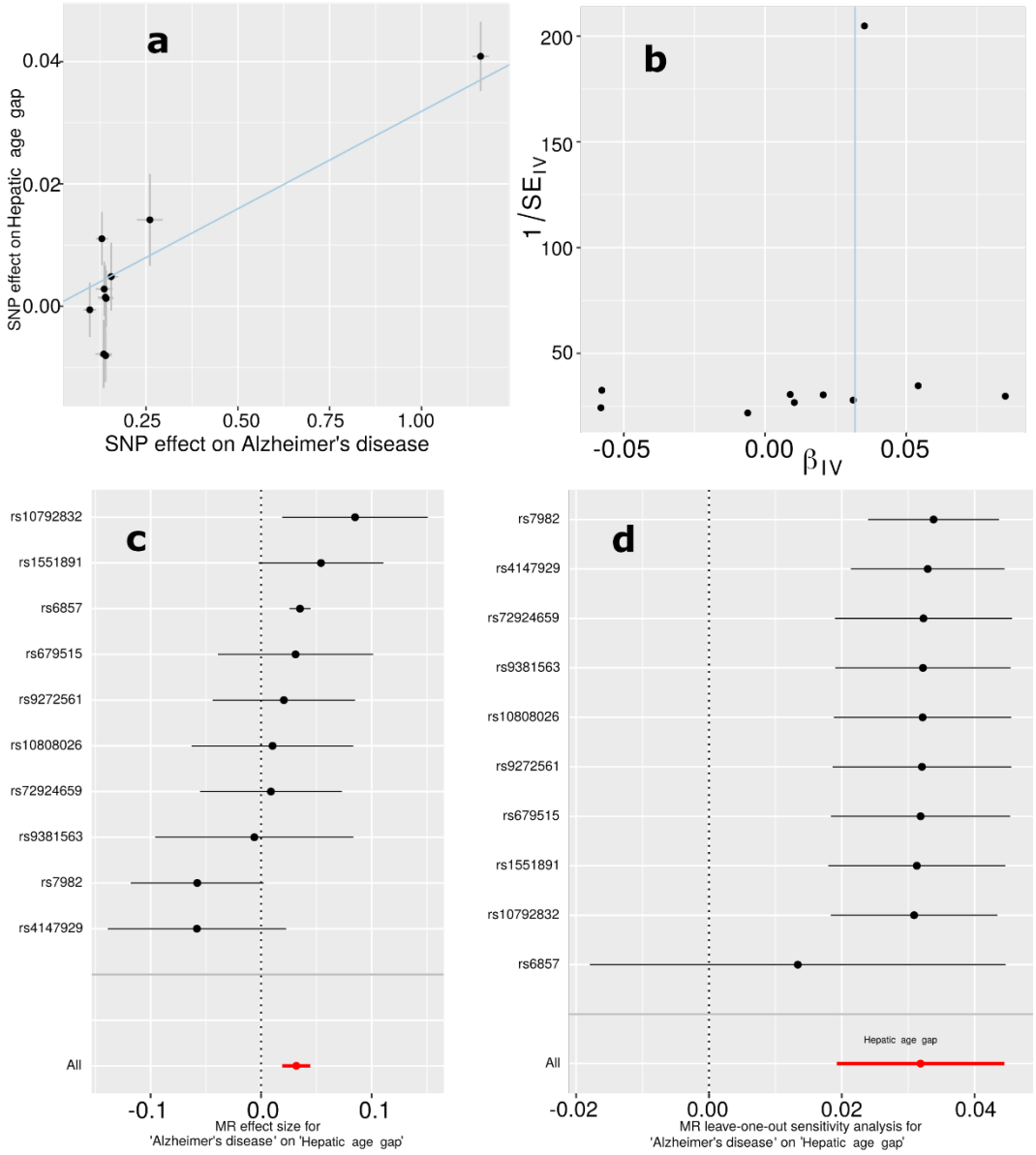

a) Scatter plot for the MR effect sizes of the exposure variable (AD, *x*-axis, SD units) and the outcome variable (hepatic BAG, *y*-axis, log OR) with standard error bars. The slopes of the regression line correspond to the causal effect sizes estimated by the IVW estimator. **b**) Funnel plot for the relationship between the causal effect of the exposure variable on the outcome variable. Each dot represents MR effect sizes estimated using each SNP as a separate instrument against the inverse of the standard error of the causal estimate. The vertical red line shows the MR estimates using all SNPs. **c**) Forest plot for the single-SNP MR results. Each line represents the MR effect (log OR) for the exposure variable on the outcome variable using only one SNP; the red line shows the MR effect using all SNPs together. **d**) Leave-one-out analysis of the exposure variable on the outcome variable. Each row represents the MR effect (log OR) and the 95% CI by excluding that SNP from the analysis. The red line depicts the IVW estimator using all SNPs.

539

eFigure 24: Mendelian randomization sensitivity check for Crohn's disease on the hepatic BAG

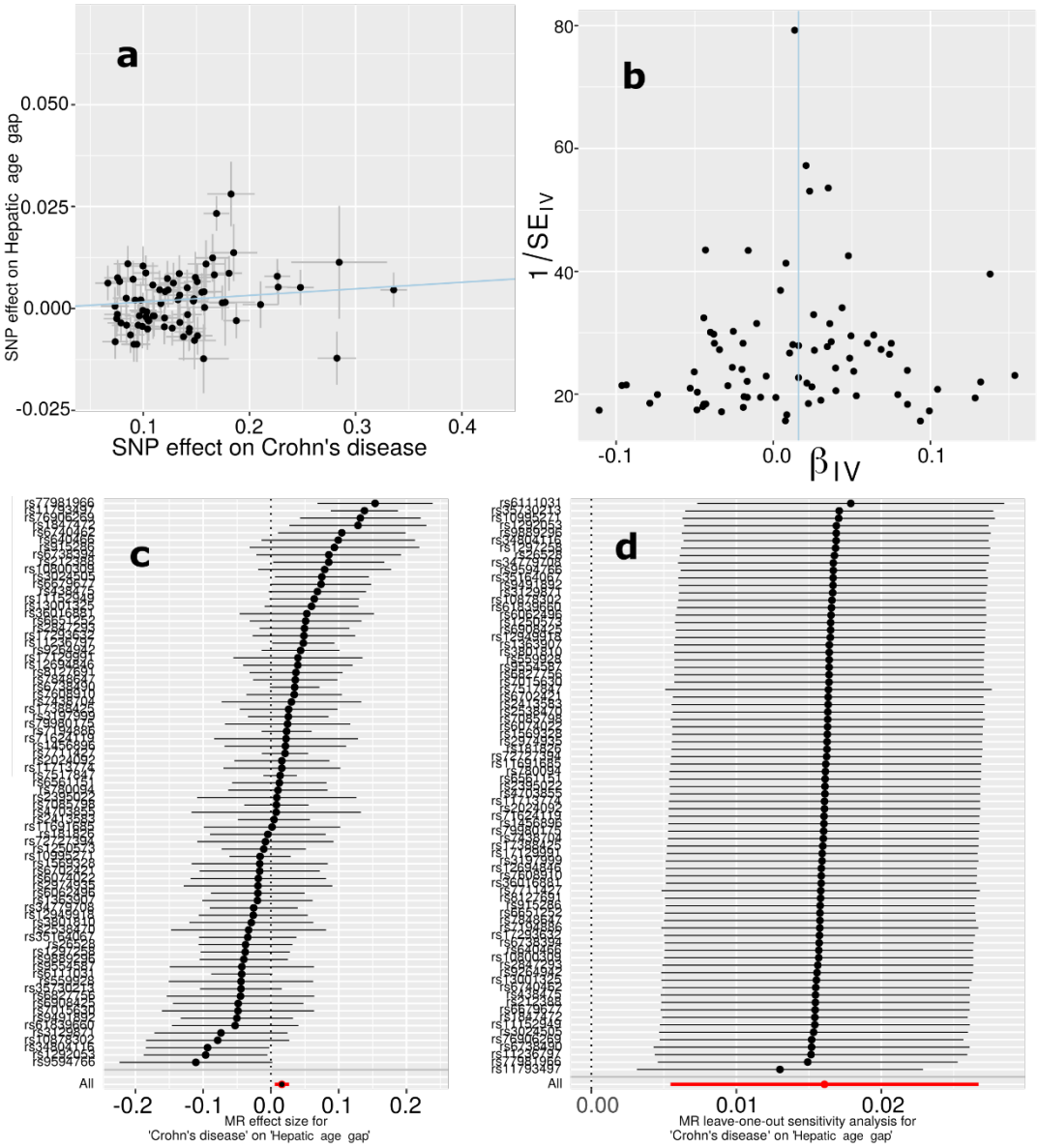

a) Scatter plot for the MR effect sizes of the exposure variable (Crohn's disease, *x*-axis, SD units) and the outcome variable (hepatic BAG, *y*-axis, log OR) with standard error bars. The slopes of the regression line correspond to the causal effect sizes estimated by the IVW estimator. **b**) Funnel plot for the relationship between the causal effect of the exposure variable on the outcome variable. Each dot represents MR effect sizes estimated using each SNP as a separate instrument against the inverse of the standard error of the causal estimate. The vertical red line shows the MR estimates using all SNPs. **c**) Forest plot for the single-SNP MR results. Each line represents the MR effect (log OR) for the exposure variable on the outcome variable using only one SNP; the red line shows the MR effect using all SNPs together. **d**) Leave-one-out analysis of the exposure variable on the outcome variable. Each row represents the MR effect (log OR) and

553 the 95% CI by excluding that SNP from the analysis. The red line depicts the IVW estimator
554 using all SNPs.
555

eFigure 25: Mendelian randomization sensitivity check for body weight on the immune BAG

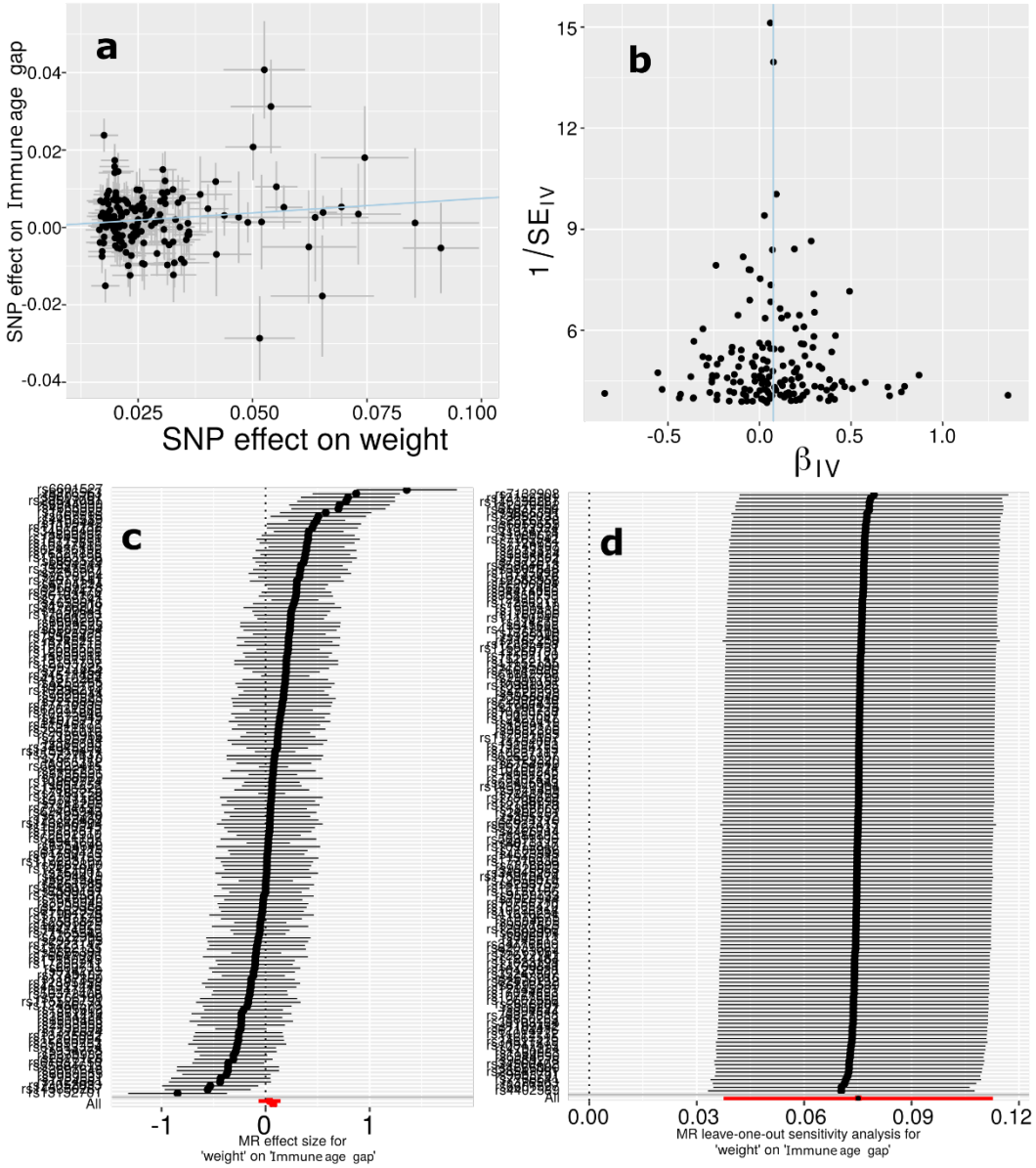

a) Scatter plot for the MR effect sizes of the exposure variable (body weight, *x*-axis, SD units) and the outcome variable (immune BAG, *y*-axis, log OR) with standard error bars. The slopes of the regression line correspond to the causal effect sizes estimated by the IVW estimator. **b**) Funnel plot for the relationship between the causal effect of the exposure variable on the outcome variable. Each dot represents MR effect sizes estimated using each SNP as a separate instrument against the inverse of the standard error of the causal estimate. The vertical red line shows the MR estimates using all SNPs. **c**) Forest plot for the single-SNP MR results. Each line represents the MR effect (log OR) for the exposure variable on the outcome variable using only one SNP; the red line shows the MR effect using all SNPs together. **d**) Leave-one-out analysis of the exposure variable on the outcome variable. Each row represents the MR effect (log OR) and

569 the 95% CI by excluding that SNP from the analysis. The red line depicts the IVW estimator
570 using all SNPs.
571

eFigure 26: Mendelian randomization sensitivity check for type 2 diabetes on the metabolic BAG

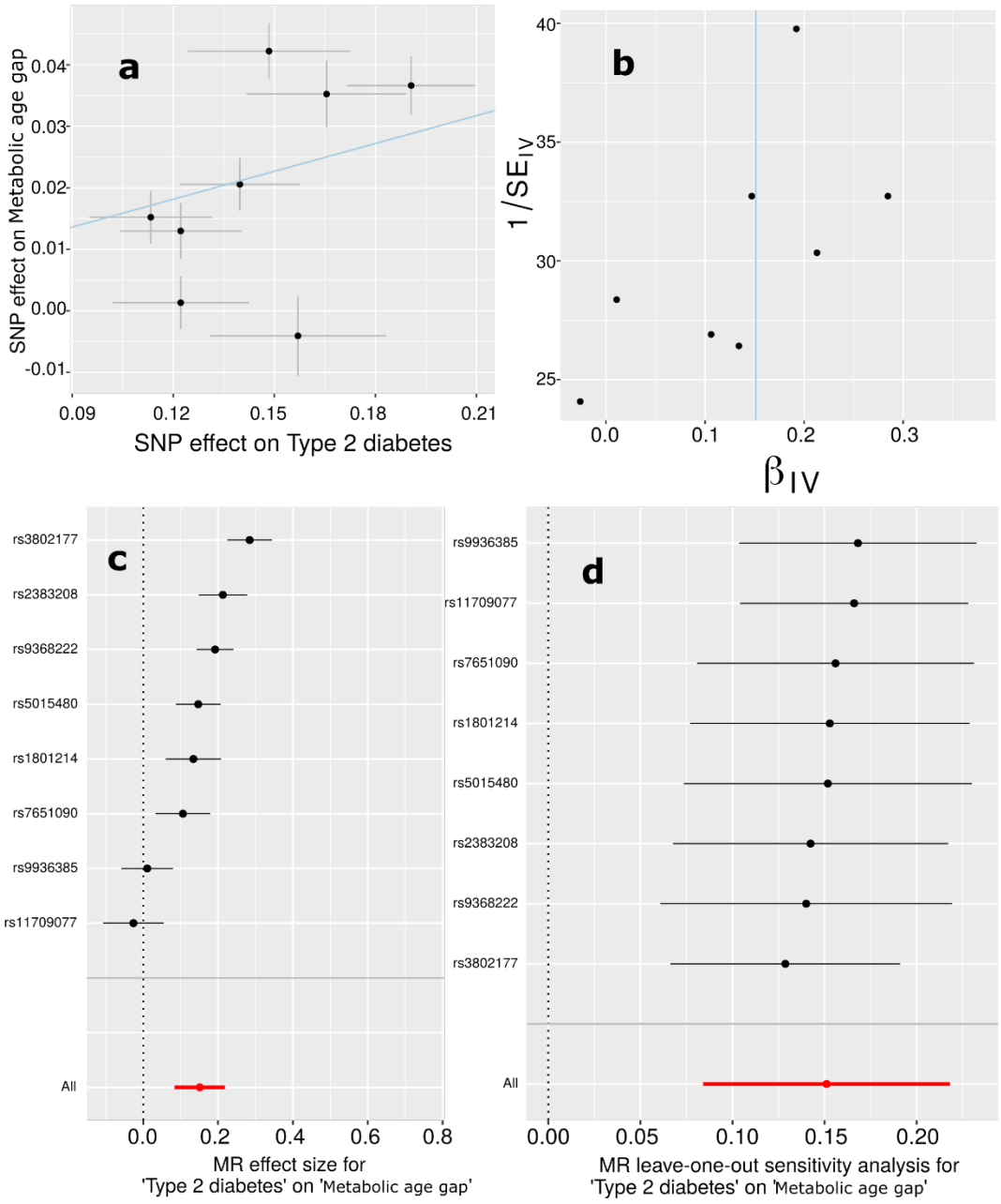

a) Scatter plot for the MR effect sizes of the exposure variable (type 2 diabetes, *x*-axis, SD units) and the outcome variable (metabolic BAG, *y*-axis, log OR) with standard error bars. The slopes of the regression line correspond to the causal effect sizes estimated by the IVW estimator. **b**) Funnel plot for the relationship between the causal effect of the exposure variable on the outcome variable. Each dot represents MR effect sizes estimated using each SNP as a separate instrument against the inverse of the standard error of the causal estimate. The vertical red line shows the MR estimates using all SNPs. **c**) Forest plot for the single-SNP MR results. Each line represents the MR effect (log OR) for the exposure variable on the outcome variable using only

583 one SNP; the red line shows the MR effect using all SNPs together. **d**) Leave-one-out analysis of
584 the exposure variable on the outcome variable. Each row represents the MR effect (log OR) and
585 the 95% CI by excluding that SNP from the analysis. The red line depicts the IVW estimator
586 using all SNPs.
587

eFigure 27: Mendelian randomization sensitivity check for AD on the musculoskeletal BAG

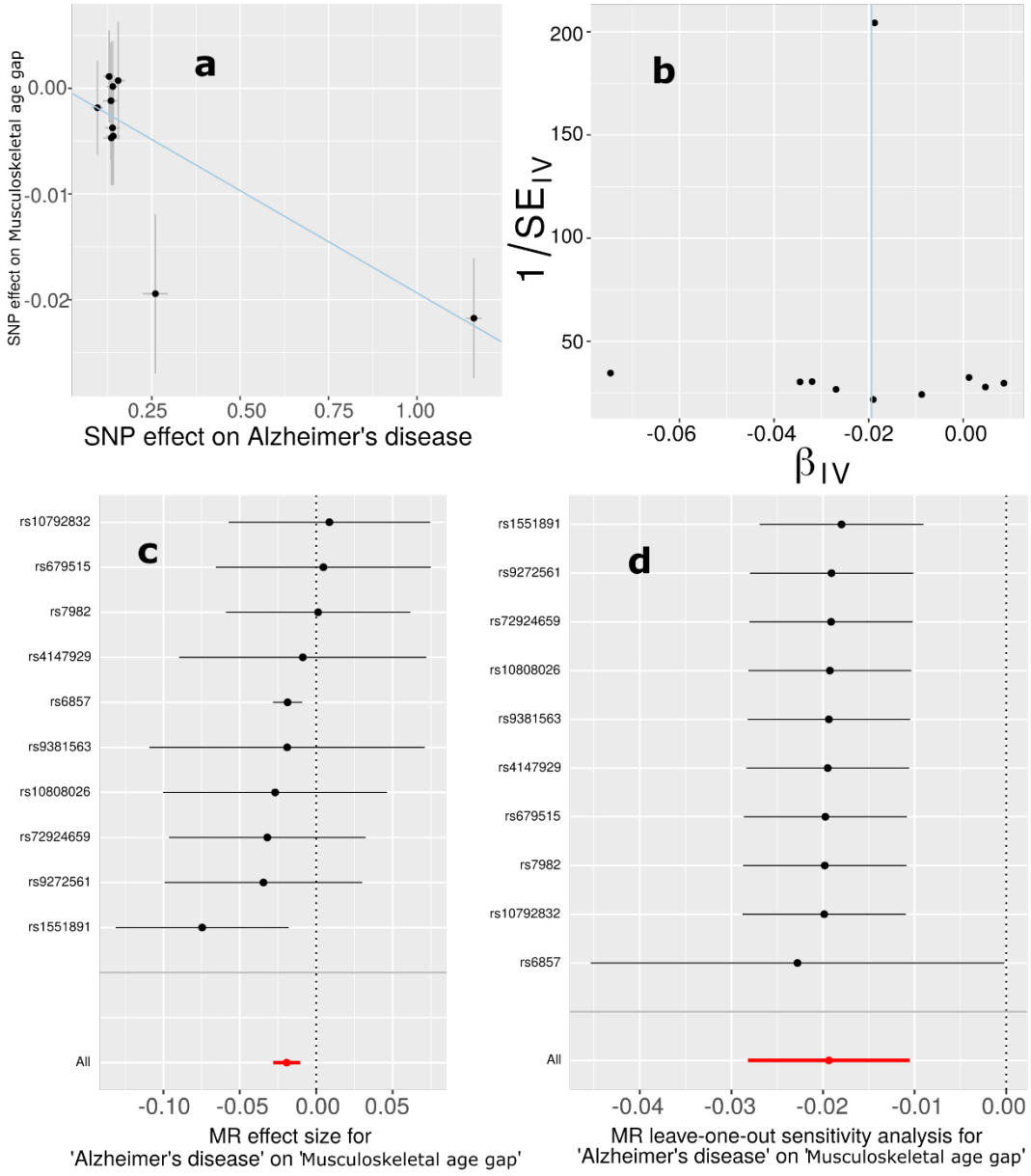

a) Scatter plot for the MR effect sizes of the exposure variable (AD, *x*-axis, SD units) and the outcome variable (musculoskeletal BAG, *y*-axis, log OR) with standard error bars. The slopes of the regression line correspond to the causal effect sizes estimated by the IVW estimator. **b**) Funnel plot for the relationship between the causal effect of the exposure variable on the outcome variable. Each dot represents MR effect sizes estimated using each SNP as a separate instrument against the inverse of the standard error of the causal estimate. The vertical red line shows the MR estimates using all SNPs. **c**) Forest plot for the single-SNP MR results. Each line represents the MR effect (log OR) for the exposure variable on the outcome variable using only one SNP; the red line shows the MR effect using all SNPs together. **d**) Leave-one-out analysis of the exposure variable on the outcome variable. Each row represents the MR effect (log OR) and the 95% CI by excluding that SNP from the analysis. The red line depicts the IVW estimator using all SNPs.

602

eFigure 28: Mendelian randomization sensitivity check for IBD on the musculoskeletal BAG

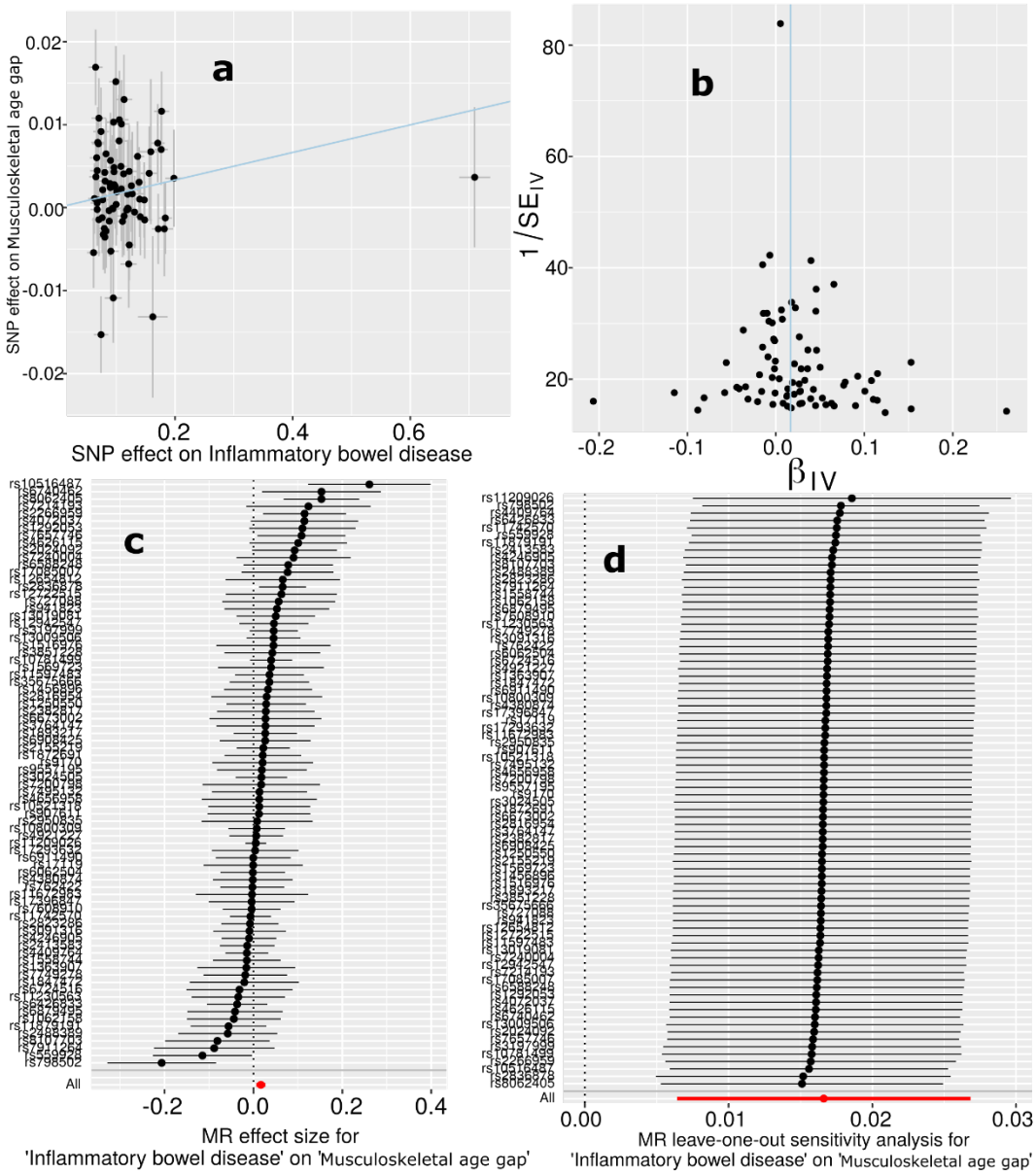

a) Scatter plot for the MR effect sizes of the exposure variable (IBD, *x*-axis, SD units) and the outcome variable (musculoskeletal BAG, *y*-axis, log OR) with standard error bars. The slopes of the regression line correspond to the causal effect sizes estimated by the IVW estimator. **b**) Funnel plot for the relationship between the causal effect of the exposure variable on the outcome variable. Each dot represents MR effect sizes estimated using each SNP as a separate instrument against the inverse of the standard error of the causal estimate. The vertical red line shows the MR estimates using all SNPs. **c**) Forest plot for the single-SNP MR results. Each line represents the MR effect (log OR) for the exposure variable on the outcome variable using only one SNP; the red line shows the MR effect using all SNPs together. **d**) Leave-one-out analysis of the exposure variable on the outcome variable. Each row represents the MR effect (log OR) and

616 the 95% CI by excluding that SNP from the analysis. The red line depicts the IVW estimator
617 using all SNPs.
618

eFigure 29: Mendelian randomization sensitivity check for PBC on the musculoskeletal BAG

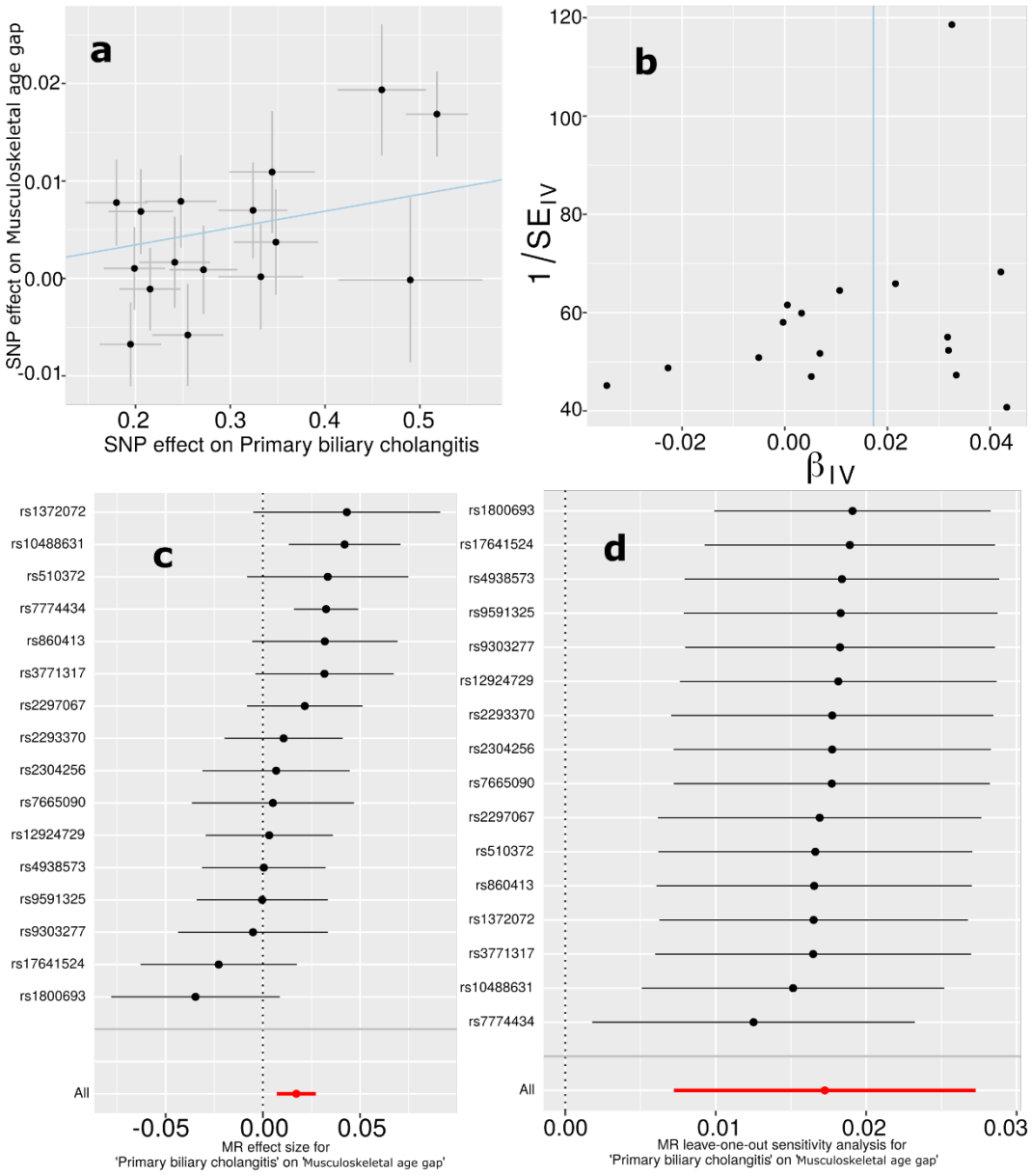

a) Scatter plot for the MR effect sizes of the exposure variable (PBC, *x*-axis, SD units) and the outcome variable (musculoskeletal BAG, *y*-axis, log OR) with standard error bars. The slopes of the regression line correspond to the causal effect sizes estimated by the IVW estimator. **b**) Funnel plot for the relationship between the causal effect of the exposure variable on the outcome variable. Each dot represents MR effect sizes estimated using each SNP as a separate instrument against the inverse of the standard error of the causal estimate. The vertical red line shows the MR estimates using all SNPs. **c**) Forest plot for the single-SNP MR results. Each line represents the MR effect (log OR) for the exposure variable on the outcome variable using only one SNP; the red line shows the MR effect using all SNPs together. **d**) Leave-one-out analysis of the exposure variable on the outcome variable. Each row represents the MR effect (log OR) and

632 the 95% CI by excluding that SNP from the analysis. The red line depicts the IVW estimator
633 using all SNPs.
634

eFigure 30: Mendelian randomization sensitivity check for weight on the musculoskeletal BAG

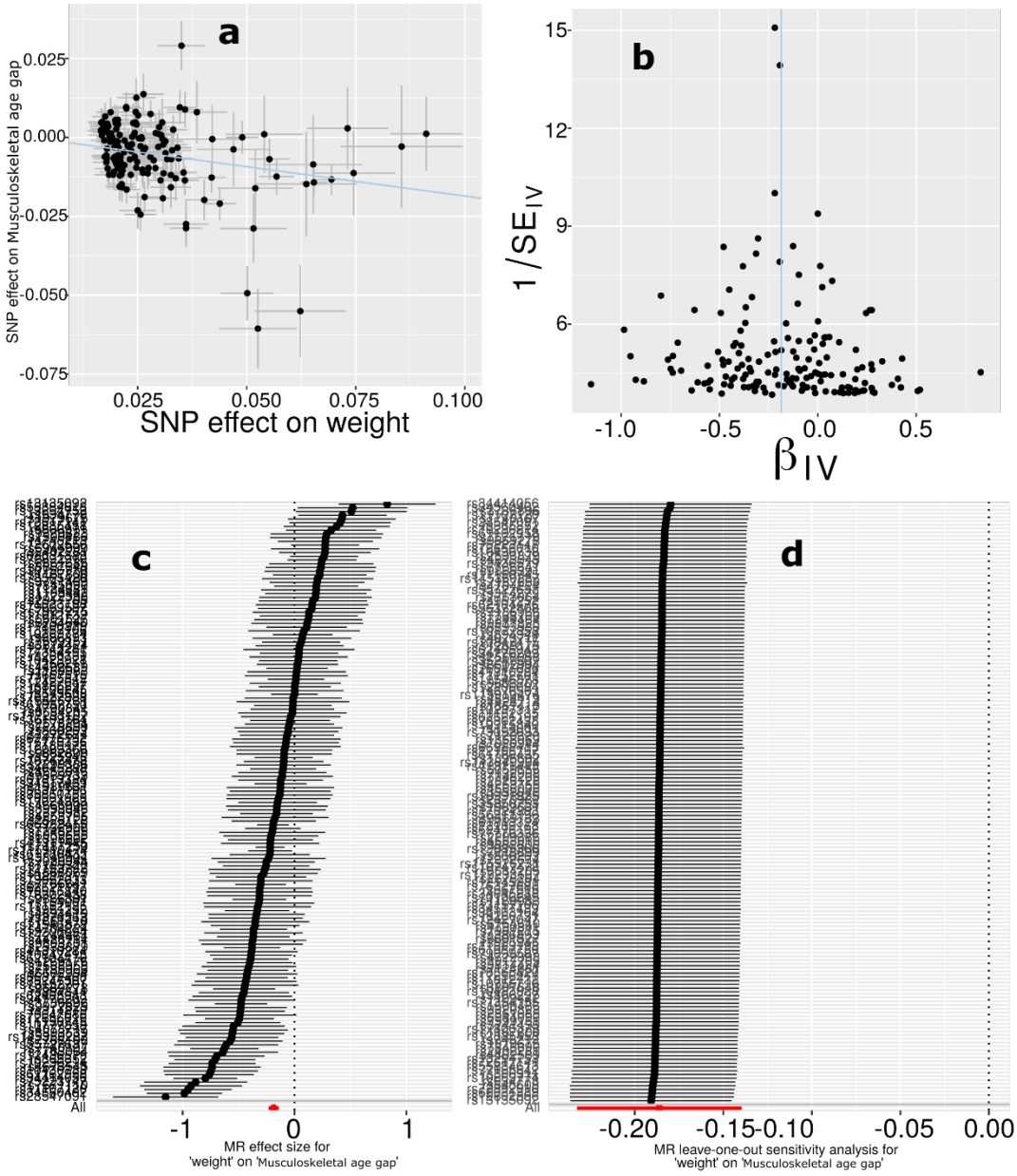

a) Scatter plot for the MR effect sizes of the exposure variable (body weight, *x*-axis, SD units) and the outcome variable (musculoskeletal BAG, *y*-axis, log OR) with standard error bars. The slopes of the regression line correspond to the causal effect sizes estimated by the IVW estimator. **b**) Funnel plot for the relationship between the causal effect of the exposure variable on the outcome variable. Each dot represents MR effect sizes estimated using each SNP as a separate instrument against the inverse of the standard error of the causal estimate. The vertical red line shows the MR estimates using all SNPs. **c**) Forest plot for the single-SNP MR results. Each line represents the MR effect (log OR) for the exposure variable on the outcome variable using only one SNP; the red line shows the MR effect using all SNPs together. **d**) Leave-one-out analysis of the exposure variable on the outcome variable. Each row represents the MR effect

(log OR) and the 95% CI by excluding that SNP from the analysis. The red line depicts the IVW estimator using all SNPs.

eFigure 31: Mendelian randomization sensitivity check for weight on the pulmonary BAG

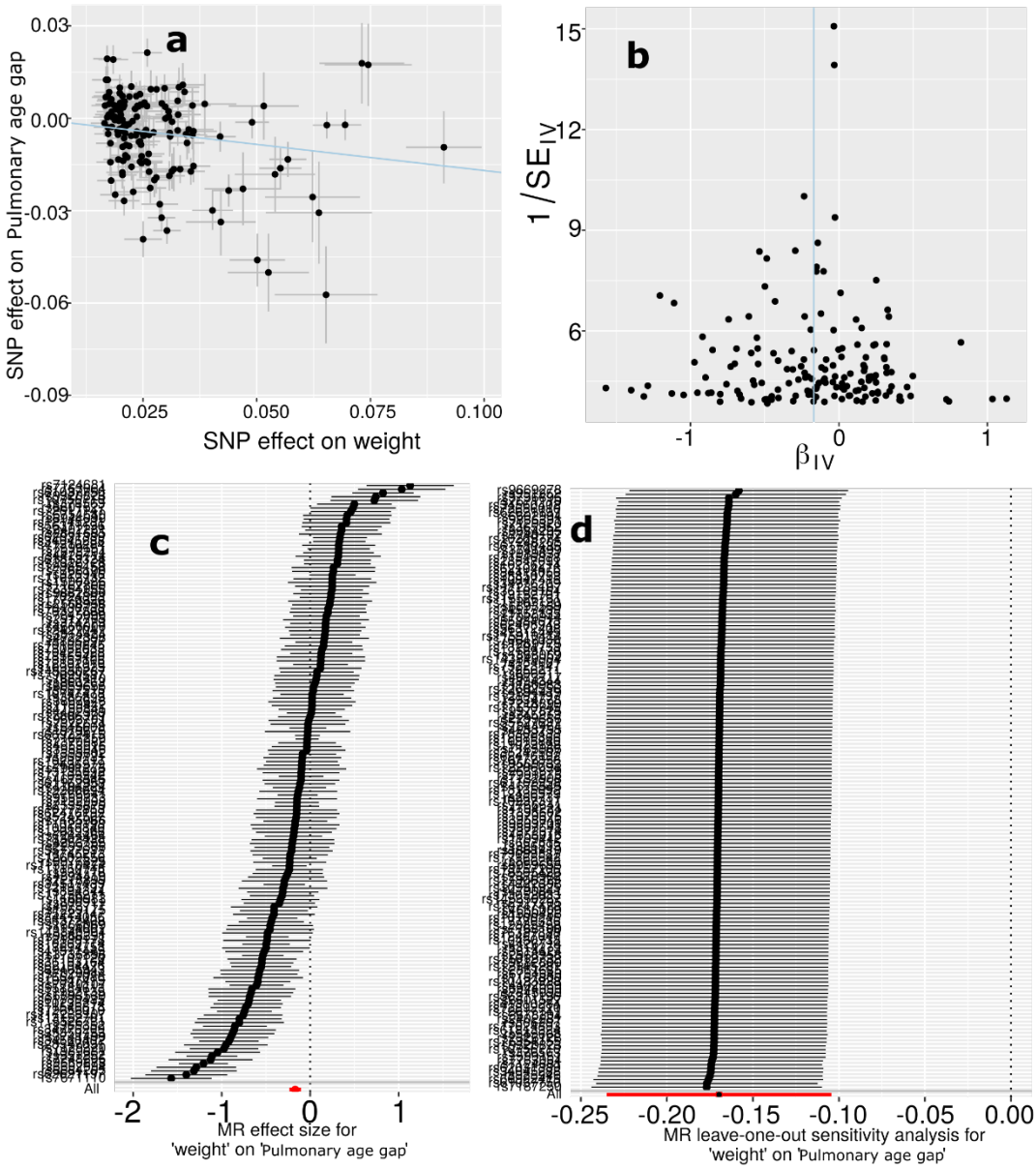

a) Scatter plot for the MR effect sizes of the exposure variable (body weight, *x*-axis, SD units) and the outcome variable (pulmonary BAG, *y*-axis, log OR) with standard error bars. The slopes of the regression line correspond to the causal effect sizes estimated by the IVW estimator. **b**) Funnel plot for the relationship between the causal effect of the exposure variable on the outcome variable. Each dot represents MR effect sizes estimated using each SNP as a separate instrument against the inverse of the standard error of the causal estimate. The vertical red line shows the MR estimates using all SNPs. **c**) Forest plot for the single-SNP MR results. Each line represents the MR effect (log OR) for the exposure variable on the outcome variable using only one SNP; the red line shows the MR effect using all SNPs together. **d**) Leave-one-out analysis of the exposure variable on the outcome variable. Each row represents the MR effect (log OR) and the 95% CI by excluding that SNP from the analysis. The red line depicts the IVW estimator using all SNPs.

eFigure 32: Mendelian randomization sensitivity check for AD on the renal BAG

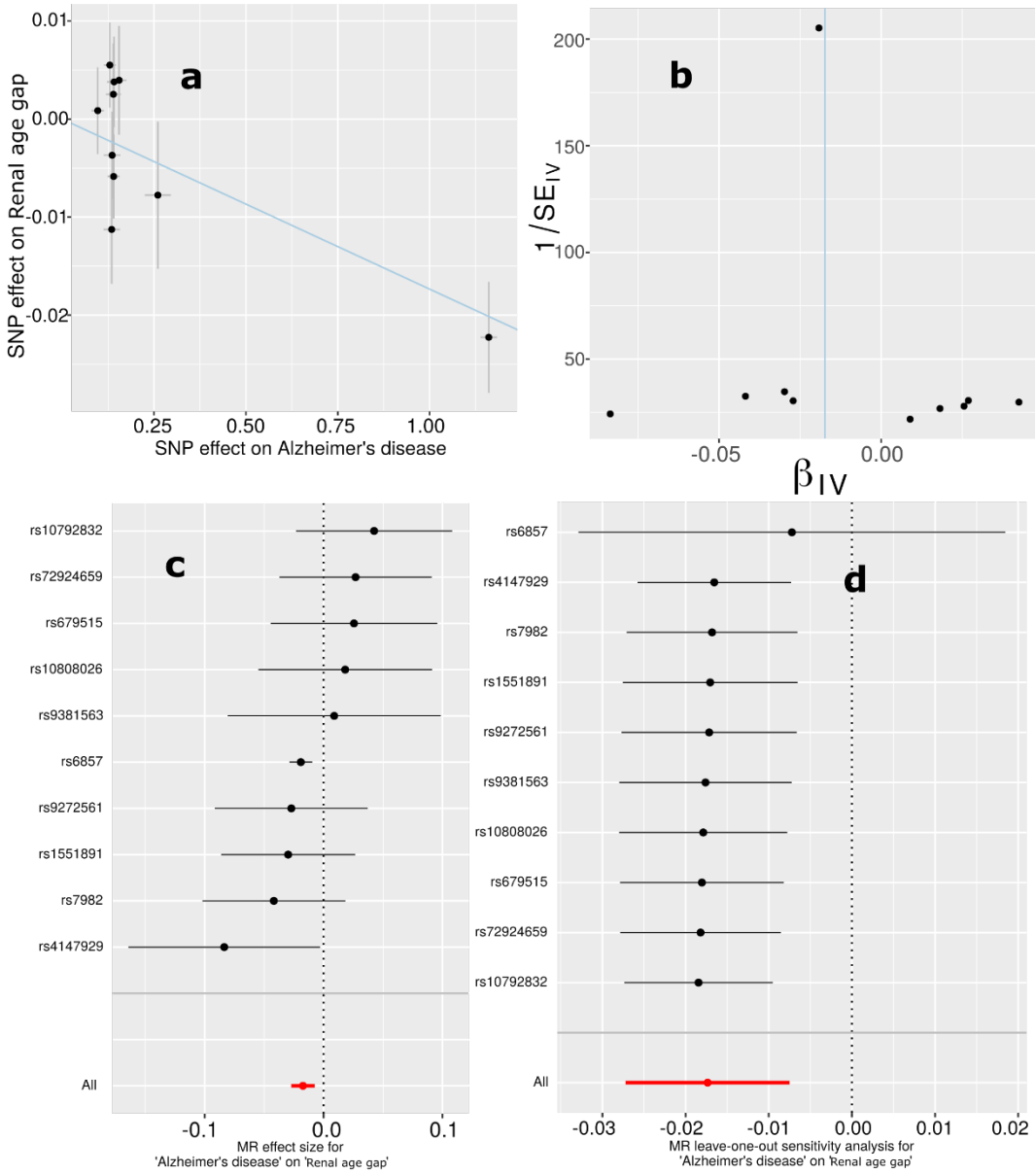

a) Scatter plot for the MR effect sizes of the exposure variable (AD, *x*-axis, SD units) and the outcome variable (renal BAG, *y*-axis, log OR) with standard error bars. The slopes of the regression line correspond to the causal effect sizes estimated by the IVW estimator. **b**) Funnel plot for the relationship between the causal effect of the exposure variable on the outcome variable. Each dot represents MR effect sizes estimated using each SNP as a separate instrument against the inverse of the standard error of the causal estimate. The vertical red line shows the MR estimates using all SNPs. **c**) Forest plot for the single-SNP MR results. Each line represents the MR effect (log OR) for the exposure variable on the outcome variable using only one SNP; the red line shows the MR effect using all SNPs together. **d**) Leave-one-out analysis of the exposure variable on the outcome variable. Each row represents the MR effect (log OR) and the 95% CI by excluding that SNP from the analysis. The red line depicts the IVW estimator using all SNPs.

eFigure 33: Mendelian randomization sensitivity check for weight on the renal BAG

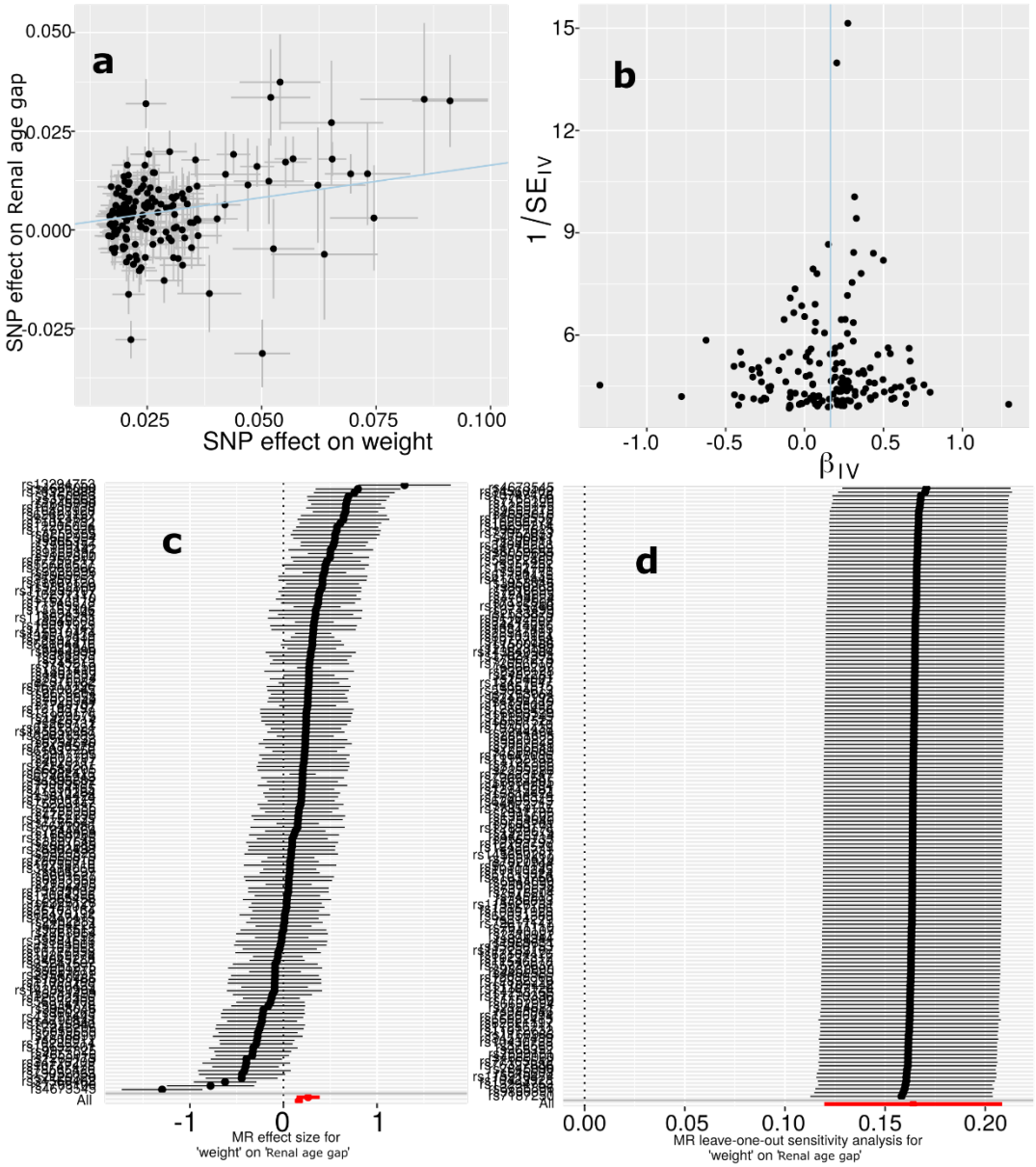

a) Scatter plot for the MR effect sizes of the exposure variable (body weight, *x*-axis, SD units) and the outcome variable (renal BAG, *y*-axis, log OR) with standard error bars. The slopes of the regression line correspond to the causal effect sizes estimated by the IVW estimator. **b**) Funnel plot for the relationship between the causal effect of the exposure variable on the outcome variable. Each dot represents MR effect sizes estimated using each SNP as a separate instrument against the inverse of the standard error of the causal estimate. The vertical red line shows the MR estimates using all SNPs. **c**) Forest plot for the single-SNP MR results. Each line represents the MR effect (log OR) for the exposure variable on the outcome variable using only one SNP; the red line shows the MR effect using all SNPs together. **d**) Leave-one-out analysis of the exposure variable on the outcome variable. Each row represents the MR effect (log OR) and the 95% CI by excluding that SNP from the analysis. The red line depicts the IVW estimator using all SNPs.

eFigure 34: Mendelian randomization sensitivity check for the brain BAG on sleep duration

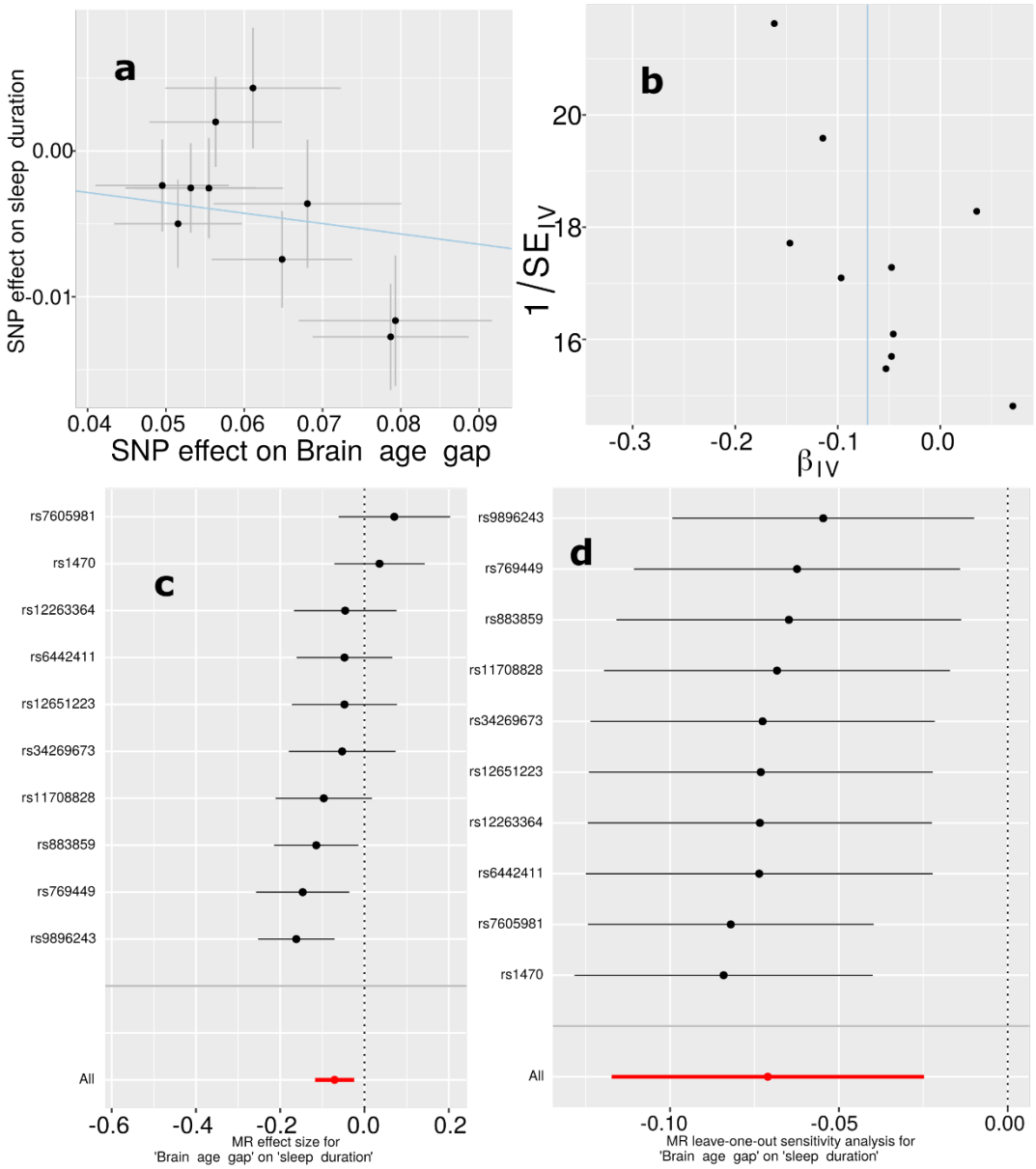

a) Scatter plot for the MR effect sizes of the exposure variable (brain BAG, *x*-axis, SD units) and the outcome variable (sleep duration, *y*-axis, log OR) with standard error bars. The slopes of the regression line correspond to the causal effect sizes estimated by the IVW estimator. **b**) Funnel plot for the relationship between the causal effect of the exposure variable on the outcome variable. Each dot represents MR effect sizes estimated using each SNP as a separate instrument against the inverse of the standard error of the causal estimate. The vertical red line shows the MR estimates using all SNPs. **c**) Forest plot for the single-SNP MR results. Each line represents the MR effect (log OR) for the exposure variable on the outcome variable using only one SNP; the red line shows the MR effect using all SNPs together. **d**) Leave-one-out analysis of the exposure variable on the outcome variable. Each row represents the MR effect (log OR) and the

706 95% CI by excluding that SNP from the analysis. The red line depicts the IVW estimator using
707 all SNPs.
708

eFigure 35: Mendelian randomization sensitivity check for the cardiovascular BAG on triglycerides to lipids ratio in very large VLDL

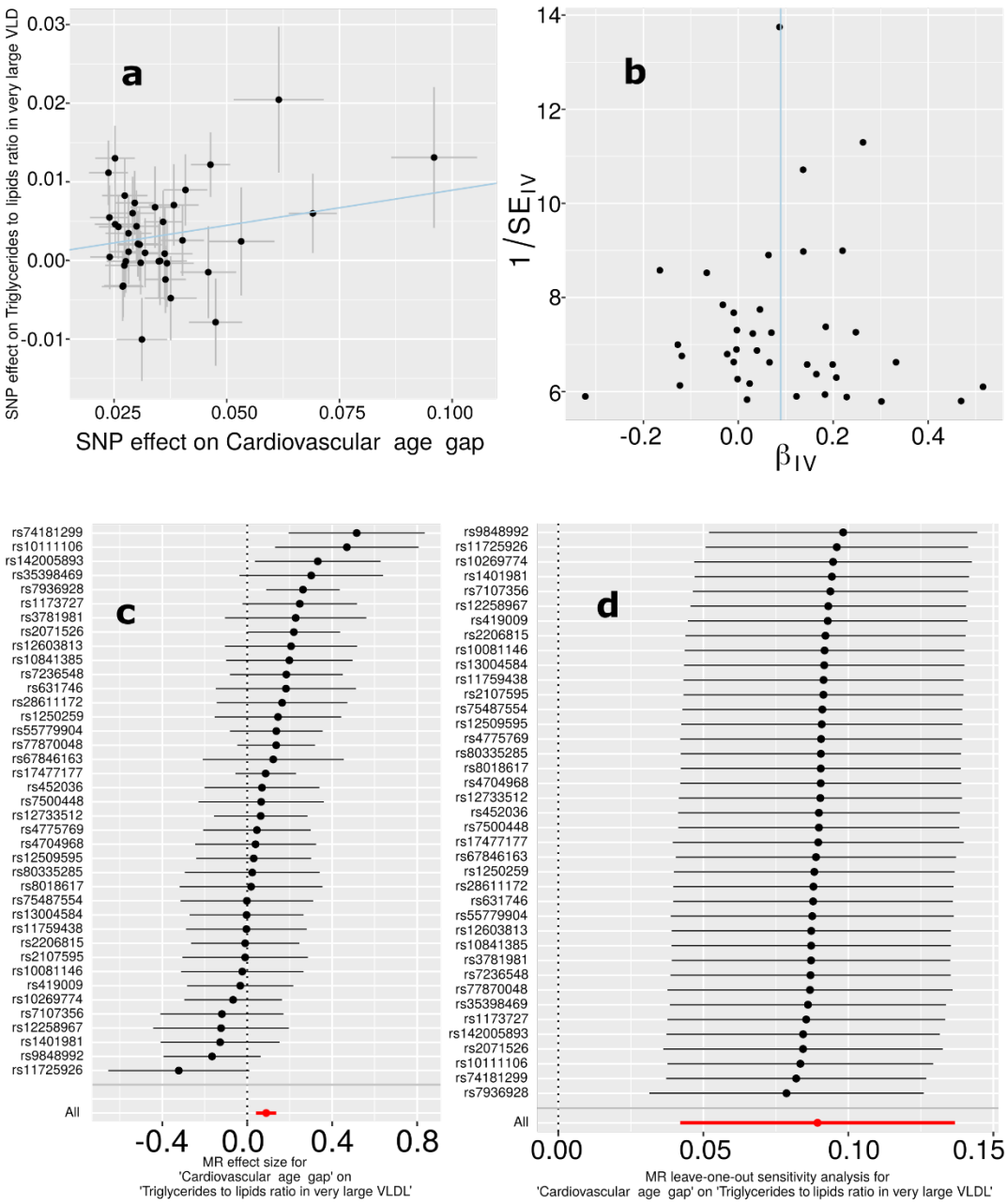

a) Scatter plot for the MR effect sizes of the exposure variable (cardiovascular BAG, *x*-axis, SD units) and the outcome variable (triglycerides to lipids ratio in very large VLDL, *y*-axis, log OR) with standard error bars. The slopes of the regression line correspond to the causal effect sizes estimated by the IVW estimator. **b**) Funnel plot for the relationship between the causal effect of the exposure variable on the outcome variable. Each dot represents MR effect sizes estimated using each SNP as a separate instrument against the inverse of the standard error of the causal estimate. The vertical red line shows the MR estimates using all SNPs. **c**) Forest plot for the single-SNP MR results. Each line represents the MR effect (log OR) for the exposure variable on the outcome variable using only one SNP; the red line shows the MR effect using all SNPs

721 together. **d**) Leave-one-out analysis of the exposure variable on the outcome variable. Each row
722 represents the MR effect (log OR) and the 95% CI by excluding that SNP from the analysis. The
723 red line depicts the IVW estimator using all SNPs.
724

eFigure 36: Mendelian randomization sensitivity check for the metabolic BAG on weight

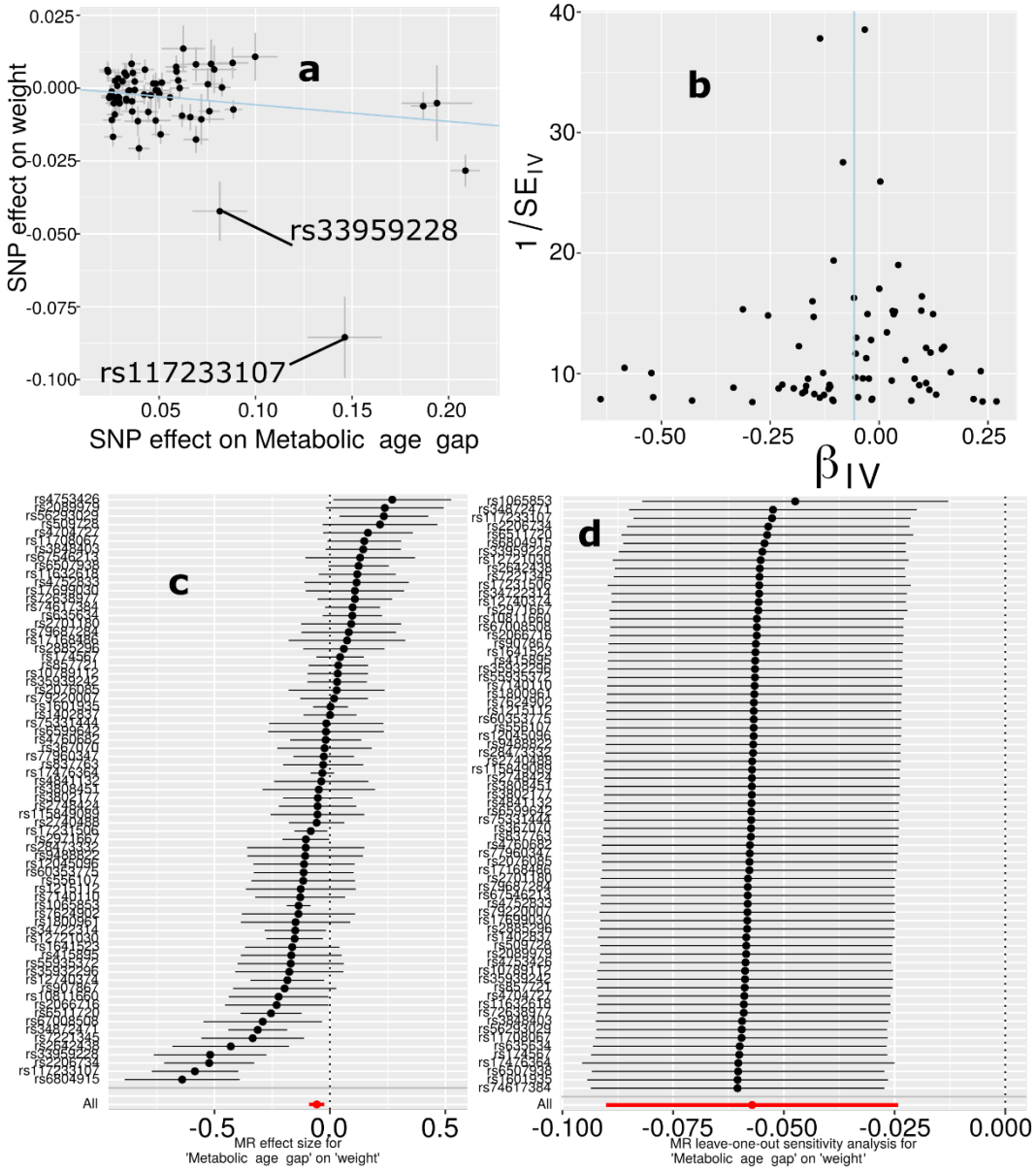

a) Scatter plot for the MR effect sizes of the exposure variable (metabolic BAG, *x*-axis, SD units) and the outcome variable (body weight, *y*-axis, log OR) with standard error bars. The slopes of the regression line correspond to the causal effect sizes estimated by the IVW estimator. **b**) Funnel plot for the relationship between the causal effect of the exposure variable on the outcome variable. Each dot represents MR effect sizes estimated using each SNP as a separate instrument against the inverse of the standard error of the causal estimate. The vertical red line shows the MR estimates using all SNPs. **c**) Forest plot for the single-SNP MR results. Each line represents the MR effect (log OR) for the exposure variable on the outcome variable using only one SNP; the red line shows the MR effect using all SNPs together. **d**) Leave-one-out analysis of the exposure variable on the outcome variable. Each row represents the MR effect (log OR) and the 95% CI by excluding that SNP from the analysis. The red line depicts the IVW estimator using all SNPs.

eFigure 37: Mendelian randomization sensitivity check for the pulmonary BAG on weight

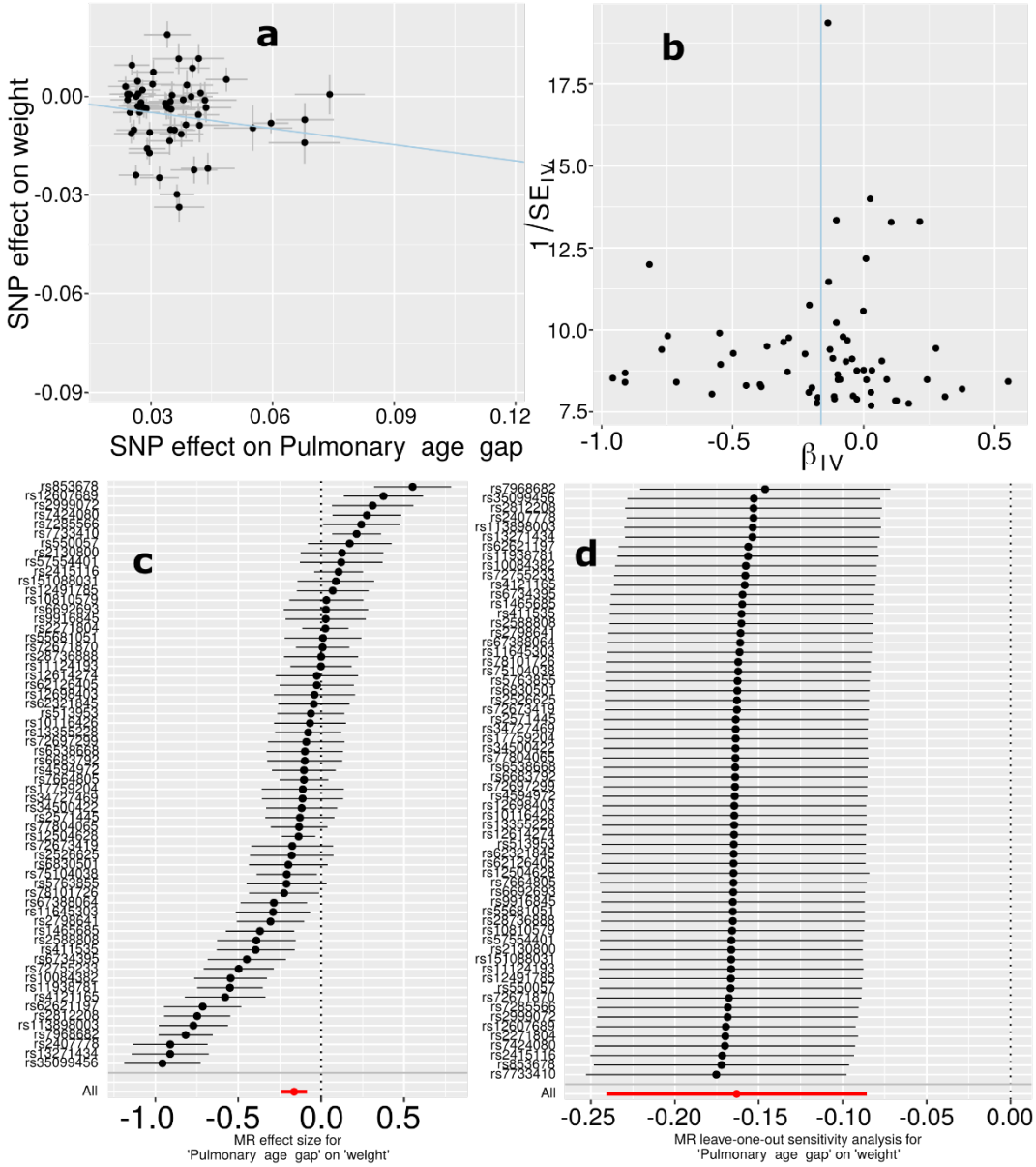

a) Scatter plot for the MR effect sizes of the exposure variable (pulmonary BAG, *x*-axis, SD units) and the outcome variable (body weight, *y*-axis, log OR) with standard error bars. The slopes of the regression line correspond to the causal effect sizes estimated by the IVW estimator. **b**) Funnel plot for the relationship between the causal effect of the exposure variable on the outcome variable. Each dot represents MR effect sizes estimated using each SNP as a separate instrument against the inverse of the standard error of the causal estimate. The vertical red line shows the MR estimates using all SNPs. **c**) Forest plot for the single-SNP MR results. Each line represents the MR effect (log OR) for the exposure variable on the outcome variable using only one SNP; the red line shows the MR effect using all SNPs together. **d**) Leave-one-out analysis of the exposure variable on the outcome variable. Each row represents the MR effect (log OR) and the 95% CI by excluding that SNP from the analysis. The red line depicts the IVW estimator using all SNPs.

eFigure 38: Causal multi-organ network between the nine biological age gaps and 17 clinical traits of chronic diseases, lifestyle factors, and cognition

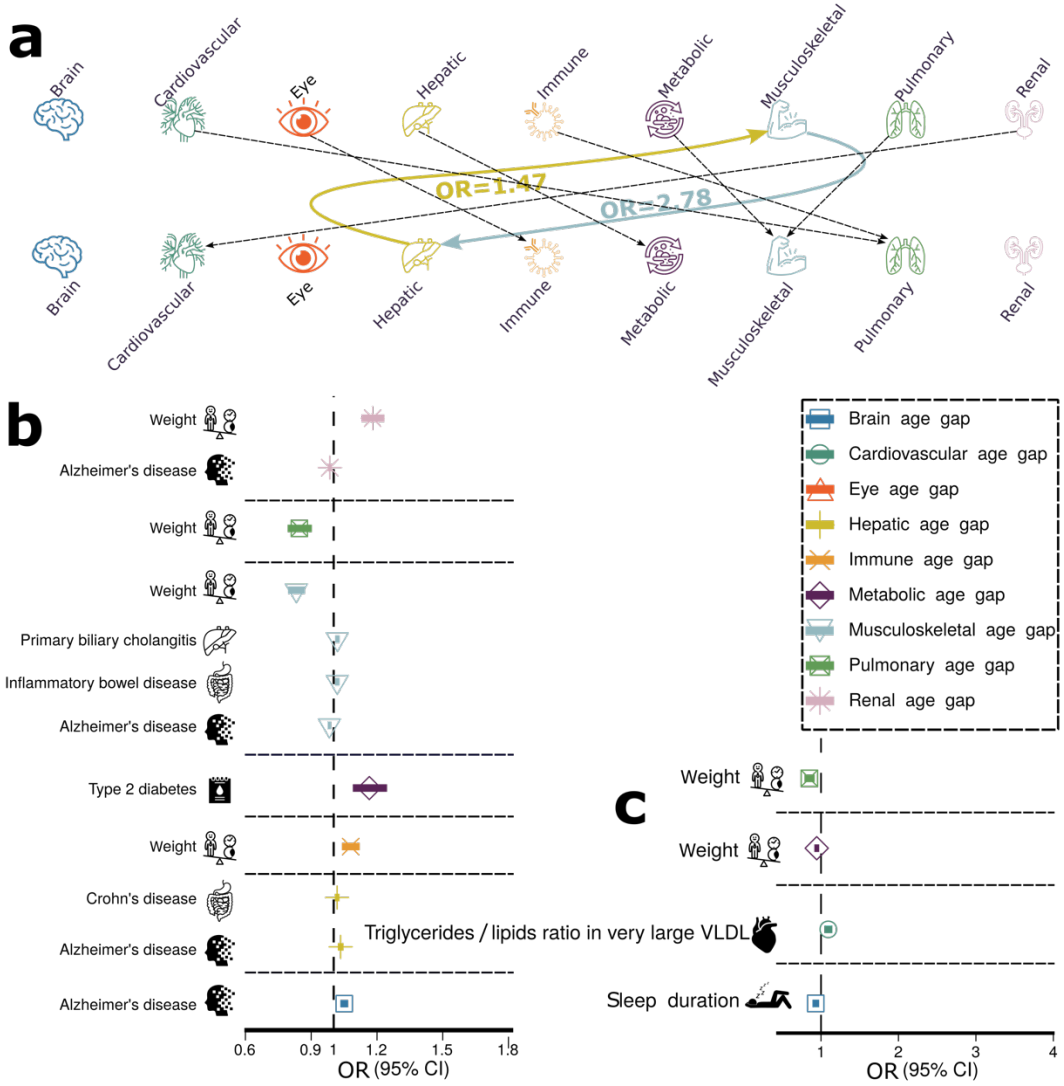

a) Causal inference between each pair of BAGs using bi-directional two-sample Mendelian randomization by excluding overlapping populations. The colored lines represent causal effects that survived the correction for multiple comparisons using the Bonferroni method; the dotted lines denote the nominal significant causal effects (P-value < 0.05). **b**) The forward Mendelian randomization investigates the causal inference of 17 unbiasedly selected exposure variables on the nine outcome variables (i.e., the nine BAGs). **c**) The inverse Mendelian randomization examines the causal inference of the 9 BAGs on the 17 clinical traits. We present the tests passing the statistical significance after adjusting for multiple comparisons using the Bonferroni correction. The OR and the 95% confidence interval are presented. Abbreviation: VLDL: very low-density lipoprotein; CI: confidence interval; OR: odds ratio.

eTable 1: Heritability estimates using the GCTA software

A) **Original sample sizes.** Original sample sizes were used to estimate the heritability for the nine organ systems.

BAG	h^2	h^2 SE	P-value	*N*
Brain	0.47	0.02	$<1x10^{-10}$	30,108
Cardiovascular	0.27	0.006	$<1x10^{-10}$	111,543
Eye	0.38	0.02	$<1x10^{-10}$	36,004
Hepatic	0.23	0.006	$<1x10^{-10}$	111,543
Immune	0.20	0.004	$<1x10^{-10}$	111,543
Metabolic	0.29	0.006	$<1x10^{-10}$	111,543
Musculoskeletal	0.24	0.004	$<1x10^{-10}$	111,543
Pulmonary	0.36	0.006	$<1x10^{-10}$	111,543
Renal	0.30	0.006	$<1x10^{-10}$	111,543

B) **Down-sampled sample sizes.** For the eight BAGs except for the brain BAG, we randomly down-sampled the original sample sizes to that of the brain BAG.

BAG	h^2	h^2 SE	P-value	*N*
Brain	0.47	0.02	$<1x10^{-10}$	30,108
Cardiovascular	0.35	0.07	$<1x10^{-5}$	30,108
Eye	0.42	0.02	$<1x10^{-5}$	30,108
Hepatic	0.18	0.07	$<1x10^{-5}$	30,108
Immune	0.19	0.07	$<1x10^{-5}$	30,108
Metabolic	0.16	0.07	$<1x10^{-5}$	30,108
Musculoskeletal	0.21	0.07	$<1x10^{-5}$	30,108
Pulmonary	0.39	0.07	$<1x10^{-5}$	30,108
Renal	0.28	0.07	$<1x10^{-5}$	30,108

C) **Brain imaging-derived phenotypes vs. 4 pulmonary features.** For the brain imaging phenotypes, we used four sets of features from our previous studies: *i*) 32 pattern of structural coavairance (PSCs) from the data-driven MuSIC atlas using T1-weighted MRI and orthogonal-projective non-negative matrix factorization[3]; *ii*) 101 GM ROIs using the ANTs (https://stnava.github.io/ANTs/) software[4]; *iii*) the 21 WM tracts for fractional anisotropy (FA) mean values[5]; and *iv*) 21 funtional node (FN) measures from resting-state functional MRI[6]. The 4 pulmonary features included forced vital capacity, forced expiratory volume, peak expiratory flow, and the ratio of forced expiratory volume to forced vital capacity. For comparison purposes, we also show the h^2estimates for the brain and pulmonary BAGs. The detailed results for all estimates are presented in **Supplementary eFile 22**. The distribution of each phenotype group is shown in the figure below.

Organ	Phenotype group	Phenotype (mean or individual)	h^2	h^2 SE	P-value
Brain	Brain feature	MuSIC[3]	0.45	0.16	$<1E^{-20}$
		GM-IDP[4]	0.39	0.16	$<1E^{-20}$
		WM-IDP[5]	0.53	0.08	$<1E^{-20}$

		FN-IDP[6]	0.29	0.06	$<1E^{-20}$
	Brain BAG	Brain BAG	0.47	0.02	$<1E^{-20}$
Pulmonary	Pulmonary feature	FVC	0.34	0.007	$<1E^{-20}$
		FEV/FVC	0.41	0.007	$<1E^{-20}$
		PEF	0.28	0.007	$<1E^{-20}$
		FEV	0.35	0.007	$<1E^{-20}$
	Pulmonary BAG	Pulmonary BAG	0.36	0.006	$<1E^{-20}$

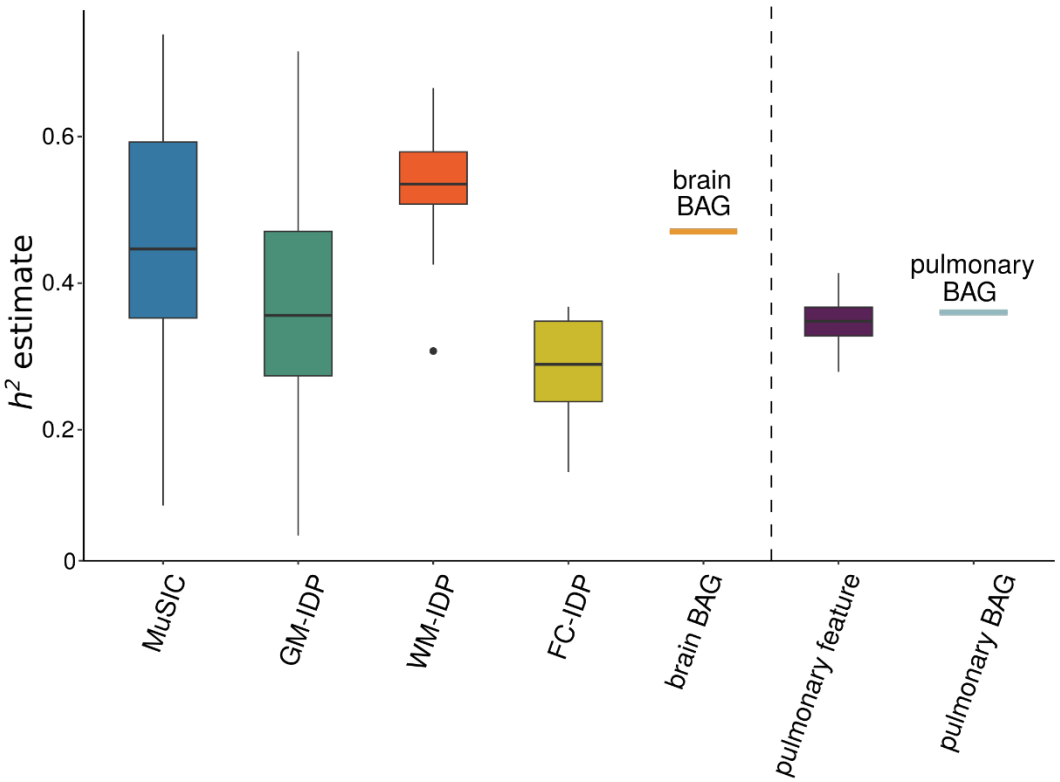

Figure. We compared h^2 estimates using GCTA between brain features and the brain BAG in contrast to pulmonary features and the pulmonary BAG. In general, our observations indicated that the brain BAG (0.47±0.02) exhibits a higher degree of heritability than the pulmonary BAG (0.36±0.06), and this pattern aligns with the heritability of the underlying features employed in their computation: Brain feature: h^2=0.42 across the four sets of brain features vs. pulmonary feature: h^2=0.34 across the four pulmonary features.

795 **eTable 2: The beta coefficient and its SE estimate from the full sample vs. the down-**
796 **sampled brain BAG comparable sample**

797 N_ISS: number of independent significant SNPs

BAG	Mean_beta_down sample	Mean_beta_full sample	SE_beta_down sample	SE_beta_fulls ample	t_beta	p_bet a	t_se	p_se	N_I SS
Cardiovasc ular	0.034802	0.035822	0.010533	0.005457	-0.513 17	0.608 293	14.08 46	**1.95E -33**	124
Eye	0.06527	0.064561	0.009967	0.009128	0.136 138	0.891 913	1.828 485	**0.069 668**	69
Hepatic	0.058408	0.057479	0.014495	0.007525	0.293 471	0.769 268	13.28 265	**2.59E -35**	289
Immune	0.043347	0.041526	0.011454	0.005948	0.682 463	0.495 312	12.78 407	**5.79E -32**	217
Metabolic	0.053834	0.052587	0.013227	0.006842	0.490 113	0.624 182	15.99 737	**1.7E-50**	422
Musculosk eletal	0.04263	0.041015	0.011109	0.005817	0.520 949	0.602 797	11.23 119	**1.44E -24**	147
Pulmonary	0.035423	0.036056	0.010959	0.005678	-0.536 29	0.591 975	20.08 143	**1.81E -67**	272
Renal	0.067828	0.068927	0.014536	0.007595	-0.233 5	0.815 446	12.87 744	**5.18E -34**	331

798

eTable 3: Genetic correlation analyses between the pulmonary BAG and the four features used to derive the BAG.

BAG	Pulmonary feature	g_c mean	g_c std	P
Pulmonary_age_gap	forced_vital_capacity_fvc_zscore	0.6409	0.0195	$6.1E^{-237}$
	fev1_fvc_ratio_zscore	0.5371	0.0316	$6.47E^{-65}$
	peak_expiratory_flow_pef	-0.7903	0.0175	$<1E^{-300}$
	forced_expiratory_volume_in_1second_fev1_zscore	0.8259	0.0111	$<1E^{-300}$

eTable 4: Selected 41 clinical traits for genetic correlation analyses. We selected the candidate studies from the GWAS Catalog for 41 clinical traits, including chronic diseases affecting multiple organ systems, education, and intelligence. To ensure the suitability of the GWAS summary statistics, we first checked that the selected study's population was European ancestry; we then guaranteed a moderate SNP-based heritability h^2 estimate and excluded the studies with spurious low h^2 (<0.05). Abbreviations are detailed in the main text.

Primary organ system	Trait	PubMed ID	Sample size
Brain	AD	30820047	63,926
	Smile-GAN-AD1	NA	33,540
	SmileGAN-AD2	NA	33,540
	SmileGAN-AD3	NA	33,540
	SmileGAN-AD4	NA	33,540
	SurrealGAN-AD1	NA	33,540
	SurrealGAN-AD2	NA	33,540
	ADHD	30478444	53,293
	ALS	27455348	36052
	ASD	30804558	46,350
	HYDRA-ASD1	37017948	14,786
	HYDRA-ASD2	37017948	14,786
	HYDRA-ASD3	37017948	14,786
	BIP	31043756	51,710
	MDD	22472876	18,759
	HYDRA-MDD1	NA	33,540
	HYDRA-MDD2	NA	33,540
	SCZ	23974872	11,244
	HYDRA-SCZ1	32103250	14,786
	HYDRA-SCZ2	32103250	14,786
	OCD	28761083	9,725
Cardiovascular	WMH	31551276	11,226
	AF	30061737	1030,836
	Stroke	29531354	446,696
Eye	Glaucoma	33627673	330,905
Hepatic	Liver fat	34128465	32,858
	PBC	34033851	24,510
Immune	SLE	26502338	14,267
	HIV	34737426	208,808
Metabolic	DB	30054458	655,666
	Hyperlipidemia	34906840	349,222
Musculoskeletal	RA	36333501	92,044
Pulmonary	Lung carcinoma	28604730	85,716
Renal	CKD	31152163	625,219
Digestive	CD	26192919	20,883
	IBD	26192919	34652
Breast	Breast cancer	29059683	139,274

Cognition	Education	23722424	126,559
	Reaction time	29844566	330,069
	Intelligence	28530673	78,308
Lifestyle	Computer use	32317632	408,815

810
811

eTable 5: Genetic correlations analyses between the nine BAGs and longevity, household income, and telomere length. We downloaded the GWAS summary statistics from Deelen et al.[7], which performed two GWASs on longevity based on the 90th survival percentile. For the household income GWAS, we downloaded from Hill et al.[8]. For the telomere length, we used GWAS summary statistics from Codd et al. [9].

BAG	Trait	g_c mean	g_c std	P	PubMed ID	Sample size
Brain_age_gap	Longevity	gc_mean	gc_std	0.0931	31413236	36,745
Cardiovascular_age_gap		-0.1588	0.0946	0.0049		
Eye_age_gap		-0.2038	0.0725	0.0719		
Hepatic_age_gap		-0.1657	0.0921	0.6182		
Immune_age_gap		0.0495	0.0993	0.9299		
Metabolic_age_gap		0.0086	0.0979	0.7605		
Musculoskeletal_age_gap		0.0328	0.1074	0.1128		
Pulmonary_age_gap		-0.1193	0.0752	0.0057		
Renal_age_gap		-0.197	0.0713	0.0323		
Brain_age_gap	Household income	-0.2089	0.0403	$2.2E^{-07}$	31874048	286,301
Cardiovascular_age_gap		-0.0679	0.0356	0.0563		
Eye_age_gap		-0.066	0.0404	0.1024		
Hepatic_age_gap		-0.1026	0.0417	0.0138		
Immune_age_gap		0.0028	0.0414	0.9464		
Metabolic_age_gap		-0.0671	0.0389	0.0841		
Musculoskeletal_age_gap		-0.2867	0.0308	$1.4E^{-20}$		
Pulmonary_age_gap		-0.1567	0.0286	$4.4E^{-08}$		
Renal_age_gap		-0.0989	0.0321	0.002		
Brain_age_gap	Telomere length	0.0273	0.0506	0.5897	34611362	472,174
Cardiovascular_age_gap		-0.0005	0.0038	0.9897		
Eye_age_gap		-0.0124	0.0439	0.7769		
Hepatic_age_gap		-0.0042	0.0306	0.9089		
Immune_age_gap		-0.1338	0.0377	0.0004		
Metabolic_age_gap		-0.0514	0.0393	0.1905		
Musculoskeletal_age_gap		0.0045	0.0333	0.8932		
Pulmonary_age_gap		-0.0993	0.0331	0.0027		
Renal_age_gap		-0.029	0.0293	0.3222		

819 **eTable 6: Causal analysis using the LCV method**. We performed causal analysis using the LCV
820 method for the bi-directional causality between hepatic and musculoskeletal BAGs, the 9 BAGs
821 and longevity, and the 9 BAGs and telomere length. GCP: genetic causality proportion.
822

Trait1	Trait2	GCP	GCP_se	P	PubMed ID	Sample size
Musculoskeletal age_gap	Hepatic_age_gap	-0.75144	0.143475	9.37E-12	NA	111,543
Brain_age_gap	Longevity (99th percentile)	-0.45597	0.208644	**0.047488**	31874048	286,301
Cardiovascular_age_gap		-0.21694	0.395088	0.547241		
Eye_age_gap		-0.07761	0.565366	0.639544		
Hepatic_age_gap		-0.53253	0.321599	0.089042		
Immune_age_gap		-0.15001	0.356513	0.868225		
Musculoskeletal_age_gap		-0.26633	0.440294	0.827824		
Metabolic _age_gap		-0.3153	0.391594	0.866896		
Pulmonary_age_gap		-0.18056	0.375253	0.210053		
Renal_age_gap		-0.33425	0.403767	0.573389		
Brain_age_gap	Telomere length	-0.05796	0.55584	0.713688	34611362	472,174
Cardiovascular_age_gap		-0.32007	0.294362	0.421771		
Eye_age_gap		-0.11877	0.49709	0.926991		
Hepatic_age_gap		-0.00755	0.332263	0.792948		
Immune_age_gap		-0.3321	0.126005	**0.002502**		
Metabolic_age_gap		-0.07943	0.45872	0.705827		
Musculoskeletal_age_gap		-0.15992	0.478106	0.821179		
Pulmonary_age_gap		-0.67193	0.198345	**3.57E-16**		
Renal_age_gap		-0.17496	0.500093	0.6767		

823

eTable 7: Selected 17 clinical traits for Mendelian randomization analyses. We unbiasedly and systematically selected 17 clinical traits, including chronic diseases affecting multiple organ systems, cognition, and lifestyle factors. The selection procedure is detailed in the main text (**Method 2J**).

Primary organ system	Trait	PubMed ID	IEU-ID (If applicable)	Number of IVs (forward MR)
Brain	AD	24162737	ebi-a-GCST002245	10
	BIP	31043756	ieu-a-1126	12
Metabolic	Type 2 diabetes	22885922	ieu-a-26	10
	Triglyceride-to-lipid ratio	32114887	met-d-XL_VLDL_TG_pct	41
Eye	Glaucoma	NA	finn-b-H7_GLAUCOMA	9
Musculoskeletal	RA	23143596	ebi-a-GCST005569	11
Hepatic	PBC	26394269	ebi-a-GCST003129	16
Digestive	CD	26192919	ieu-a-12	77
	IBD	23128233	ieu-a-292	81
Breast	Breast cancer	29059683	ieu-a-1126	86
Cognition	Reaction time	NA	Local-UKBB	18
Lifestyle	Coffee intake	NA	Local-UKBB	11
	Fresh fruit	NA	Local-UKBB	15
	Tea intake	NA	Local-UKBB	12
	Sleep duration	NA	Local-UKBB	8
	Summer outdoor activity hour	NA	Local-UKBB	14
	Body weight	NA	Local-UKBB	161

References

1. Bowden, J. *et al.* A framework for the investigation of pleiotropy in two-sample summary data Mendelian randomization. *Stat Med* **36**, 1783–1802 (2017).
2. Burgess, S. & Thompson, S. G. Interpreting findings from Mendelian randomization using the MR-Egger method. *Eur J Epidemiol* **32**, 377–389 (2017).
3. Wen, J. *et al.* Novel genomic loci and pathways influence patterns of structural covariance in the human brain. 2022.07.20.22277727 Preprint at https://doi.org/10.1101/2022.07.20.22277727 (2022).
4. Zhao, B. *et al.* Genome-wide association analysis of 19,629 individuals identifies variants influencing regional brain volumes and refines their genetic co-architecture with cognitive and mental health traits. *Nat Genet* **51**, 1637–1644 (2019).
5. Zhao, B. *et al.* Common genetic variation influencing human white matter microstructure. *Science* **372**, (2021).
6. Zhao, B. *et al.* Common variants contribute to intrinsic human brain functional networks. *Nat Genet* **54**, 508–517 (2022).
7. Deelen, J. *et al.* A meta-analysis of genome-wide association studies identifies multiple longevity genes. *Nat Commun* **10**, 3669 (2019).
8. Hill, W. D. *et al.* Genome-wide analysis identifies molecular systems and 149 genetic loci associated with income. *Nat Commun* **10**, 5741 (2019).
9. Codd, V. *et al.* Polygenic basis and biomedical consequences of telomere length variation. *Nat Genet* **53**, 1425–1433 (2021).